

1 **Response to the review by A. Benedetti on “Development studies towards an 11-year global gridded**
2 **aerosol optical thickness reanalysis for climate and applied applications”**

3
4 Thank you very much for the thorough review of this paper and the appreciation of this work. Here are
5 our replies to your specific comments (Original comments are in italic. Replies are in normal font).

6
7
8 *Main comments:*

9 *1. Title could be shortened: “An 11-year Global Gridded Aerosols*
10 *Optical Thickness Reanalysis for Climate and Related Applications”*

11
12 Answer: Thank you for the suggestion! The title is shortened now as suggested.

13
14 *2. Random and systematic in observations and background are not discussed at all. I know this is a sticky*
15 *subject which has been dealt with in previous papers, but I would like to see a few sentences on the*
16 *matter to remind the reader of the importance of a correct definition of the error matrices.*

17
18 Answer: To address this concern, a short paragraph is added in section 2.3.2 right below the section
19 title.

20 “Both observational and model errors could contain systematic bias, either of which could be removed
21 or minimized through pre-processing. For example, our quality assurance (QA) and quality control (QC)
22 methodology (Section 2.3.3) attempts to remove systematic bias as much as possible from the AOD
23 observations. Likewise, the tuning process described in Section 2.4 attempts to remove systematic bias
24 from the model background. Thus, both model background and observations are assumed to be
25 unbiased in NAVDAS-AOT.”

26
27 *3. The importance of the source and precipitation tuning is well emphasized, but the reader is left with*
28 *no feeling of what the reanalysis would do without the tuning. Is it possible to add something to address*
29 *that?*

30
31 Answer: Yes. We have included in the appendix a discussion about the tuning impact on the natural
32 model and its impact compared with the AOT data assimilation process. Four model runs with different
33 configurations were conducted for a year, including NAAPS without tuning, NAAPS with tuning, NAAPS
34 without tuning but with AOT data assimilation, and the reanalysis version, which is with both tuning and
35 AOT assimilation. A table is added, showing the 550nm modal AOT bias, RMSE, r^2 and linear regression
36 slope against AERONET from the four model runs. The seasonal mean global distributions of the total,
37 fine and coarse AOTs are also shown in two figures in the appendix. Basically, with the sources and sinks
38 tuning, RMSE decreases about half, bias and r^2 also significantly improved for the natural model. The
39 numbers are comparable with those of the DA run without tunings. AOT partitioning between the fine
40 and coarse mode AOTs are also better in the runs with the tuning.

41
42

43 4. *The trend analysis is a terrific addition to the paper in terms of science, but I feel it possibly belongs to*
44 *another publication altogether as this is already a very long paper. I leave this to the discretion of the*
45 *authors and the editor.*

46
47 Answer: Thank you for your interest and the suggestion. The trend analysis here is meant to provide an
48 evaluation of the AOT reanalysis product from another viewing point besides the validation with
49 AERONET observations. So we would like to keep the trend analysis as a part of the paper. This point is
50 also mentioned in the introductory part of section 3.3. "This helps to evaluate the reanalysis from
51 another perspective." But you are correct, that this does open up the field in trying to understand the
52 nature of aerosol trends through the use of reanalysis datasets.

53
54
55 *Other comments/typos:*

56 *Line 108: explain what modal means*

57
58 Answer: "modal" in this paper means the fine mode, coarse mode AOTs and the total AOT. In the draft,
59 "550nm modal AOT reanalysis" is replaced with "550nm modal (fine mode, coarse mode and total) AOT
60 reanalysis". Also the bracket and the content in the bracket "(fine mode, coarse mode and total)" in line
61 110-111 are deleted (as it is repeating the above information).

62
63 *Line 177: is the cloud structure retained from the model?*

64
65 Answer: Yes. In the draft "in which cloud structure is retained....." is replaced with "in which cloud
66 structure from the model is retained...."

67
68 *Line 235: perhaps another symbol can be used*

69
70 Answer: assuming you refer to "RH", which is the relative humidity. Now it is replaced with "r"
71 throughout the text.

72
73 *Line 260: what is the definition of the Monin-Obukhov length? Please add.*

74
75 Answer: right after "...and L is the Monin-Obukhov length" add ", which is a measure of the stability of
76 the surface layer (Obukhov, 1971, Eq. 26).". Also added the following new reference in the reference
77 section.

78 Obukhov, A.M : Turbulence in an atmosphere with a non-uniform temperature (English Translation).
79 Boundary-Layer Meteorology 2: 7–29, 1971.

80
81 *Line 316: "diel"?*

82
83 Answer: "Diel" means denoting or involving a period of 24 hours. To avoid confusion, "diel" is now
84 replaced with "daily".

85
86 *Line 432: "assimilatable"?*

87

88 Answer: “assimilatable” means the data is with good quality and can be assimilated in the data
89 assimilation system.
90 Change from “but it is expected that improvements in Collection 6 will be assimilatable (Shi et al.,
91 2013).” to “but it is expected that improvement in Collection 6 will be made and the data could be
92 assimilated (Shi et al. 2013).”

93
94 *Line 595: often the analysis correction are called “increments” in the literature*
95

96 Answer: thanks! The 2.4.2 section title is changed from “Tuning with AOT assimilation correction field”
97 to “Tuning with AOT assimilation correction/increment field”.

98
99 *Line 947: Over Indonesia ENSO events tend to produce large positive anomalies due to prolonged*
100 *drought and associated intense fires. The recent 2015 season was exceptional in that regard. This will*
101 *surely mask the small negative trend reported over the 2003-2013 period and shown in figure 13 (which*
102 *is fact does not reach the significance level). Again, the trend analysis is super-interesting, but I believe*
103 *deserves full attention in a separate paper.*
104

105 Answer: thank you for your interest and the suggestion. The trend analysis here is meant to provide
106 another perspective as for validation of the AOT reanalysis product. This point is also mentioned in the
107 introductory part of section 3.3. “This helps to evaluate the reanalysis from another perspective.”

108 *Figure 10-12 are a masterpiece of synthesis.*

109 Answer: Thank you!

110

111 **Response to review #2 on “Development studies towards an 11-year global gridded aerosol optical**
112 **thickness reanalysis for climate and applied applications” by P. Lynch et al.**

113

114 We would like to thank the anonymous reviewer for their comments on this paper. We are very happy
115 to hear that “The manuscript is well written, well-structured and enjoyable to read.” Here are our
116 replies to the reviewer’s specific comments (Original comments are in italic. Replies are in normal font).

117

118

119 General comments:

120 *1. I did not find description about dust and sea salt bins. Does the model has multiple bins for dust and*
121 *sea salt aerosols? If it is true, can you add lines about that (i.e., number of bin and radii of each bin)?*

122

123 Answer: the model does not have multiple bins for dust and sea salt aerosols, instead it has single mass
124 bin for each specie. Section 2.2.2 states “Aerosol microphysics are treated relatively simply in NAAPS.
125 This is in response to the computational needs of an efficient operational forecast model, its operational
126 requirements (e.g., forecast severe visibility reducing events) and the fact that in comparison with the
127 uncertainties in source functions as well as transport meteorology, microphysics is relatively well
128 constrained. Dry mass concentrations are forecasted with Equation 1 and AOT for each aerosol species
129 is computed assuming an effective particle size with respect to mass. Aerosol particles in NAAPS are
130 treated as external mixture of the aforementioned species and do not interact with each other. With
131 these assumptions, extinction and AOT can be calculated using bulk values of optical properties that
132 have been derived from theory and observations.” And “The bulk mass extinction, scattering, and
133 absorption efficiencies, along with single scattering albedo and asymmetry factor for the four aerosol
134 species at wavelength $\lambda = 550$ nm are given in Table 1.”

135

136 *2. (If the model has multiple dust and sea salt bins,) How did you separate dust and sea salt bins into the*
137 *fine and coarse-mode particles when you derive the fine and coarse AOT? Finer dust and sea salt bins*
138 *should be considered as the fine-mode.*

139

140 Answer: please see the reply above and also the introductory part of section 3. “Dust and sea salt are
141 considered coarse-mode aerosols and the ABF and smoke aerosols are considered fine-mode aerosols,
142 given the simple microphysics of the NAAPS model.”

143

144 *3. The tuning concluded a great variation in some parameters. For example, in some regions, smoke*
145 *emissions became less than half, and dust erodibility was doubled. I imagine that the tuned parameters*
146 *raises a large increment in simulation results, but there was no information about that. Can you show*
147 *how much the tuning modify model results (e.g., total emissions of smoke and dust, and distribution and*
148 *mean value of AOT)? Moreover, the readers will be interested in how much impact the tuning process*
149 *has comparing to the assimilation process.*

150

151 Answer: Thanks for raising this question. To answer this question, we have included in the appendix a
152 discussion about the tuning impact on the natural model and its impact compared with the AOT data
153 assimilation process. 4 model runs with different configurations were conducted for a year, including
154 NAAPS without tuning, NAAPS with tuning, NAAPS without tuning but with AOT data assimilation, and
155 the reanalysis version, which is with both tuning and AOT assimilation. A table is added, showing the
156 550nm modal AOT bias, RMSE, r^2 and linear regression slope against AERONET from the 4 model runs.
157 The seasonal mean global distributions of the total, fine and coarse AOTs are also shown in two figures
158 in the appendix. The values of total emissions, and the global mean values of AOTs are also given.

159 Basically, with the sources and sinks tuning, RMSE decreases about half, bias and r2 also significantly
160 improved for the natural model. The numbers are comparable with those of the DA run without tunings.
161 AOT partitioning between the fine and coarse mode AOTs are also better in the runs with the tuning.
162

163
164 *Specific comments:*
165 *Section 2.3.1: Its my understanding that you updates the 3-dimensional NAAPS mass concentration in the*
166 *assimilation process. Why did you use the 2-dimensional AOT vector as control parameter (or state*
167 *vector) instead of the 3-dimensional mass concentration vector in equation (14)? What is the advantage*
168 *of you using this method?*

169
170 Answer: This is because the 2-dimensional AOT can be obtained from vastly available observations (e.g.,
171 from MODIS, which has a global daily coverage). But 3-dimensional mass concentration is not available
172 from observations. Direct observations of mass concentrations are limited with sparsely distributed
173 ground-based surface measurements and flight measurements during field campaigns. The 2-D data
174 assimilation of AOT is to take advantage the superior spatial and temporal coverage of the satellite
175 observations.

176
177
178 *P10481, L15: Did you have a criteria for iterations of the tuning?*

179
180 Answer: No specific criteria, but no more than five times of tuning for one region and one aerosol
181 specie. The tuning is empirical and it differs for regions and species.

182
183 *P10483, L14: Does the tuning factor has seasonal variation or temporal trend during the reanalysis*
184 *period?*

185
186 Answer: The tuning factor does not have seasonal variations. The calculated factors for each species and
187 regions are based on two seasons of 3 years. For a single tuning factor, it differs slightly from year to
188 year and season to season to a certain range. An average over the 6 seasons was taken to generalize this
189 tuning factor for the reanalysis. This information is already included in section 2.4.1. The tuning factor
190 for dust erodibility changes twice over the 11 years to accommodate the land surface parameterization
191 changes in the meteorological analysis. This information is now included in section 2.4.1.

192
193 *Section 4.4: There is another limitation. The satellite observations provide a column amount of total*
194 *aerosols (i.e. AOT), but has difficulty to get vertical profiles and information about each aerosol*
195 *component.*

196
197 Answer: This is true. The paper is about reanalysis on AOT, not the 3-dimensional mass concentrations
198 of each aerosol species, so this point was not originally mentioned. But it is now added in section 4.4.

199
200 *Figure 10-12: They are interesting, but some results are put outside of the frame.*

201 Answer: Figures 10-12 are replotted with all results inside of the frame.

202

203 **List of all relevant changes made in the manuscript**
204

- 205 1. Title is shortened as “An 11-year Global Gridded Aerosols Optical Thickness Reanalysis for Climate
206 and Applied Sciences”
- 207 2. A short paragraph is added in section 2.3.2 right below the section title.
208 “Both observational and model errors could contain systematic bias, either of which could be
209 removed or minimized through pre-processing. For example, our quality assurance (QA) and quality
210 control (QC) methodology (Section 2.3.3) attempts to remove systematic bias as much as possible
211 from the AOD observations. Likewise, the tuning process described in Section 2.4 attempts to
212 remove systematic bias from the model background. Thus, both model background and
213 observations are assumed to be unbiased in NAVDAS-AOT.”
- 214 3. Added Appendix “Impact of tuning of sources and sinks vs. AOT data assimilation upon model
215 performance” at the end of the manuscript, which included one table and two figures.
- 216 4. Line 126 (corresponding to the new draft) “550nm modal AOT reanalysis” is replaced with “550nm
217 modal (fine mode, coarse mode and total) AOT reanalysis”. Also the bracket and the content in the
218 bracket “(fine mode, coarse mode and total)” in line 130 are deleted (as it is repeating the above
219 information).
- 220 5. Line 195 “in which cloud structure is retained.....” is replaced with “in which cloud structure from
221 the model is retained....”
- 222 6. The symbol of relative humidity “RH” is replaced with “*r*” throughout the text and also in Eq. 2 and
223 Eq. 6 . Single symbol in the equation cannot be marked up, so the whole equation of Eq. 2 and 6 are
224 marked up.
- 225 7. Line 276, to explain what Monin-Obukhov length is, right after “....and L is the Monin-Obukhov
226 length” add “, which is a measure of the stability of the surface layer (Obukhov, 1971, Eq. 26). ”.
- 227 8. Added in the reference section.
228 “Obukhov, A.M : Turbulence in an atmosphere with a non-uniform temperature (English
229 Translation). Boundary-Layer Meteorology 2: 7–29, 1971. ”
- 230 9. To avoid confusion, “diel” is now replaced with “daily” (“diel only appeared once in the text).
- 231 10. Line 483, Change from “but it is expected that improvements in Collection 6 will be assimilatable
232 (Shi et al., 2013).” to “but it is expected that improvement in Collection 6 will be made and the data
233 could be assimilated (Shi et al. 2013).”

- 234 11. 2.4.2 section title is changed from “Tuning with AOT assimilation correction field” to “Tuning with
235 AOT assimilation correction/increment field”.
- 236 12. Figures 10-12 are replotted with wider frames.
- 237 13. In section 2.4.1, added “For a single tuning factor, it differs slightly from year to year and season to
238 season to a certain range. An average over the six seasons is taken to generalize this tuning factor
239 for the reanalysis.” after the 1st sentence of the last paragraph. Also added “The tuning factor for
240 soil erodibility changes twice over the 11 years to accommodate the land surface parameterization
241 changes in the meteorological analysis. ” at the end of the last paragraph.
- 242 14. In section 4.4. , added “Satellite AOT retrievals characterize the optical properties of a column, and it
243 does not carry any information about aerosol vertical profiles or speciation. So the total AOT is
244 constrained through AOT data assimilation. The relative vertical profile in 3-D extinction and
245 speciation of the aerosols are uniformly varied to match the posterior AOT.” in the middle of the
246 paragraph after “However, the data assimilation system, associated with the assimilatable data, also
247 has limitations.”
- 248 15. Font of the square of the Pearson correlation coefficient “ r^2 ”, is changed from italic to normal, i.e.,
249 “ r^2 ” throughout the text and tables (to avoid confusion with the symbol of relative humidity “ r ” ,
250 which r in italic).

251

252 **Marked-up manuscript**

253 A Little Note:

254 Red color is used for mark-up.

255 Single symbol in the equations cannot be marked up, so the whole equation of Eq. 2 and 6 are marked
256 up (“RH” are replaced with “r”) with yellow color.

257 “ r^2 ”s which are marked up for font change from italic to normal may not complete (some are updated
258 but not marked-up. Sorry for the inconvenience).

259

260 **An 11-year Global Gridded Aerosol Optical Thickness Reanalysis for**
261 **Climate and Applied Sciences**
262

263 Peng Lynch¹, Jeffrey S. Reid², Douglas L. Westphal², Jianglong Zhang³, Timothy F. Hogan², Edward J.
264 Hyer², Cynthia A. Curtis², Dean A. Hegg⁴, Yingxi Shi³, James R. Campbell², Juli I. Rubin⁵, Walter R.
265 Sessions^{1,6}, F. Joseph Turk⁷, and Annette L. Walker²

266

- 267 1. Computer Sciences Corporation Inc., Monterey, CA, USA
268 2. Marine Meteorology Division, Naval Research Laboratory, Monterey, CA, USA
269 3. Dept. of Atmospheric Science, University of North Dakota, Grand Forks, ND, USA
270 4. Dept. of Atmospheric Science, University of Washington, Seattle, WA, USA
271 5. National Research Council Postdoctoral Research Associate, Monterey, CA, USA
272 6. Dept. of Atmospheric and Oceanic Sciences, University of Wisconsin-Madison, WI, USA
273 7. Jet Propulsion Laboratory, Pasadena, CA, USA

274

275 Correspondence to: Peng Lynch, CSC Inc., Mail: Marine Meteorology Division, Naval Research
276 Laboratory, 7 Grace Hopper Ave, Stop 2, Monterey, CA 93943. Email: peng.lynch.ctr@nrlmry.navy.mil

277

278 **Abstract**

279 While standalone satellite and model aerosol products see wide utilization, there is a significant
280 need in numerous climate and applied applications for a fused product on a regular grid.

281 Aerosol data assimilation is an operational reality at numerous centers, and like meteorological
282 reanalyses, aerosol reanalyses will see significant use in the near future. Here we present a
283 standardized 2003 - 2013 global 1x1 degree and 6-hourly modal aerosol optical thickness (AOT)

284 reanalysis product. This dataset can be applied to basic and applied earth system science
285 studies of significant aerosol events, aerosol impacts on numerical weather prediction, and
286 electro-optical propagation and sensor performance, among other uses. This paper describes
287 the science of how to develop and score an aerosol reanalysis product. This reanalysis utilizes a
288 modified Navy Aerosol Analysis and Prediction System (NAAPS) at its core and assimilates
289 quality controlled retrievals of AOT from the Moderate Resolution Imaging Spectroradiometer
290 (MODIS) on Terra and Aqua and the Multi-angle Imaging SpectroRadiometer (MISR) on Terra.
291 The aerosol source functions, including dust and smoke, were regionally tuned to obtain the
292 best match between the model fine and coarse mode AOTs and the Aerosol Robotic Network
293 (AERONET) AOTs. Other model processes, including deposition, were tuned to minimize the
294 AOT difference between the model and satellite AOT. Aerosol wet deposition in the tropics is
295 driven with satellite retrieved precipitation, rather than the model field. The final reanalyzed
296 fine and coarse mode AOT at 550nm is shown to have good agreement with AERONET
297 observations, with global mean root mean square error around 0.1 for both fine and coarse
298 mode AOTs. This paper includes a discussion of issues particular to aerosol reanalyses that
299 make them distinct from standard meteorological reanalyses, considerations for extending such
300 a reanalysis outside of the NASA A-Train era, and examples of how the aerosol reanalysis can be
301 applied or fused with other model or remote sensing products. Finally, the reanalysis is
302 evaluated in comparison with other available studies of aerosol trends, and the implications of
303 this comparison are discussed.

304 **1.0 Introduction**

305 The importance of aerosol particles in the atmosphere and climate system is recognized across the
306 earth sciences. Long implicated in climate change investigations (e.g., IPCC 2007; 2013), aerosol
307 particles influence countless other aspects of science and society. Obvious impacts include biologic and
308 visual air quality, including health outcomes (Laden et al., 2000; Kappos, et al., 2004), defense
309 operations, and transportation (Wilkinson et al., 2012). Further, aerosol particles interfere with many
310 aspects of earth system surveillance, such retrievals of sea surface temperature (e.g., May et al., 1992;
311 Reynolds, 1989; Robock, 1989) and ocean color (e.g., Gordon, 1997) and land use systems (Song et al.,
312 2001). Aerosols can also affect atmospheric retrievals or radiances used to constrain temperature,
313 water vapor, and CO₂ in numerical weather prediction models (Houweling, et al., 2005). In all of the
314 above cases, contiguous spatial and temporal sampling of aerosol loadings is critical. Monitoring
315 solutions using satellite data alone must cope with variable orbits (polar, high inclination or
316 geostationary) and sampling times. Based on this large basic applied science need, there is considerable
317 demand for consistent gridded aerosol products constructed for numerous applications.

318 To meet aerosol monitoring requirements, the climate and earth systems science community has
319 historically presented aerosol data as either a free-running model (with the advantage of regularly
320 gridded and timed products, e.g., Tanaka et al., 2003; Miller et al., 2006; Morcrette et al., 2009; Colarco
321 et al., 2010; Pérez et al., 2011), or irregularly-timed and located satellite data (e.g., Mishchenko et al.,
322 1999; Torres et al., 2002; Hsu et al., 2004; Levy et al., 2010; Kahn et al., 2010). In both cases, the
323 products are underdetermined. Models have poorly-resolved emissions, evolution, and sinks, and can be
324 affected by errors in the underlying meteorological model, whereas satellite data has limited coverage
325 and underdetermined retrievals based on assumptions that lead to a series of spatially and temporally-
326 correlated biases (e.g., Shi et al., 2011a). Ultimately, models and remote sensing products present

327 different aspects of atmospheric characteristics. When model and satellite products are compared,
328 contextual and sampling biases appear (e.g., Zhang and Reid, 2009). For daily and more rapid analysis,
329 such as for many specific earth system science process study questions or intersensor correction,
330 neither approach can adequately represent the full state of the aerosol system.

331 To bridge modeling and remote sensing data sources, numerous operational numerical weather
332 prediction centers have embarked on sophisticated aerosol data assimilation efforts of both passive and
333 lidar satellite sensors (e.g., Collins et al., 2001; Weaver et al., 2007; Zhang et al., 2008, 2011; Benedetti et
334 al., 2009; Sekiyama et al., 2010). Satellite products are screened, empirically corrected and assimilated
335 into models to provide systematic best-available analyses of the aerosol environment. The next step in
336 this process is to develop best-available reanalyses for community use. Just as meteorological reanalysis
337 such as the NCAR/NCEP (eg., Kalnay et. al., 1996) and ECMWF (eg., Uppala et. al., 2005; Dee et. al.,
338 2011) are commonly applied for meteorological applications, aerosol reanalyses are likely to be destined
339 to be useful data sources for initial analysis or systematic global studies for aerosol sciences.

340 Like meteorological reanalyses, aerosol reanalyses are generated through a rerun of a model that
341 assimilates historical observational data. Aerosol reanalyses aim to be a best-available, contiguous,
342 gridded product with consistent temporal reporting. It combines advantages of data accuracy from
343 satellite products and data consistency from modelling. The data should have good spatial and temporal
344 coverage and be easy to use. But an aerosol reanalysis is not simply just a rerunning of the model with
345 aerosol data assimilation. First, strict quality assurance and quality control processes need to be applied
346 to the satellite data that goes into an assimilation system, such that the model input is as consistent as
347 possible over the reanalysis period. Biased retrievals in the data assimilation system could result in
348 erroneous features that can propagate in the short term. Lack of consistency in the model or data can
349 lead to artifacts that could be mistaken for climatological trends or spurious aerosol events. Second,

350 the performance of the underlying aerosol forward model should be optimized to its upper limit through
351 a series of tunings to the aerosol sources and wet/dry removal processes. This helps to avoid large and
352 frequent corrections via the data assimilation cycle, so that the natural model field is as close as possible
353 to the satellite product and the final reanalysis product is smooth and fluent in space and time.

354 In this paper, we present the Naval Research Laboratory's development of an aerosol reanalysis
355 product for applied science use through the assimilation of NASA Terra and A-train satellite sensors into
356 the Navy Aerosol Analysis and Prediction System (NAAPS). The goal is to provide a best available AOT
357 product for applications that require this parameter. As the system develops and verification datasets
358 become available, the publically-released analysis will include many other aspects of the aerosol system,
359 including three dimensional concentrations and radiative effects such as fluxes and heating rates. Our
360 goals for the initial development of the NAAPS reanalysis and this paper are threefold.

- 361 a) *Development of a baseline applications dataset:* NAAPS has always been operationally focused,
362 with frequent operational transitions. In support of basic research and climatology applications,
363 however, the NAAPS model often requires re-runs with updated parameterizations. With
364 individual case studies being examined dozens of times per year, we wish to support such
365 endeavors by developing an accurate AOT product that is consistent in quality and time.
- 366 b) *Development of a baseline verification dataset:* Any application of the baseline dataset will
367 require a comprehensive description of the NAAPS model when run in reanalysis mode, and
368 how this differs from the operational version of NAAPS. The methods and data for characterizing
369 the reanalysis performance must be carefully examined and documented.
- 370 c) *Development of a framework for future development:* We wish to investigate the degree a
371 reanalysis represents the true atmospheric state and the extent that it can be used to study
372 climatologically-relevant aerosol features like trend and radiative impacts. As more satellite

373 products mature, they can also be incorporated into the reanalysis. The analysis presented here
374 is intended to be a template for characterization of future reanalysis datasets as they become
375 available.

376 While the aerosol system is a highly complex internal mixture of anthropogenic, biogenic, open
377 burning and wind driven emissions, ultimately it is AOT and its simple partition into fine and coarse
378 mode contributions that we can actually measure and verify globally. Reanalyses on atmospheric gas
379 composition and/or aerosols are also in development at ECMWF (Inness et al., 2013) and NASA (Buchard
380 et al., 2015). The aerosol models used for generating these reanalyses are independent in their
381 underlying meteorology, as well as aerosol sources, sinks, microphysics and chemistry. The AOT
382 assimilation methodologies, the observed AOT data to be assimilated, and the pre-assimilation
383 treatments of input data are also different. Validation of multivariate reanalyses of atmospheric
384 composition is a very complex task, and a comprehensive evaluation is needed. This study focuses
385 exclusively on the development and validation of a 550nm modal (fine mode, coarse mode and total)
386 AOT reanalysis.

387 In this paper, we provide an up-to-date description of the primary NAAPS model, noting differences
388 between the reanalysis and operational versions. Our emphasis is on the development of a modal (~~fine
389 mode, coarse mode and total~~) NAAPS AOT analysis. We describe the methods used to tune modeled
390 aerosol processes. The data assimilation system used to fuse the model and observations is described,
391 as well as the satellite data products used in the reanalysis. This is followed by a basic description of the
392 reanalyzed global fine and coarse mode 550nm AOT fields and their verification. We conclude with a
393 brief synopsis and discussion of our findings. We provide documentation of strengths and pitfalls of
394 reanalysis products including advice on interpreting like products. For example, we discuss how the data
395 assimilation system affects diurnal aerosol representation or how long term trends are represented in

396 the simulation that has static industrial emissions. We also discuss the difficulty in keeping
397 meteorological input consistent at decadal levels. We conclude with a project synopsis and outlook for
398 future experiments.

399

400 **2.0 Description of Model: NAAPS and NAVDAS-AOT**

401 The foundation of this AOT reanalysis is the Navy Aerosol Analysis and Prediction System (NAAPS)
402 and its associated aerosol data assimilation components. NAAPS is an offline aerosol transport model,
403 which has seen wide use in the community for global aerosol lifecycle research, contextual information,
404 field mission planning, and operations.

405 The original NAAPS model was based on the Danish Eulerian Hemispheric Model (Christensen,
406 1997), although since then there have been a number of upgrades to model advection and microphysics.
407 NAAPS has been run quasi-operationally at NRL since 1998, and became the world's first operational
408 global aerosol model in 2006 with implementation at the Fleet Numerical Meteorology and
409 Oceanography Center (FNMOC). The Navy Atmospheric Variational Data Assimilation System (NAVDAS)
410 for Aerosol Optical Thickness (NAVDAS-AOT; Zhang et al., 2008) was operationally implemented in 2010.
411 The system assimilates quality assured and quality controlled 2-dimensional MODIS AOT at 550 nm. In
412 its current operational configuration, NAAPS makes 6-day forecasts, 4 times a day at 1080x540 global
413 (1/3 degree) spatial resolution and 42 vertical levels driven by truncated T425L60 resolution Navy Global
414 Environmental Model (NAVGEM) meteorology (Hogan et al., 2014). Papers describing the development
415 of the operational NAAPS include Witek et al. (2007) for sea salt, Reid et al. (2009) for biomass burning
416 smoke and Westphal et al. (2009) for dust. Updates to the operational model can be found at
417 <http://www.nrlmry.navy.mil/aerosol/>.

418 In converting NAAPS from a forecast model to a reanalysis system for the A-train 2003-2013
419 time period, we desire a system that is consistent spatially and temporally in time and fits within our

420 computational constraints. This requires, at times, significant departures from the operational model,
421 and some reduction in resolution. In this section, we describe the NAAPS model configured for
422 reanalysis mode, its AOT assimilation package and the associated MODIS, MISR and precipitation
423 satellite data used to initialize and assimilate into the model. We also describe the tuning processes
424 necessary to help ensure spatial and temporal consistency within the reanalysis period.

425 2.1 Meteorology fields

426 The current operational version of NAAPS is driven by NAVGEM (Hogan et al., 2014), a global
427 T425L60 spectral model that is only available since September 2013. The NAAPS reanalysis described in
428 this paper is driven by the recently-decommissioned Navy Operational Global Atmospheric Prediction
429 System (NOGAPS) analysis fields for 2003-2013. A full NAVGEM reanalysis is under construction that will
430 allow higher horizontal and vertical resolution to better constrain future runs of the reanalysis. The
431 NOGAPS model is a global model that is spectral horizontally and energy-conserving finite-difference
432 (sigma coordinate) in the vertical (Hogan and Rosmond, 1991; Hogan and Brody, 1993). Four times a
433 day, the weather forecast models provide 6-day forecasts of the dynamical and surface analysis fields to
434 NAAPS at 3-hr intervals. The reanalysis uses only the 00, 06, 12, and 18Z analyses with the associated 3-
435 hr forecast fields to make up the 3-hr time series of dynamical forcing. NOGAPS variables used by
436 NAAPS are the topography, sea ice, surface stress, surface heat flux, surface moisture flux, surface
437 temperature, surface wetness, snow cover, stratiform precipitation, convective precipitation, lifting
438 condensation level, cumulus fractional coverage, cumulus cloud height, surface pressure, three
439 components of the wind, temperature, and relative humidity. For data assimilation, NOGAPS uses the
440 NRL Atmospheric Variational Data Assimilation System (NAVDAS), which is still used operationally for
441 assimilation of a large variety of conventional and satellite-based observations (Daley et al., 2001). While
442 NOGAPS has had some resolution changes over the 2003-2013 study period (ranging from T159 to

443 T319), spectrally truncated NOGAPS meteorology data is incorporated into the NAAPS reanalysis for
444 each 6 hour time step at the prescribed 1x1 degree resolution.

445 As the primary sink of aerosol particles, the precipitation component of NOGAPS is worth special
446 attention. Often in large scale models the parametrized precipitation schemes for tropical regimes
447 generate widespread light precipitation, while the long-term total precipitation amount is comparable
448 to observations (Dai, 2006, Sun et al., 2007). Similarly, global models also have difficulty placing
449 significant convective cells, particularly moderately-sized squall lines or coastal thunderstorms. Diurnal
450 precipitation cycles are also poorly represented by numerical models. These characteristics of model
451 precipitation are shown to affect removal of aerosol particles and can have significant impact on
452 regional AOT simulations (Wilcox and Ramanathan, 2004; Xian et al., 2009). For the reanalysis, tropical
453 precipitation from NOAA Climate Prediction Center (CPC) MORPHing technique (CMORPH, Joyce et al.,
454 2004) is used whenever available to improve aerosol wet deposition in the manner described in Xian et
455 al., (2009), in which cloud structure [from the model](#) is retained but precipitation flux is changed
456 accordingly. CMORPH combines infrared (IR) and passive microwave data (PMW) retrieved from
457 instruments onboard multiple geostationary and lower-orbiter satellites. CMORPH was chosen for this
458 role as it appears to have the best representation of temporal and spatial patterns of tropical
459 precipitation among satellite precipitation products (Janowiak et. al, 2005; Sapiano and Arkin, 2009).

460

461 2.2 Aerosol Model

462 As noted above, NAAPS is a global aerosol model originated in the mid-1990's from a
463 hemispheric sulfate chemistry model developed by Christensen (1997). Dust, sea salt and smoke have
464 been added to the original model, and are documented in Westphal et al., (2009), Witek et al., (2007)
465 and Reid et al., (2009), respectively. Given that what is commonly referred to as regional pollution or

466 haze is a result of complex anthropogenic and biogenic emissions and chemistry, here we replaced the
 467 simplified Christensen (1997) SO₂ and sulfate chemistry. As elaborated in Section 2.2.6, anthropogenic
 468 SO₂, sulfate and organics, are combined with biogenic emissions to form an anthropogenic and biogenic
 469 fine (ABF) aerosol particle species.

470 2.2.1 Aerosol Model Dynamics

471 The equations solved in the model have the form

$$472 \quad \frac{\partial q_i}{\partial t} = - \left(u \frac{\partial q_i}{\partial x} + v \frac{\partial q_i}{\partial y} + \dot{\sigma} \frac{\partial q_i}{\partial \sigma} \right) + \left(K_x \frac{\partial^2 q_i}{\partial x^2} + K_y \frac{\partial^2 q_i}{\partial y^2} + K_z \frac{\partial(\Gamma^2 K_z \frac{\partial q_i}{\partial \sigma})}{\partial \sigma} \right) + P_i - Q_i \quad , \quad (1)$$

473 where q_i is the mass mixing ratio (kg kg⁻¹) for the species i , $q_i = c_i/\rho$, where c_i is the mass concentration
 474 (kg m⁻³) and ρ is the density of air (kg m⁻³), x and y are the horizontal coordinates (longitude and
 475 latitude), σ is the terrain-following vertical coordinate that ranges from 1 at the surface to 0 at the
 476 model top, $u, v, \dot{\sigma}$ are the advection velocity in the x, y and the vertical directions of the σ -coordinates,
 477 K_x and K_y are horizontal diffusion coefficients that are assumed to be constant ($K_x = K_y = 6 \times 10^4 \text{ m}^2 \text{ s}^{-1}$),
 478 And K_z is the vertical diffusion coefficient based on the Monin-Obukhov similarity theory for the surface
 479 layer (Obukhov, 1971). The K_z profile is extended to the whole boundary layer by using a simple
 480 extrapolation (Hertel et al., 1995). Finally, $\Gamma = d\sigma/dz$ (m⁻¹). P_i are the sources and Q_i are the sinks for
 481 the species i .

482 Equation 1 is solved on a spherical grid with 1° x 1° horizontal resolution and 25 vertical irregular
 483 σ -coordinate levels in the reanalysis product presented here. The average depth of the first layer is ~30
 484 meters, and consecutive layers gradually increase in depth towards the top layer, which ends at ~18 km
 485 (70hpa). Advection is calculated using a semi-Lagrangian scheme (Staniforth and Cote, 1991), with
 486 departure points calculated using the method of Ritchie (1987). Horizontal and vertical diffusion are
 487 calculated with a finite-element method (e.g., Bathe, 2006).

488 2.2.2 Aerosol Optical Properties in NAAPS

489 Aerosol microphysics are treated relatively simply in NAAPS. This is in response to the
 490 computational needs of an efficient operational forecast model, its operational requirements (e.g.,
 491 forecast severe visibility reducing events) and the fact that in comparison with the uncertainties in
 492 source functions as well as transport meteorology, microphysics is relatively well constrained. Dry mass
 493 concentrations are forecasted with Equation 1 and AOT for each aerosol species is computed assuming
 494 an effective particle size with respect to mass. Aerosol particles in NAAPS are treated as external
 495 mixture of the aforementioned species and do not interact with each other. With these assumptions,
 496 extinction and AOT can be calculated using bulk values of optical properties that have been derived from
 497 theory and observations. The calculations for scattering (b_{scat} , m^{-1}), absorption (b_{abs} , m^{-1}) and extinction
 498 coefficients (b_{ext} , m^{-1}), plus the integrated optical depth (τ , unitless) are, respectively

499
$$b_{scat,i}(\lambda, x, y, \sigma) = c_i(x, y, \sigma) \alpha_{scat,i}(\lambda) f_i[r(x, y, \sigma)] \quad , \quad (2)$$

500
$$b_{abs,i}(\lambda, x, y, \sigma) = c_i(x, y, \sigma) \alpha_{abs,i}(\lambda) \quad , \quad (3)$$

501
$$b_{ext,i}(\lambda, x, y, \sigma) = b_{scat,i}(\lambda, x, y, \sigma) + b_{abs,i}(\lambda, x, y, \sigma) \quad , \text{ and } (4)$$

502
$$\tau_i(\lambda, x, y) = \int_1^0 b_{ext,i}(\lambda, x, y, \sigma) \frac{1}{\Gamma} d\sigma \quad , \quad (5)$$

503 where α_{ext} , α_{scat} and α_{abs} are the mass extinction, scattering, and absorption efficiencies respectively
 504 ($m^2 g^{-1}$), and f_i is a scattering hygroscopic growth factor.

505 The bulk mass extinction, scattering, and absorption efficiencies, along with single scattering
 506 albedo and asymmetry factor for the four aerosol species at wavelength $\lambda = 550$ nm are given in Table 1.
 507 For ABF, dust and sea salt, the values are taken from the optical properties of aerosol and clouds-OPAC
 508 database (Hess et al., 1994). The chosen coefficients for ABF are weighted towards the more-absorbing
 509 aerosol particles that are generated by less-developed countries that dominate global aerosol fields

510 (Dubovik et al., 2002). Optical properties for smoke are treated similarly, with both empirical
511 derivations and theory derived from Reid et al. (2005a, b).

512 The effect of humidity on particle light scattering for each aerosol species is represented by the
513 Hanel (1976) formulation of the hygroscopic growth factor $f_i(RH)$ (unitless), defined as

$$f_i(r) = \left[\frac{(1-r)}{(1-r_o)} \right]^{-\Gamma_i}, \quad (6)$$

514 where RH is the relative humidity, Γ_i is an empirical species-dependent exponent and RH_o is the
515 reference relative humidity that is set equal to 30%. In NAAPS, Γ_i is taken as 0.5 for ABF particles
516 assuming 40% sulfate and 60% organic aerosols. In comparison, Γ_i is 0.63 for sulfate (Hanel, 1976),
517 0.18 for smoke (Reid et al., 2005b), 0.46 for sea salt (Hegg et al. 2002; Ming and Russell, 2001), and zero
518 for dust (Li-Jones et al., 2002). A maximum allowed RH is 95%. We assume absorption α_{abs} is not
519 affected by humidity.

Formatted: Font: Italic

Formatted: Font: Italic

520 2.2.3 Sink processes in NAAPS

521 Dry deposition to the surface is accounted for through a decrease of the aerosol concentration
522 in the lowermost model layer, assuming a dry deposition flux

$$523 F_{DDi} = c_{1i} v_{di}, \quad (7)$$

524 where c_{1i} is the mass concentration (kg m^{-3}) in the first layer above the surface for the species i , and v_{di}
525 is the dry deposition velocity, which is a function of aerosol type and surface type.

526 For particle deposition over water, the dry deposition velocity v_d is set to 0.0002 m s^{-1} for
527 anthropogenic and biogenic fine particles, 0.0003 m s^{-1} for smoke loosely following the theoretical
528 relation between over water v_d and particle radius in Slinn and Slinn (1980), assuming bulk effective
529 radius listed in Table 1 for the two types of aerosols. v_d is set to 0.001 m s^{-1} over water for dust particles
530 after tuning to minimize AOT corrections through the data assimilation process (more details in section

531 2.4.2). Dry deposition of sea salt to open water is given by the formula in Slinn and Slinn (1980),
532 assuming a dry mass mean radius near 1.5 μm , and written as

$$v_{dss} = C_d U_{10}, \quad (8)$$

533 where $C_d = 1.3 \times 10^{-3}$ is the drag coefficient, and U_{10} the wind speed at 10 meters above the sea
534 surface in m s^{-1} .

535 For particle deposition over land, the method of Walcek et al. (1986) is used and the explicit
536 expression for v_d is the same as in Christensen (1997; Eq. (9)), which is a function of surface friction
537 velocity and Monin-Obukhov length, which is a measure of the stability of the surface layer (Obukhov,
538 1971, Eq. 26). This is written as

$$v_d = \begin{cases} \frac{u_*}{a} \left(1 + \left(\frac{-300}{L} \right)^{2/3} \right) & \text{for } L < 0 \\ \frac{u_*}{a} & \text{for } L > 0 \end{cases}, \quad (9)$$

539 where u_* is the surface friction velocity in m s^{-1} , $a = 500$ (except for a forest with leaves, where $a = 100$),
540 and L is the Monin-Obukhov length. v_d is calculated using Eq. (9) for all the aerosol species in the model.

541 Gravitational settling is also applied to the aerosol particles in the model. Dry deposition is only
542 applied in the lowermost model layer, whereas gravitational sedimentation takes place within the whole
543 vertical domain except the lowermost model layer, as it is taken into account in v_d .

544 The wet deposition of particles is assumed to be similar to that for sulfate aerosol, based on a
545 simple scavenging ratio formulation (e.g. Iversen, 1989). The scavenging coefficient is calculated in the
546 same way as in Witek et al. (2007), as a function of the precipitation mass flux with different below-
547 cloud and in-cloud scavenging ratios, written as

548

$$W(\sigma) = \begin{cases} \frac{\Lambda_{bc}}{H} \frac{P_a(\sigma)}{\rho_w} & \text{below cloud scavenging} \\ \frac{\Lambda_c}{H} \frac{P(\sigma)}{\rho_w} & \text{in cloud scavenging} \end{cases}, \quad (10)$$

549 where $P_a(\sigma)$ and $P(\sigma)$ ($\text{kg m}^{-2}\text{s}^{-1}$) are the total downward flux densities of precipitation mass at a
 550 given σ -level below or in a precipitating cloud, respectively. H is an effective thickness for scavenging
 551 (set to 1000 m), $\Lambda_{bc} = 1 \times 10^5$ is the below-cloud scavenging ratio, $\Lambda_c = 7 \times 10^5$ is the in-cloud
 552 scavenging ratio, and ρ_w is the density of water.

553 2.2.4 Dust

554 Dust emissions occur whenever the friction velocity exceeds a threshold value, snow depth is
 555 less than a critical value, and the surface moisture is less than a critical value (Westphal et al., 1988).

556 The dust emission flux follows the equation

$$557 F_{dust} = c e_f u_*^4, \quad (11)$$

558 where e_f is the erodible fraction of a grid box (unitless), u_* is the surface friction velocity with the
 559 threshold value of 0.6 m s^{-1} for dust mobility, and c is a scaling constant of $4.5 \times 10^{-7} \text{ g m}^{-2} \text{ s}^{-1}$. In the
 560 operational version of NAAPS, the erodibility map is empirically derived from the United States
 561 Geological Survey Land Cover Characteristic Database and Total Ozone Mapping Spectrometer Aerosol
 562 Index values (Walker et al., 2009). While in general the operational version of NAAPS has good dust
 563 scores, NAAPS clearly has a high bias for dust for the Sahara. For the reanalysis, the use of Ginoux et al.
 564 (2001) dust sources mitigated much of this bias. The Ginoux et al. (2001) erodibility map associates dust
 565 sources with topographic depressions and has many of the same features as seen in Westphal et al.
 566 (1988), yet its geologic input data tightened individual source areas.

567 Regional source tuning is also applied in the NAAPS reanalysis, which is described in Section 2.4.

568 Dust is emitted into the bottom two layers of the model (below 100m) when friction velocity exceeds
 569 the threshold and surface wetness is below a critical value (0.4). Then, dust is transported by model

570 dynamics both horizontally and vertically in the boundary layer and the free troposphere. Dust removal
571 includes sedimentation, dry deposition and wet removal, which is constrained with CMORPH
572 precipitation within the tropics. Dust is assumed to be totally hydrophobic and hence the hygroscopic
573 growth factor is set to 1.

574 2.2.5 Sea Salt

575 The sea salt component for operational NAAPS and the NAAPS reanalysis was developed by
576 Witek et al. (2007). Sea salt emissions are driven dynamically by sea surface wind. The sea salt dry mass
577 flux F_{ssa} ($\text{kg m}^{-2}\text{s}^{-1}$) from the surface is based on the whitecap method and the Monahan's formulation of
578 the source function (Monahan et al., 1986), and has the empirical form

$$F_{ssa} = a_s U_{10}^{b_s} \quad , (12)$$

579 where U_{10} is the wind speed at 10 meters above the sea surface in m s^{-1} , $a_s = 1.37 \times 10^{-13}$ and $b_s = 3.41$.

580 Dry deposition of sea salt over water is proportional to the sea surface wind speed, following Slinn and
581 Slinn (1980) and over land follows Eq. (9). Sea salt particles are assumed to undergo hygroscopic growth
582 depending on ambient atmospheric relative humidity, following the growth rate shown in Eq. (6). Sea
583 salt scattering coefficient is based on swelled particles, while absorption coefficient is assumed not
584 effected by the swell.

585 2.2.6 Anthropogenic and biogenic fine particles (ABF)

586 The most significant change to NAAPS microphysics for the reanalysis is the development of a
587 method to account for complex anthropogenic and biogenic species while not significantly increasing
588 the computational cost of the model. Originally, the only anthropogenic emissions and predictive
589 variables within NAAPS were SO_2 and sulfate. However, organic species constitute one of the most
590 important contributors to the mass of atmospheric aerosols (Zhang et al, 2007, Jimenez et al, 2009), and
591 indeed commonly dominate the submicron aerosol mass and AOT. This organic aerosol mass, while

592 having a significant component attributable to primary organic aerosol (POA) emission, is predominantly
593 secondary organic aerosol (SOA; i.e., created in the atmosphere from volatile organic carbon (VOC)
594 precursors in the gas phase, such as, isoprene, terpenes and aromatics; e.g., Zhang et al, 2007). These
595 precursors are largely biogenic in origin. Ultimately, the complex chemical interactions between
596 anthropogenic and biogenic emissions result in a photochemical soup that cannot be directly linked to a
597 single origin.

598 For realistic simulation of AOT, primary and secondary organic aerosols must both be included in
599 the NAAPS model in some form. To be consistent with the NAAPS reanalysis' philosophy of simple and
600 tractable physics, the sulfur-related species has been replaced with a bulk anthropogenic and biogenic
601 fine (ABF) mass category to account for the entire class of anthropogenic and biogenic emissions and
602 their secondary particle products. This species class includes all accumulation mode particles, including
603 biogenic marine, outside of open biomass burning, as described in Section 2.2.7. The first component of
604 this mixture is the original sulfur chemistry. Sulfate aerosols are produced by chemical processes in the
605 atmosphere from gaseous precursors, mainly sulfur dioxide (SO₂) from anthropogenic sources and
606 dimethylsulfide (DMS) from biogenic sources. For NAAPS reanalysis, SO₂ emissions are updated from
607 GEIA Version 1A (i.e., 1985) (Benkovitz, 1996) to Monitoring Atmospheric Composition &
608 Climate/CityZen EU projects (MACCity) inventory 2005-2010 average (Granier et al., 2011, Diehl et al.,
609 2012), which reflects the increased emission in India and China over the past decade and also includes
610 monthly variation. DMS emission fluxes at the air-sea interface are computed using the Saltzman (1993)
611 parameterization, with the monthly DMS seawater concentrations from Lana et al. (2011). DMS are
612 immediately converted to 95% sulfur dioxide and 5% sulfate in the model. SO₂ chemistry follows
613 Hoffmann and Calvert (1985), in which oxidation of sulfur solution (S(IV)) by hydrogen peroxide (H₂O₂)
614 and dissolved ozone (O₃) are considered climatologically. We assume background oxidants H₂O₂ and O₃

615 are not depleted by reactions. Ultimately, sulfur chemistry accounts for roughly one half of all non-
616 biomass burning fine mode AOT.

617 Inclusion of POA in the NAAPS reanalysis is straightforward, including the major VOC species
618 that act as precursors for the SOA. We apply the 2005-2010 monthly-mean MACCity data base for
619 anthropogenic (industrial and transport) emissions of POA and SOA precursors (Granier et al, 2011), the
620 Bond et al (2004) biofuels data with a monthly scaling factor based on Jeong (2011), and the Precursors
621 of Ozone and their Effects in the Troposphere (POET) climatological monthly emissions inventory for
622 biogenic VOC's (Olivier et al, 2003). For the actual SOA formation process, the Volatility Basis Set (VBS)
623 approach has been adopted (Donahue et al, 2006; Ahmadov et al, 2012). This greatly reduces both the
624 number of necessary precursor species and the number of SOA products from the vast numbers needed
625 to explicit represent SOA formation and evolution by formulating the conversion process in terms of a
626 limited number of precursor species and volatility classes (four in our case) for the reaction products.
627 The reaction yields for the various VBS classes, upon which the approach ultimately depends, are
628 derived from numerous chamber studies as cited, for example, in Ahmadov et al (2012) and Donahue et
629 al (2006). Phase partitioning is done as per Pankow (1994).

630 To further simplify the inclusion of organic aerosols in the NAAPS model, both the POA and SOA
631 are calculated in a "preprocessor" at model initialization. For the SOA, this includes calculation of the
632 yield of SOA product mass from the emissions inventory VOC's, based on the VBS model, and the
633 treatment of this mass as a primary aerosol emission, similar to the POA. Utilizing the similarity in
634 microphysical and optical properties of OA and sulfate, the model carries POA and SOA together with
635 sulfate as aforementioned "anthropogenic and biogenic fine". This approach has some obvious
636 shortcomings, but it carries minimal computational cost and has much improved the simulation of AOT,
637 especially the model bias and correlation with AERONET over India, China and Eastern United States.

638 2.2.7 Biomass Burning Smoke

639 Biomass burning has a wide coverage globally, from the tropics to the high latitudes, and it
640 significantly impacts the total light absorption budget (Bond et al., 2013). Unlike other aerosol sources
641 that are meteorologically driven (e.g., dust and sea salt) or prescribed in a seasonal or monthly inventory
642 (e.g., pollution), smoke emissions have significant variability that hinders easy parameterization.
643 Configuring the NAAPS model with biomass burning aerosols as a separate species permits explicit
644 hypothesis testing about the sources, sinks, and optical properties of these aerosols. Operational NAAPS
645 has adopted the satellite active fire hotspot based approach through the Fire Locating and Modeling of
646 Burning Emissions (FLAMBE1.0; Reid et al., 2009; Hyer et al., 2013). The model converts the smoke
647 emission to total mass injected by multiplying by the fire size. This value is then divided by the area of
648 the grid cell and the fire duration to create a flux as an hourly input to the model. FLAMBE can use
649 satellite fire products from either geostationary sensors, which offer faster refresh rates and
650 observation of the full diurnal cycle, or polar orbiters, which have greater sensitivity. Polar orbiting
651 | satellites have significant biases not only in their ~~daily~~ sampling pattern, but also additional artifacts
652 | from day to day shifts in the orbital pattern (e.g., Heald et al., 2003, Hyer et al., 2013). Over the
653 reanalysis period, multiple changes in the geostationary constellation posed a challenge for consistency
654 of the smoke source function. Therefore, a polar-only version of FLAMBE was created for the reanalysis.

655 Given that the NAAPS reanalysis coincides with the NASA EOS system, MODIS-based fire
656 products and emissions are applied. MODIS orbits have a 16-day repeat cycle, with daily coverage of the
657 globe excepting small gaps between orbits at the equator. Areas that are not covered one day are
658 centered on the orbit the next. The Fire Inventory from NCAR (FINN, Wiedinmyer et al. 2011), which is
659 also based on MODIS active fire detections, uses a 3-day moving average to account for gaps and orbital
660 variations. After testing multiple coverage corrections, we found that for the reanalysis a simple two-day
661 maximum (previous day and present day) fire signal largely mitigated orbital effects and thick clouds in a

662 tractable way. This correction is consistent with the self-sustained nature of regional fire emissions, and
663 further improves upon the scores presented in Reid et al. (2009).

664 Smoke injection height combined with boundary layer mixing has a strong influence on how
665 smoke is dispersed. Most plumes are observed as constrained within the planetary boundary layers,
666 especially within the tropics and subtropics (Tosca et al., 2011, Campbell et al., 2013). Large boreal fires
667 can pump smoke to higher altitudes, though these fires constitute only a very small portion of the total
668 fires and global budget of AOT (Fromm and Servranckx, 2003; Kahn et al., 2008). In NAAPS, smoke is
669 injected into the bottom four layers of the model, which is approximately the bottom 400 m of the
670 model. Tuning of injection height to match observed aerosol vertical profiles is feasible in regional
671 studies (e.g., Wang, et al., 2013). However, we use the uniform injection height in NAAPS, considering
672 that boundary layer processes generally quickly mix aerosols well within the boundary layer or below
673 the models significant inversion height to produce a result similar to the observations of Kahn et al.
674 (2008).

675

676 2.3 AOT assimilation

677 The core of the NAAPS AOT reanalysis is AOT assimilation using the Navy Atmospheric
678 Variational Data Assimilation System for Aerosol Optical Thickness (NAVDAS-AOT; Zhang et al., 2008).
679 NAVDAS-AOT is a system that, by default, assimilates quality-controlled two-dimensional MODIS AOT at
680 550 nm into NAAPS. It additionally has the ability to perform three-Dimensional (3DVAR) assimilation
681 using the Cloud Aerosol Lidar with Orthogonal Polarization (CALIOP) product of Campbell et al. (2010) in
682 Zhang et al. (2011). The main impact of 3DVAR assimilation is redistribution of aerosol mass vertically,
683 while conserving the total column mass and AOT. CALIOP data is available for only part (2006-2013) of
684 the reanalysis period, therefore, in this first study we perform 2DVAR AOT assimilation only.

685

686 2.3.1 Formulation of NAVDAS-AOT

687 The NAAPS prognostic variable is the 3D aerosol mass concentration. A 2DVAR approach is
688 adopted for AOT assimilation simply because AOT retrievals from MODIS and MISR are a column-
689 integrated aerosol optical property. The 2DVAR AOT assimilation is realized through three steps:

690 (1) Convert NAAPS mass concentration AOT:

$$\tau_{b\lambda} = H_{m_\tau}(C_m) + \epsilon_{b\lambda} \quad , (13)$$

691 where $\tau_{b\lambda}$ is the background (prior analysis) AOT vector, C_m is the NAAPS mass concentration, and H_{m_τ} is
692 the forward operator that represents the conversion of NAAPS mass concentration to AOT. $\epsilon_{b\lambda}$ is the
693 error in $\tau_{b\lambda}$ introduced by the H_{m_τ} operator;

694 (2) 2-D variational assimilation of the AOT field:

$$\tau_{a\lambda} = \tau_{b\lambda} + P_b H^T [H P_b H^T + R]^{-1} [\tau_{o\lambda} - H(\tau_{b\lambda})] \quad , (14)$$

695 where $\tau_{a\lambda}$ is the analysis AOT vectors, $\tau_{o\lambda}$ is the observation AOT vector, and H is the observation
696 operator that represents any necessary spatial and temporal interpolations from the background to
697 observational space. P_b and R are the background error covariance and observational error covariance
698 matrices, respectively. The analysis field can be considered as the background ($\tau_{b\lambda}$) plus a correction
699 term (the second term on the right hand side of Eq. 14), which is the difference between the
700 observation and background vectors weighted by the ratio of background error covariance matrix to
701 total error covariance matrix in the observational space;

702 (3) Convert the analysis AOT vectors to NAAPS mass concentration:

$$C_m = H_{\tau_m}(\tau_{a\lambda}) + \epsilon_m \quad , (15)$$

703 where H_{τ_m} is the backward operator that performs the conversions from AOT to NAAPS mass
704 concentration. In the backward operation, a scaling factor is applied to the vertical profile of aerosol
705 mass based on the ratio of the AOT correction and background AOT, while keeping the hygroscopic

706 growth rate (Eq. 6) unchanged. ε_m is the error in C_m introduced by the H_{τ_m} operator. Both ε_m and $\varepsilon_{b\lambda}$ can
707 be transformed as part of the error term of $\tau_{b\lambda}$, which is assumed to be zero for this study.

708

709 2.3.2 Observational and background model error covariance matrices

710 Both observational and model errors could contain systematic bias, either of which could be
711 removed or minimized through pre-processing. For example, our quality assurance (QA) and quality
712 control (QC) methodology (Section 2.3.3) attempts to remove systematic bias as much as possible from
713 the AOT observations. Likewise the tuning process described in Section 2.4 attempts to remove
714 systematic bias from the model background. Thus, both model background and observations are
715 assumed to be unbiased in NAVDAS-AOT.

716 In NAVDAS-AOD, observational errors are assumed to be uncorrelated. Thus, only observational
717 error variances are needed. The error variances for the gridded satellite AOT data are computed by the
718 summation of instrumental error variances and sample error variances (Zhang et al., 2008). The
719 instrumental error variance is estimated through the comparison of satellite and ground-based
720 sun-photometer data as shown in Zhang and Reid (2006) and Shi et al., (2011a) for MODIS “Dark
721 Target”, and Shi et al., (2014) for MISR aerosol products. The sample error variance measures the
722 variance in the gridded mean (or the representative error variance). For a 1° latitude by 1° longitude
723 grid, the sample error variance is derived by the spatial variance of the AOT data of the grid divided by
724 the number of observations that are used in computing the gridded mean value.

725 The background error covariance is computed for any given two horizontal model grids m and n
726 based on the following equation

727
$$P_b^{mn} = [S_b^m]^{1/2} C_b^{1/2} [S_b^n]^{1/2}, \quad (16)$$

728 where P_b^{mm} is the background error variance for horizontal grid locations of m and n. S_b^m and S_b^n are
729 the model error variances at grid locations m and n, respectively. C_b is the horizontal background error
730 correlation between the two grid locations. Similar to observational error variances, model error
731 variances are also estimated using ground based sun-photometer data, and the values are reported in
732 Zhang et al., (2008). The C_b values are computed using the second order auto-regressive (SOAR)
733 approximation (Daley and Barker, 2001),

734
$$C_b(m, n) = (1 + R_{mn} / L) \exp(-R_{mn} / L) \quad . (17)$$

735 Here R_{mn} is the great circle distance between m and n. L is the horizontal error correlation length. The
736 horizontal error correlation length is estimated through evaluating the differences in AOT between
737 satellite observations and 6-hour model forecasts as a function of horizontal distance. L is set to 200 km
738 for this study based on Zhang et al., (2008).

739

740 2.3.3 Input data for NAVDAS-AOT and its preprocessing treatment

741 The basis of input data for the reanalysis is operational MODIS Collection 5 AOT (Levy et al.,
742 2007; 2010; Remer et al., 2005; 2008) and Multi-angle Imaging SpectroRadiometer (MISR) AOT products
743 (Martonchik et al., 2009, Kahn et al., 2009, Kahn et al., 2010). MODIS Deep Blue for Collection 5 is not
744 used here due to bias issues, but it is expected that improvements in Collection 6 will be made and the
745 data could be assimilated~~assimilatable~~ (Shi et al., 2013). Extensive quality assurance (QA) and quality
746 control (QC) procedures applied to the MODIS C5 AOT are conducted as described in Zhang et al. (2006)
747 and Shi et al. (2011a) for over water and Hyer et al. (2011) for over land. These QA/QC procedures are
748 especially important for this application, because the analysis must be heavily weighted to the
749 observations to allow assimilation for correct for errors such as missing dust and smoke sources. Under

750 these circumstances, the impact of noisy data is large and proper filtering and correction of data is
751 critical. QA/QC procedures implemented for MODIS and MISR AOT include a) strict checks for removal of
752 possible cloud contamination, b) corrections for the lower boundary condition, such as wind speed to
753 correct for white caps and specular reflection over water and surface albedo over land, and c) aerosol
754 micro-physical corrections based on derived fine mode fraction over water and regionally over land. This
755 strict quality assuring and quality control procedure is necessary to remove outliers and minimize
756 erroneous aerosol features in MODIS that would adversely impact the model and propagate through the
757 system. Currently, the total global data loss through screening of MODIS is about 40%, with a reduction
758 of absolute errors of 10–30% over water (Zhang et al., 2006; Shi et al., 2011a). Over-land, the QA/QC
759 procedures reduce data volume by ~60% and improve the global fraction of MODIS AOT within $0.05 \pm$
760 20% of AERONET (Hyer et al., 2011). The data are aggregated into a $1^\circ \times 1^\circ$ grid that matches the model
761 resolution where additional buddy checks are applied.

762 A benefit of a reanalysis is that observations that are not timely enough to be incorporated into
763 an operational run can be utilized. Thus, while MODIS products are used in all versions of NAAPS, for the
764 reanalysis we can make use of MISR. Though narrower in swath than MODIS, and thus providing less
765 relative coverage, MISR has two key benefits. First, MISR is on Terra and its imaging swath is in the
766 MODIS sun-glint region. Hence, MODIS plus MISR completes the MODIS swath with full coverage.
767 Second, the MISR over-land algorithm has an advantage over retrievals conducted with other sensors in
768 its handling of the lower boundary condition, provided that $AOT < 0.8$. In particular, there are large
769 spatially-correlated discrepancies between the retrieved MODIS and MISR AOT in regions of high albedo
770 as a result of deficiencies in the MODIS lower boundary condition (Shi et al., 2011b). Notable regions of
771 discrepancy between MODIS and MISR include the Andes Mountains, Saharan Africa, the Arabian
772 Peninsula and Central Asia (Shi, et al., 2011b). Further, MISR can retrieve AOT in desert region at high
773 efficacy where the operational MODIS Collection 5 “Dark Target” products cannot, thus providing

774 further coverage in desert regions. Quality-assuring (QA) and quality control (QC) procedures, including
775 the use of MODIS cloud mask products to reduce cloud contamination in MISR data sets and applying
776 various quality checks and empirical corrections on MISR Level 2 aerosol products, are conducted to
777 generate data assimilation (DA) quality data sets (Shi et al., 2011c, 2014). Then the data are aggregated
778 into a 1° latitude by 1° longitude grid.

779 Data assimilation using NAVDAS-AOT is used to produce a new analysis after every six hours of
780 NAAPS integration time. The MODIS and MISR Level 2 aerosol products are typically acquired in a 6-hr
781 range centered on the nominal valid time of the analysis (i.e., 0, 6, 12 and 18 UTC) from NASA data
782 servers. Then QA/QC processes convert MODIS and MISR level 2 data into filtered, corrected, and
783 aggregated AOT observations with associated uncertainty estimates for assimilation in NAVDAS-AOT.
784 After QA/QC processes, the general pattern of data coverage from MODIS and MISR for each
785 assimilation cycle is shown in Fig. 1. The observed geographic pattern is attributed to the fact that
786 MODIS and MISR AOT retrievals are limited to daytime and a limited range of sun-sensor geometries.
787 The longitudinal range for which MODIS and MISR data is available in a given assimilation cycle is limited
788 because Terra and Aqua are in sun-synchronous orbits with equatorial overpass time of 10:30 and 13:30
789 local solar time, respectively.

790 For the MODIS sensors, overlapping coverage between Terra and Aqua over the 6-hr data
791 acquisition period does occur and a mean of Terra and Aqua weighted to the number of Level 2
792 retrievals from each sensor. The contribution of each individual sensor to the total volume of the MODIS
793 DA quality data is about 50% on average, although this number is highly variable on the 6-hrly basis,
794 with the variability depending on the observability of the sensors (e.g., cloudy vs. non-cloudy, land vs.
795 ocean, etc...). Because of its narrower swath compared to MODIS, the data volume of the MISR DA-
796 quality data is only about 22% on average of that of MODIS. Approximately half of the MISR DA-quality

797 data overlaps with MODIS. When overlapping of MISR and MODIS 1°x1° 6-hrly DA-quality data occurs,
798 the mean of the two is taken for final assimilation purpose.

799 The seasonal geographic distribution of the total number of 6-hrly 1°x1° fused MODIS and MISR
800 DA quality AOT data averaged over 2003-2013 is shown in Fig. 2 (left column). Areas with high cloud
801 coverage, including the ITCZ and the subtropical stratus cloud deck regions, have relatively less data. In
802 the polar regions, cloud contamination often exists in satellite-retrieved AOT data, leading to elevated
803 AOTs. The Southern Oceans is an example of cloud-enhanced MODIS AOT, for instance (Toth et al.,
804 2013). As a result, high-latitude AOT data are filtered out in the QA/QC process. The cut-off latitudes for
805 AOT data to be assimilated are 40°S over water for the southern hemisphere and 80°N for the northern
806 hemisphere. In addition, because MODIS and MISR AOT observations are only available during daylight,
807 and thus there are no observations during polar nights, this results in more data counts in boreal
808 summer than in boreal winter. Fig. 2 also shows that areas with bright desert (e.g., Saharan Africa, the
809 Arabian Peninsula and Central Asia), or snowy/icy surfaces (e.g., Andes Mountains, Greenland and high
810 latitude in boreal winter) have relatively less data to be assimilated, as these regions are mainly filled in
811 by MISR retrievals that have a revisit time of seven days on average rather than a revisit time of one day
812 by MODIS.

813 The start date of the reanalysis is 1 January 2003, based on the availability of the observational
814 data used in the reanalysis. Terra MODIS and MISR AOT data are first available in March, 2000, and Aqua
815 MODIS AOT is first available in July 2002. An additional consideration is CMORPH precipitation data,
816 which is used to replace model precipitation within the tropics, is not available until December 2002.
817 Since the required spin-up time for the aerosol model is one month, the reanalysis starts at 1 January,
818 2003. Figure 3 shows the time evolution of 6-hrly data counts of the global MODIS, MISR and the fused
819 1°x1° grid DA quality AOT in dots and their center-point thirty-day running average in solid lines.
820 Throughout the reanalysis time period (2003-2013), the data counts of the DA quality data are relatively

821 stable, despite small dips in December 2003 in both MISR and MODIS and October 2008 in MISR due to
822 the upstream data being unavailable. The data count of the fused MODIS and MISR DA quality data is
823 about 3800 during boreal summer and 2400 during boreal winter, on average. This essentially follows
824 the seasonal variation of the MODIS DA quality data count, which makes up about 80% of the total fused
825 MODIS and MISR DA quality data. Half of the remaining 20% is attributed to MISR alone and half is
826 attributed to the overlapping MISR and MODIS DA quality data. The seasonal variation of data volume is
827 mainly related to the fact that more AOT data are discarded for the southern hemisphere high latitudes
828 than the northern hemisphere high latitudes as a result of cloud contamination, and no observations are
829 available during polar nights (Fig. 2).

830

831 2.4 Tuning studies

832 While AOT data assimilation from sensors such as MODIS and MISR improves NAAPS
833 performance (Zhang et al. 2014), the natural NAAPS model performance is equally important for
834 generating a final reanalysis product that aims to match observations. Previous studies have shown that
835 aerosol source functions, inherent within the natural runs, are one of the largest uncertainties with
836 respect to aerosol modeling of AOT (e.g., Kinne et al., 2003). As a result, a series of source-tuning
837 exercises have been carried out on the natural model, using AERONET and satellite AOT observations for
838 constraint. The tuning exercises consisted of running the model multiple times while iteratively adjusting
839 model source and sink parameters. Smoke emissions and dust erodibility, for regions as shown in Fig. 4
840 with some additional divisions as shown in Table S1, were tuned by iterative comparison between
841 NAAPS model output without data assimilation and AERONET data, as described in Section 2.4.1.
842 Emissions for some regions not covered by AERONET, as well as aerosol sink parameters, were
843 constrained using the AOT assimilation correction field as described in Section 2.4.2. A list of the
844 corrections applied is given in Table S1. The range of variation in optical properties of dry aerosols

845 reported in the literature (e.g., Hess et al., 1998; Kinne et al., 2003) is small compared to other
846 uncertainties, therefore we adopted the optical properties described in section 2.2.2 without additional
847 tuning.

848 2.4.1 Tuning of aerosol sources with AERONET

849 The AErosol RObotic NETwork (AERONET, <http://aeronet.gsfc.nasa.gov>), a ground-based global
850 scale sun photometer network, has been providing high-accuracy measurements of aerosol properties
851 since the 1990s (Holben et al., 1998; Holben et al., 2001). AERONET instruments measure sun and sky
852 radiance at several wavelengths, ranging from the near ultraviolet to near infrared during daytime. It is
853 often used as the primary standard for validating satellite products and model simulations (e.g., Kahn et
854 al., 2010; Levy et al., 2010; Colarco et al., 2010). Since there are no AERONET data at 550nm,
855 measurements from multiple wavelengths (380nm to 1020nm) were used to estimate both fine and
856 coarse mode AOTs at 550nm, based on the Spectral Deconvolution Method (SDA) of O'Neill et al. (2001,
857 2003). Extracted fine and coarse mode AOTs from AERONET AOTs are then compared to ABF plus
858 smoke and sea salt plus dust, respectively. The SDA product has been verified using in situ
859 measurements (Kaku et al., 2014) and has been shown to be able of capturing the full modal
860 characteristics of fine and coarse particles while avoiding the uncertainties that come from using static
861 diameter thresholds, at 0.8 or 1.0 μm for example. Further, the SDA has also been shown to eliminate
862 any potential cloud bias in fine mode AOTs from AERONET (Chew et al., 2011), although thin cirrus
863 contamination into the coarse model AOT can still be problematic in some regions such as Southeast
864 Asia and Equatorial Africa (Chew et al., 2011; Huang et al. 2011).

865 Only cloud-screened, quality-assured Level 2 AERONET data are used in this study (Smirnov et
866 al., 2000), and the sites are marked with black dots in Fig. 4. Within the reanalysis time period, nearly
867 600 regular sites provided valid observational data. AERONET Distributed Regional Aerosol Gridded

868 Observation Networks (DRAGON) observations are concentrated over a small area and a short period of
869 time, and they are excluded from this study to avoid the effect of uneven sampling on the results from
870 the statistical analysis. Spatially, the 1x1 degree grids in which the AERONET Level 2 data fall within are
871 identified, and the model AOT is sampled from these identified model grids. Temporally, AERONET Level
872 2 data are binned into 6-hrly intervals centered at the model synoptic output times of 00, 06, 12 and 18
873 UTC and then averaged within the bins. The model AOT at 550nm is sampled consistently with
874 AERONET: we extract the model AOT at a site using only times when AERONET had measurements. A
875 second approach is tested, in which the model data is interpolated onto AERONET observation times.
876 Validation results from the two methodologies are similar.

877 Empirical regional tuning of smoke and dust emissions is based on the fine and coarse mode
878 AOT comparisons with AERONET. The globe is divided into sixteen regions, as shown in Fig. 4, each
879 having their own distinct aerosol characteristics. For example, South America, South Africa, Peninsular
880 Southeast Asia, and Insular Southeast Asia have a prevailing smoke aerosol species during burning
881 seasons, while North Africa and Southwest Asia are dust dominated. East Asia and Indian Peninsular
882 have mixed dust and pollution. Regional emission tuning factors were generated by using the regional
883 bias and slope of the linear regression between pair-wise NAAPS and AERONET AOT. This is done for
884 2009-2011 when AERONET data is more abundant than earlier years. Seasonally, data are grouped into
885 the boreal winter/spring (December to next-May) and boreal summer/fall (June to November) time
886 periods. These bi-seasonal temporal stratifications account for the major monsoonal and climatic shifts
887 in the atmosphere while preserving major aerosol seasons such as, for the boreal summer/fall, the
888 August-October biomass burning seasons in South Africa, South America, and Maritime Continent, the
889 June-August African dust season, and the U.S. and European summer haze seasons.

890 Regional emission factors, in the form of linear scaling factors applied to the original source
891 functions for smoke and dust, are derived for each aerosol active season for the three years. [For a single](#)

892 [tuning factor, it differs slightly from year to year and season to season to a certain range. An average](#)
893 [over the six seasons is taken to generalize this tuning factor for the reanalysis. The resulting seasonal](#)
894 [factors are then averaged over the three years and applied over the entire time series.](#)The model is
895 then run using the corrected emissions and the results are validated regionally against AERONET to
896 determine whether the tuning improved bias, correlation, and root mean square error (RMSE).
897 Additionally, the fine/coarse mode AOT time series of NAAPS and AERONET are reviewed for each site in
898 the region to ensure the tuning is sensible. This process is repeated iteratively to refine the tuning. In
899 the supplemental Table 1, the values of the regional multipliers for smoke emission based on the two-
900 day maximum MODIS-only FLAMBE data base are listed. Also provided are the regional multipliers for
901 soil erodibility, which are used to modify the dust source (Ginoux et. al., 2001). [The tuning factor for soil](#)
902 [erodibility changes twice over the 11 years to accommodate the land surface parameterization changes](#)
903 [in the meteorological analysis.](#)
904

905 2.4.2 Tuning with AOT assimilation correction/[increment](#) field

906 The total number of operational AERONET sites has grown to over 300 in recent years. However,
907 the network's global coverage is uneven with the majority of sites located over land where they are
908 easily accessible. The available AERONET data is often not representative of major aerosol impact
909 regions, and it does not optimally sample for the biases that remote sensing products may have (Shi et
910 al., 2011b). In particular, open oceans have few AERONET sites.

911 In regions with sparse AERONET data coverage, aerosol sources and parameters, such as
912 sedimentation and dry deposition for ocean regions, are tuned using satellite AOT assimilation
913 correction/[increment](#) fields. The monthly means of the daily AOT corrections (i.e., the difference
914 between the assimilation posterior and the model prior) are a good indicator of the model performance
915 globally. The correction maps can be used to quickly identify geographic regions where the model

916 succeeds or does poorly. A region in which the data assimilation consistently suppresses aerosol mass
917 could indicate a region with excessive aerosol emissions, or deficient removal, with the assumption that
918 aerosol transport has much smaller uncertainty.

919 Since satellite products have uncertainties, especially over land, we rely on source corrections
920 inferred from AERONET except where there are no representative sites close to the known source area
921 (e.g., southern African biomass burning region). Over the ocean where AERONET has only a few sites
922 globally, satellite data assimilation plays an irreplaceable role, not only because of the good spatial and
923 temporal coverage of satellite AOT data, but also because of its much smaller uncertainty compared to
924 the over-land AOT product (Hyer et al., 2011). Dust dry deposition velocity over water is tuned based on
925 the AOT correction over the tropical Atlantic where African continent dust outflow is located, and is set
926 to 0.001 m s^{-1} . To minimize the AOT correction over global ocean, especially high-latitude regions where
927 surface wind is large, we also update the sea salt dry deposition velocity over water from a constant to a
928 function of surface wind speed following Eq. (8). This effectively reduces the negative AOT correction
929 over high-wind regions. This approach does not account for possible sources of error, including sea salt
930 emission parameterization, biases in surface wind that drives emission and biases in boundary layer
931 relative humidity that affects hygroscopic growth of the sea salt particles. In particular, our approach
932 assumes that meteorological fields are correct, and implements correction solely to the uncertain
933 parameters of aerosol sources and sinks.

934

935 **3.0 Reanalyzed Aerosol Optical Thickness**

936 In this section, we focus on evaluating the reanalysis AOT at 550 nm apportioned into fine and
937 coarse mode contributions. The sum of the fine and coarse mode AOTs constitutes the total AOT. These
938 are what we consider the key reanalysis output variables. Dust and sea salt are considered coarse-mode
939 aerosols and the ABF and smoke aerosols are considered fine-mode aerosols, given the simple

940 microphysics of the NAAPS model. Seasonally, the boreal winter/spring (December to next-May, ie.,
941 DJFMAM) and boreal summer/fall (June to November, ie., JJASON) time periods are investigated. When
942 performing bi-seasonal long-term averaging, we use only data in June 2003-May 2013 time period, so
943 that each individual month has an even weighting.

944

945 3.1 Global distribution of AOT and seasonal variability

946 The bi-seasonally averaged total, fine, and coarse mode AOTs at 550nm for the 2003-2013 time
947 period are presented in Fig. 5. Results are shown for the reanalysis and a parallel model run using tuned
948 source and sink parameters but without AOT data assimilation. The fused MODIS-MISR DA-quality AOT
949 for the same time period are shown in Fig. 2 (right column) for comparison. The total AOTs for both the
950 NAAPS runs with and without AOT data assimilation look very similar to the fused DA-quality MODIS-
951 MISR AOT. Prominent fine mode features include pollution over East Asia and India, as well as biomass
952 burning in South Africa, South America and the Maritime Continent in JJASON. Distinguishable coarse
953 mode features include Saharan dust, Arabian and central Asian dust, and the circumpolar sea salt belt
954 over the Southern Ocean. For DJFMAM, the total AOTs for both the NAAPS runs with and without AOT
955 data assimilation also look very similar to the fused DA-quality MODIS-MISR AOT. As for the fine-mode
956 AOT, in addition to the year-round pollution over East Asia and India, biomass burning in central Africa
957 and Peninsular Southeast Asia shows up for the DJFMAM season. As for the coarse-mode AOT, dust over
958 Sahara, Sahel, Arabian Peninsula and East Asia are clear and the circumpolar sea salt belt over the
959 southern ocean is persistent. The seasonal global average total AOTs for over-ocean and over-land from
960 the reanalysis are also similar to those of the fused DA-quality MODIS-MISR AOT. The NAAPS run
961 without AOT assimilation has slightly higher global average total AOTs for over-ocean and over land,
962 mainly attributed to higher fine mode AOT averages.

963 The similarity between the NAAPS runs with and without AOT data assimilation implies that the
964 AOT correction by the data assimilation process is small and the whole model tuning process is effective.
965 The resemblance between the reanalysis (NAAPS with AOT data assimilation) AOT and the fused MODIS-
966 MISR AOT indicates that the data assimilation system works well in adjusting model fields to the closest
967 observations. In this study, the model tuning process is considered equally as significant as the AOT data
968 assimilation in influencing the final reanalysis. As the DA-quality satellite AOT data can reflect relatively
969 small global coverage (Fig. 1, Fig. 2), areas not covered by the DA-quality satellite AOT would be highly
970 impacted by the natural model (NAAPS without data assimilation). [More details on the impact of tuning](#)
971 [versus the DA on the model performance are provided in Appendix A.](#)

972 For this type of comparison (Fig. 5), which is done with all available model and satellite data, we
973 should also expect some difference between the satellite retrievals and the reanalysis, resulting from
974 contextual biases in satellite products such as clear sky biases (Zhang and Reid, 2009). Satellite retrievals
975 for AOT mainly occur over clear sky, while the model depicts both clear and cloudy situations. Aerosol
976 conditions can be very different between clear and cloudy sky, which is often associated with weather
977 systems. For example, during the South America and Africa burning season (corresponding to JJASON),
978 the southeast outflow regions from the southeast coast of the continents into the southern oceans are
979 found to have lower seasonal average AOT for clear sky compared to cloudy/all sky, as smoke plumes
980 are often transported along with the cloud system (Zhang and Reid, 2009). This clear sky bias is also
981 discernable comparing MODIS AOT and the reanalysis AOT (Fig. 2 and Fig. 5).

982

983 3.2 Validation with AERONET

984 For validation purposes, we use the quality-assured AERONET Level-2 product. The reanalysis
985 AOTs are compared with AERONET 6-hrly total, fine and coarse mode AOTs at 550nm.

986 3.2.1 Global overview

987 Over the reanalysis period (2003-2013), the number of AERONET observations that can be
988 paired with model data gradually increases with time (Fig. 6a). The daily volume of global 6-hrly
989 AERONET data has more than doubled in 2012 compared with 2003. The data count in 2013 decreases
990 slightly due to the long processing time required for validating AERONET Level 2 data (instruments need
991 to be removed from the field and recalibrated (Smirnov et al., 2000)). As there are more AERONET sites
992 in the northern hemisphere than in the southern hemisphere and AERONET measurement only occurs
993 during daytime, there are more AERONET observations during boreal summers than winters. Polar and
994 high-latitude sites have few or no observations in winter, which raises a temporal sampling issue in
995 validation for these regions. AERONET sampling also covaries with the seasonal AOT assimilation cycle,
996 as high-latitude regions are less influenced by AOT assimilation during the wintertime.

997 Despite the uneven seasonal sampling, the ninety-day running average of the root mean square
998 error (RMSE) of reanalysis AOTs is quite stable throughout the reanalysis time period (Fig. 6b), at around
999 0.1 for both fine and coarse mode AOTs and 0.14 for the total AOTs. Daily average RMSE can
1000 occasionally exceed 0.4.

1001 Figure 7 provides the comparison of the pair-wise 6-hrly reanalysis AOT and AERONET AOT for
1002 all of the available global sites during the reanalysis time period. The normalized data density is shown
1003 in color. AOT data from AERONET and the reanalysis are binned at a resolution of 0.01 and density of
1004 each bin is colored relative to the maximum density in the sample. Also shown are the basic statistics of
1005 the comparison: the total number of stations and the 6-hrly observations, bias, root-mean-square error
1006 (RMSE), square of the Pearson correlation coefficient (r^2), and the linear regression parameters of the
1007 Theil-Sen method (Theil, 1950; Sen, 1968). The slope of the Theil-Sen linear regression is defined as the
1008 median of the slopes determined by all pairs of two-dimensional sample points. It is a robust linear

1009 regression that is insensitive to outliers and more accurate than the least-squares regression for
1010 potentially skewed data. For reference, also shown is the linear least square regression line, which is
1011 more sensitive to outliers.

1012 For both JJASON and DJFMAM, the global reanalysis fine-mode AOT has a small positive bias of
1013 slightly less than 0.01, while the coarse-mode AOT has a negative bias close to -0.02. The resulting bias
1014 for total AOT is -0.01. It is noteworthy that perhaps a portion of the AERONET coarse mode bias is due to
1015 cirrus contamination (Chew et al., 2011), which will be mitigated in the next major revision of AERONET
1016 data. The RMSE values for both fine and coarse mode 6-hrly AOTs are ~ 0.1 , except that the RMSE of the
1017 coarse AOT is a little higher (0.11) during DJFMAM and a little lower during JJASON (0.08). The
1018 seasonality of RMSE for coarse mode AOT is more apparent than that of the fine mode AOT, which is
1019 consistent with Fig. 6. RMSE for the total AOT is 0.14 for both seasons, consistent with Fig. 6 as well. r^2
1020 is close to 0.65 for fine mode AOT and close to 0.61 for coarse mode AOT for both seasons. r^2 for the
1021 total AOT is about 0.7, which is slightly better than the individual fine/coarse mode AOTs. The slope of
1022 the Theil-Sen regression lines is greater than 1 (around 1.3) for the fine mode AOT, less than 1 (around
1023 0.8) for the coarse mode AOT, and very close to 1 for the total AOT for both seasons. All of the above
1024 statistical numbers indicate that the fine mode AOT has a small high bias while the coarse mode AOT has
1025 a small low bias on average and globally. There is little seasonal difference in the mode statistics (fine,
1026 coarse and total modes) for the whole globe.

1027 As monthly data is often used in climate studies, we also evaluate the reanalysis monthly
1028 averaged AOTs (Fig. 8). Monthly averages are obtained only when the total number of 6-hrly AERONET
1029 data exceeds ten. For validation purposes, the monthly average reanalysis AOT is calculated based on
1030 the available 6-hrly data that can be paired with AERONET data. With the high frequency signals (e.g.,
1031 daily variability) smoothed out, the monthly average exhibits a better match with AERONET data over

1032 all. For both seasons and all modal AOTs, the monthly averages in the scatter plots are more aligned
1033 with the 1:1 lines, RMSE is roughly 50% lower (0.07 for total AOT, 0.05 for fine and coarse mode AOTs),
1034 and r^2 about 0.2 higher on average (with a maximum of 0.90 for the total AOT in DJFMAM and a
1035 minimum of 0.74 for the coarse AOT in JJASON). While absolute bias is unaffected by averaging, there
1036 appears a slope bias in linear regression results. Sites that may have a low background punctuated by
1037 severe events will appear in the regression differently from sites with a consistent but high background.
1038 This results in slope bias in regression of monthly averaged AOT values, demonstrating the dangers of
1039 applying monthly mean data to downstream calculations such as radiative forcing. Such calculations
1040 need to be conducted at the finest spatial and temporal scales achievable, with accounting for
1041 resolution effects.

1042 Figure 9 shows the cumulative distribution function (CDF) of AOT errors compared with
1043 AERONET for total, fine and coarse AOTs, respectively, using 6-hrly data. As a reassurance, the CDF of
1044 AOT errors compared with MODIS and MISR DA quality data is also shown. Because the seasonal
1045 differences for the global validation statistics are small, the two seasons are combined for the CDF
1046 analysis. As expected, the reanalysis total AOT is in good agreement with MODIS and MISR DA quality
1047 AOTs, though slightly less agreement with MISR than MODIS is found as the relative number of MISR
1048 data involved in AOT assimilation is much less. More than 95% of the reanalysis total AOT has an AOT
1049 error falling in the AOT error range of $[-0.05, 0.05]$ compared with MODIS or MISR. The reanalysis AOT
1050 has larger errors with respect to AERONET. The crossing points of the CDF curves and the zero AOT error
1051 line (and the $-0.1/+0.1$ error lines) show that about 35% fine mode AOT has a low bias (4% with error
1052 less than -0.1) and the other 65% has a high bias (6% with error greater than 0.1) compared to
1053 AERONET. For coarse mode AOT, about 60% has a low bias (7% with error less than -0.1) and 40% has a
1054 high bias (2% with error greater than 0.1). For the total AOT, about 44% has a low bias (10% with error
1055 less than -0.1) and 56% has a high bias (8% with error greater than 0.1). On average the fine AOT has a

1056 slight high bias and the coarse AOT has a slight low bias, which is consistent with the scatter plot result
1057 (Fig. 7).

1058 3.2.2 Regional Evaluation

1059 Figures 10, 11, and 12 show box-whisker plots of the pair-wise comparisons of regional
1060 reanalysis 6-hrly modal AOT vs AERONET: percentiles marked in the plots are 95%, 90%, 75%, 50%, 25%,
1061 10% and 5%, for the regions defined in Fig. 4 for 2003-2013. Also shown are regional mean AOTs
1062 designated by a diamond for AERONET and “+” for the reanalysis. Detailed statistics associated with Fig.
1063 10-12 (including separation into two seasons) are provided in the supplemental material. These include
1064 seasonal means and medians of the reanalysis and AERONET, along with reanalysis bias, RMSE, r^2 , Theil-
1065 Sen linear regression parameters and number of valid data points for each region and the globe.

1066 In general, the reanalysis follows the regional variation found in AERONET for fine-mode, coarse-
1067 mode and total AOTs. For the fine mode AOT, the reanalysis matches well with AERONET with respect
1068 to the regional means, medians, and variance. However, the results vary by region (Fig. 10). The
1069 regional means and medians are the same or slightly larger than those of AERONET for all regions,
1070 except East Asia and insular Southeast Asia, where the means are smaller than AERONET. The high AOT
1071 regions are the developing East Asia, Indian subcontinents, Peninsular and Insular Southeast Asia. These
1072 regions also have the highest RMSE values varying between 0.15 and 0.2, while RMSE values of other
1073 regions are all below 0.1. The low bias in mean fine mode AOT in East Asia and insular Southeast Asia is
1074 mostly due to the model’s inability to capture the magnitude of large fine aerosol events (e.g. extreme
1075 pollution and biomass burning events). The correlation coefficients (r^2) of most regions fall between 0.5
1076 and 0.9. The best performing region is South America, whose r^2 is greater than 0.8, indicating the
1077 reanalysis captures the temporal variation in fine mode aerosols, which are attributed mostly to biomass

Formatted: Font: Not Italic

Formatted: Font: Not Italic

1078 burning smoke. Regions with worse r^2 include West Continental United States (W. CONUS), North Africa,
1079 SW Asia and insular Southeast Asia, with r^2 around 0.4-0.5.

Formatted: Font: Not Italic

Formatted: Font: Not Italic

1080 The coarse mode AOT, overall, agrees less well with AERONET than the fine mode AOT with
1081 respect to the regional means, medians, variances and correlations (Fig. 11). Many regions have
1082 generally very low coarse AOT; RMSE for these regions will be low, but r^2 will also be low due to the
1083 small dynamic range. The most prominent high coarse mode AOT regions are the dusty North Africa and
1084 Southwest Asia domains. The moderate coarse mode AOT regions are dust-influenced Indian
1085 subcontinent, East Asia and Central America. These regions have relatively large RMSE (between 0.1 and
1086 0.2), except central America (<0.1), compared to other regions (<0.1). Except for Southwest Asia, the
1087 oceanic region, North America boreal, W. CONUS and Australia, where the reanalysis mean coarse mode
1088 AOT is comparable to that of AERONET, other regions show mean low biases. The low bias, relative to
1089 the mean AOT, is generally small, except for Peninsular and insular Southeast Asia. The bias over these
1090 regions is attributed largely to the known thin cirrus contamination in AERONET L2 data (Chew et al.,
1091 2011; Huang et al., 2011). Thin cirrus cloud is a significant challenge for sun photometer aerosol optical
1092 depth measurement, as it is easily miscategorized as coarse-mode aerosols by the instrument. The
1093 persistent occurrence of high thin cirrus cloud over these regions elevates the mean coarse mode AOT
1094 and thus the mean total AOT substantially. For example, at Singapore, a representative site for the
1095 insular Southeast Asia, 34% of AERONET L2 AOT data is found to be coincident with Micro-Pulse Lidar
1096 Network (MPLNET)-observed cirrus clouds (Chew et al, 2011). The estimated range of positive AOT bias
1097 in AERONET L2 data over Singapore, due to unscreened cloud presence, ranges from 0.03 to 0.06. Taking
1098 this estimated AOT bias of AERONET L2 data into account, the reanalysis coarse-mode AOT would be
1099 very close to reality. A similar situation exists for the peninsular Southeast Asia, based on the estimated
1100 cirrus cloud contamination in AERONET data at the regionally representative Pimai, Thailand site (Huang
1101 et al., 2011).

Formatted: Font: Not Italic

1102 | The correlation coefficients r^2 of the coarse mode AOT are less than those of the fine mode AOT
1103 | for most regions, except for north Africa, SW Asia, Europe-Mediterranean and India, which have strong
1104 | dust influence. Insular and Peninsula SE Asia have the worst correlations as expected, mostly because of
1105 | the cirrus cloud contamination in AERONET data. Other regions which have small AOT variations (e.g.
1106 | dynamical data range less than 0.1) tend to have small r^2 s, e.g., north American Boreal and W. CONUS.

Formatted: Font: Not Italic

Formatted: Font: Not Italic

1107 | The total AOT, which is the sum of the coarse-mode AOT and fine-mode AOT, has a validation
1108 | feature that combines the validation properties of the two AOT modes (Fig. 12). The regional variation
1109 | of total AOT follows that of AERONET well. The variance of the reanalysis for each region is smaller
1110 | overall than that of AERONET, suggesting the difficulty in capturing extreme events with the model and
1111 | assimilation system and a tendency to underestimate the magnitude of extreme events and
1112 | overestimate in very clean conditions. A smaller AOT variance is known to be a typical model behavior
1113 | among aerosol models (Kinne et al., 2006; Sessions et al., 2015) and is a persistent challenge to the
1114 | aerosol modelling community. The reanalysis does not perform as well with respect to mean bias and
1115 | RMSE over East Asia, Indian subcontinent, insular and peninsular Southeast Asia, where complicated
1116 | aerosol environments often exist. For example, dust is often mixed with various kinds of pollutants over
1117 | East Asia and the Indian subcontinent, which hinders satellite AOT retrievals and impacts model
1118 | performance through AOT data assimilation. Over insular Southeast Asia, constant high cloud cover
1119 | poses significant observability issues (Reid et al., 2013), reducing the availability of successful satellite
1120 | retrievals of AOT, in addition to artificial high AOTs caused by cirrus contamination in AERONET data.
1121 | This region also has a complicated fire regime that is systematically undersampled by the observations
1122 | used to drive the smoke emissions in the model (Miettinen et al., 2013). The large discrepancies
1123 | between the reanalysis and AERONET for coarse AOTs over insular and peninsular Southeast Asia affect
1124 | the reanalysis means and medians for total AOTs, but to a lesser degree, since fine mode aerosols are
1125 | the dominant aerosol type for the these regions. Most regions have r^2 between 0.5 and 0.8. W. CONUS

Formatted: Font: Not Italic

1126 | has the smallest r^2 , which is about 0.376, among all regions, reflecting the challenge for the model to
1127 | simulate the small variance of the AOT there.

Formatted: Font: Not Italic

1128 3.2.3 Site-by-site validation

1129 | Site-by-site validation of the NAAPS reanalysis was conducted relative to the International
1130 | Cooperative for Aerosol Prediction (ICAP) Multi Model Ensemble (ICAP-MME, Sessions et al., 2015) as a
1131 | baseline. Overall, ICAP-MME was shown to outperform any individual models with regard to RMSE in
1132 | 550nm AOT forecast (Sessions et al., 2015). By ranking, the ICAP-MME was typically first or second
1133 | against all models at individual sites using one-year worth of data. Since most of the ICAP models
1134 | include AOT assimilation as well, the NAAPS reanalysis was compared to the ICAP-MME. The twenty-one
1135 | AERONET sites used in the ICAP-MME study were agreed upon by the world's major center developers,
1136 | as the most representative of each region. The same two seasonal periods (DJFMAM and JJASON of
1137 | 2012) are used. In Fig. 4, these sites are marked with red squares. The ICAP-MME is run daily at 00 UTC
1138 | for 6-hrly forecasts out to 120 hr. The best available ICAP MME data (closest to analysis) for this
1139 | comparison is the consensus mean of 6-hr forecast at 00 UTC; thus, the NAAPS reanalysis is at an
1140 | advantage in this comparison due to the lagged AOT assimilation cycle in the ICAP-MME.

1141 | Table 2 shows the name of each site, its location and the prevailing aerosol type, along with all
1142 | statistics relating to the total AOT at 550nm for the two seasons. The same statistics for fine and coarse
1143 | mode AOTs are listed in Tables 3 and 4, respectively. The values of bias and RMSE are *in bold, bold with*
1144 | *underline, and italic, depending on whether the reanalysis performance is the same, better, or worse*
1145 | *than the ICAP MME mean 6-hr forecast, respectively. Over a majority of the sites, the total AOT of the*
1146 | *reanalysis is the same or better than the ICAP-MME with respect to bias and RMSE. The exceptions are*
1147 | *the Beijing and Solar Village AERONET sites. Singapore is uncertain, as the low biases in fine mode AOT*
1148 | *contributes less than half of the total low bias, implying the dominant bias is the coarse mode AOT bias,*

1149 *which is affected by thin cloud contamination in AERONET data. Cases, where the reanalysis is the same*
1150 *or better than the ICAP-MME in bias and RMSE occur less for the coarse-mode AOT than for the total*
1151 *AOT. On the one hand, the total AOT is assimilated in the reanalysis while the coarse mode AOT is not.*
1152 *So, the total AOT is better constrained with satellite observations. On the other hand, the ICAP-MME*
1153 *consensus mean for dust/coarse mode AOT includes an additional independent aerosol model relative to*
1154 *the total AOT consensus (five vs. four models), which makes the dust AOT ensemble exhibit better*
1155 *performance among all the models compared with the total AOT ensemble performance (Sessions, et. al.*
1156 *2015).*

1157 The AOT seasonal difference is very clear for sites with outstanding seasonal aerosol features.
1158 For example, higher total and fine AOT values attributed to biomass burning are observed in JJASON
1159 over Alta Floresta, Rio Branco, and Singapore and in DJFMAM over Chiang Mai. Seasonal differences are
1160 also found over Ilorin with higher AOT in DJFMAM relative to JJASON, due to both dust and biomass
1161 burning activities. It is generally true that absolute bias and RMSE increase with increasing values of
1162 AOT, so a seasonal variation in bias and RMSE is also discernable for the sites with large seasonal AOT
1163 variations. r^2 of the above sites in their biomass burning seasons are generally very good (above 0.8
1164 except for Singapore), indicating that the reanalysis captures the timing and variability of large smoke
1165 episodes quite well.

1166 Overall, the sign of the bias and the order of magnitude of the bias and RMSE values for the
1167 selected sites are consistent with the regional evaluations in Fig. 10-12 (and the supplemental tables).
1168 For high AOT sites (e.g., Banizoumbou, Beijing, Chiang Mai, Gandhi College, Ilorin and Kanpur), the
1169 reanalysis generally has a low bias, as a result of the model and/or the data assimilation system being
1170 incapable of capturing the amplitude of high AOT events. An exception is Solar Village, though its
1171 dominant aerosol species, which is dust/coarse mode aerosol, is also biased low in AOT during DJFMAM.

Formatted: Font: Not Italic

1172 Low bias in high AOT events is quite common among aerosols models (Kinne et al., 2006; Sessions et al.,
1173 2015). The discrepancy can arise solely as a function of spatial and temporal resolution: the average AOT
1174 for a grid cell in an aerosol plume will be systematically lower than the peak observed point AOT in that
1175 plume. However, shortcomings of aerosol sources or insufficient representation of near-source aerosol
1176 processes can also cause bias. Sometimes the discrepancy can be reduced by AOT assimilation, but the
1177 probability of a successful retrieval declines for higher AOT events, and this phenomenon is amplified by
1178 the application of AOT QA/QC procedures. The largest departure for both seasons in total AOT occurs
1179 over Beijing, where the coarse mode bias contributes a little more to the total bias in DJFMAM and the
1180 fine mode bias contributes a little more in JJASON. Among all sites, the maximum RMSE occurs over
1181 Beijing in both seasons for the total and the fine mode AOT and in DJFMAM for coarse mode AOT.
1182 JJASON RMSE is smaller for the reanalysis than for the ICAP-MME, implying that global models uniformly
1183 don't do well here. Correlation coefficient r^2 of the coarse mode AOT at Beijing is also the worst for both
1184 seasons, while r^2 values for the fine and total AOTs are reasonable (0.54 in DJFMAM and 0.76 in JJASON
1185 for total AOT, and a little better for fine AOT). The frequent mixture of pollution, dust, and clouds, along
1186 with varying surface properties also hinders satellite retrievals, not only reducing the number of
1187 successful retrievals but also contributing to large errors in retrieved AOT (e.g, Shi et al., 2011b; Zhang et
1188 al., 2014). Similar situations exist for Ilorin, where Sahelian biomass burning system is often mixed with
1189 dust episodes in DJFMAM, and for Gandhi College and Kanpur, the two Indian sites, in both seasons.

Formatted: Font: Not Italic

Formatted: Font: Not Italic

1190 For moderate to low AOT sites, including Cart Site, Chapais, GSFC, Minsk, Moldova, Monterey
1191 and Palma de Mallorca, the reanalysis performs well, with the biases falling between -0.02 and 0.02,
1192 RMSE values less than half of their site mean AOTs for all modes (all less than 0.07), and r^2 between
1193 0.42 and 0.85. Over Crozet Island, a remote oceanic site in the Southern Indian Ocean, the reanalysis has
1194 a relative large high bias (compared to its very low mean) likely due to overestimation of sea salt. On the

Formatted: Font: Not Italic

1195 contrary, the fine mode AOT has a slight low bias, which may be an indication of insufficient DMS
1196 emission or too much removal.

1197 Several sites are affected by similar aerosol sources at different distances, allowing us to
1198 examine transport phenomena using these sites. Banizoumbou, which is located deep in the Sahara, has
1199 the largest bias (negative) and RMSE, and the lowest r^2 for the coarse and total AOT modes among all
1200 the African-dust-impacted sites. Capo Verde, located on an island off the west coast of North Africa, has
1201 high coarse mode AOT, but with much smaller bias and RMSE and high correlation (r^2 is ~ 0.88 for
1202 DJFMAM and ~ 0.77 for JJASON for both total and coarse AOTs), benefiting from AOT assimilation.
1203 Farther downwind of north Africa and across the Atlantic Ocean, Ragged Point in Barbados, shows even
1204 smaller biases and RMSEs and very high correlation (r^2 greater than 0.81 for total AOT in both season,
1205 and for coarse AOT in JJASON). Palma de Mallorca, which is a receptor site for Saharan dust transported
1206 across the Mediterranean Sea, has bias, RMSE and correlation similar to Ragged Point.

Formatted: Font: Not Italic

Formatted: Font: Not Italic

1207 The performance of the reanalysis has a tendency to increase with the distance from the source
1208 region, especially over water. The main reasons for this are 1) aerosol models normally have larger
1209 uncertainties in aerosol sources than aerosol transports (Kinne et al., 2003), 2) there is limited satellite
1210 AOT data over the bright desert regions for the model to assimilate (Fig. 2), while there are a lot more
1211 opportunities for the model AOT to be corrected by assimilation along dust transport paths, and 3) the
1212 atmosphere acts to smooth out near-source variability that is often at finer scales than the effective
1213 resolution of the model. These effects can also be seen when comparing the reanalysis performance
1214 over Beijing and Baengyeong, an island site in South Korea downwind of Beijing, for both fine and
1215 coarse mode AOTs.

1216 3.3 AOT trend

1217 There is debate over the use of AOT reanalyses to document and understand climatic trends,
1218 similar to the debate associated with meteorological reanalysis. However, the decadal trends derived
1219 from the reanalysis are largely in line with other studies using stand-alone satellite products (Zhang and
1220 Reid, 2010; Hsu et al., 2012) for a similar time period. This helps to evaluate the reanalysis from another
1221 perspective. Figure 13 shows the trend of the deseasonalized total AOT over the whole reanalysis period
1222 (2003-2013), using the same calculation method as in Zhang and Reid (2010), where the significance of
1223 the trend analysis is estimated following the method of Weatherhead et al. (1998). Many areas show
1224 trends consistent with the satellite-only results of Zhang and Reid (2010) and Hsu et al. (2012): Indian
1225 Bay of Bengal, Arabian Peninsula and Arabian Sea, Bohai Sea in East Asia and the downwind region of
1226 South African biomass burning area, which have a positive trend, and the east coast of North America,
1227 Europe, central South America biomass burning area and Southern Indian Ocean, which have a negative
1228 trend. The reanalysis also exhibits a weak negative trend off the coast of dusty West Africa that is
1229 similar to other studies, though not statistically significant. The non-trend (zero trend) region with
1230 statistical significance in the south subtropical Pacific Ocean is also consistent with other studies.

1231 An arguable trend appears in the Maritime Continent, where Zhang and Reid (2010) report a
1232 non-significant positive trend while Hsu et al. (2012) and our reanalysis here report a non-significant or
1233 significant negative trend based on slightly different study periods (Study periods are 2000-2010, 1998-
1234 2010, and 2003-2013 in Zhang and Reid, Hsu et al. and this paper, respectively). Because 1997-1998 was
1235 a strong El Nino period and 2010-2012 are La Nina years, corresponding to strong and weak fire
1236 activities in the Maritime Continent, respectively, trends for these different periods can be expected to
1237 differ systematically. Studies show that the climate and the associated fire/smoke activity in the
1238 Maritime Continent are controlled by ENSO on the inter-annual time scale (e.g., Reid et al., 2012; van
1239 der Werf et al., 2004). The Maritime Continent is anomalously dry during El Nino years and experiences
1240 more fire activity and thus smoke aerosols compared to La Nina years, and there is a good correlation

1241 between ENSO and AOT there (e.g., Hsu et al., 2012; Xian et al, 2013). The different AOT trends over the
1242 maritime continents obtained with the use of slightly different time periods suggest the importance of
1243 checking the possible controlling climate variability on aerosol trend analysis depending on the time
1244 scales of interest. Similarly, the negative AOT trend in north Africa and off the coast of West Africa is
1245 likely impacted by the Atlantic Multidecadal Oscillation (AMO), North Atlantic Oscillation (NAO) and
1246 ENSO activities as Saharan dust is also shown to be correlated with these climate variabilities (Evan et
1247 al., 2006; Hsu et al. 2012; Wang et al., 2012).

1248 This reanalysis uses non-trending source functions for sulfate, DMS, organic aerosol emissions
1249 and dust erodibility. It is worth noting that even with static source functions and no volcanic source, the
1250 data assimilation has successfully picked up the positive trend downwind of the Hawaiian Islands due to
1251 the enhanced degassing activity of the Kilauea volcano since 2008 (e.g. Beirle et al., 2014). In a parallel
1252 model run, where AOT data assimilation is turned off, trends disappear over the east coast of North
1253 America and Europe or change sign over the Bay of Bengal while retaining their signs in most other
1254 regions (not shown). This indicates that AOT trends over the eastern US, Europe and Bay of Bengal are
1255 related to anthropogenic emission changes. Opposite to the trend shown in the DA run, West African
1256 and the downwind subtropical Atlantic region show a strong positive trend in the natural run. There
1257 could be many possible reasons, such as an artifact of stronger surface wind in the meteorological
1258 model over the study period, or changes in vegetation which are not captured in the meteorological
1259 model or the dust source function.

1260 The positive trend over the Southern African biomass burning area and its downwind
1261 subtropical Atlantic region and the negative trend over central South America biomass burning region
1262 are by and large a result of increasing fire emissions over Southern Africa and decreasing fire emissions
1263 over South America exhibited in FLAMBE (not shown). The smoke emission trends in the above regions

1264 are consistent with the trends found with other satellite fire detection products for the same time
1265 period (Giglio et al., 2013). Trends over other regions are most likely relevant to climate variability or
1266 changes in climate, especially changes in meteorological variables that covary with aerosol processes.
1267 For example, the aforementioned negative trend over the Maritime Continent is very likely closely
1268 related to ENSO cycles. In another example, the decreasing dust trend in the North Africa dust outflow
1269 region of the tropical Atlantic is shown to be caused mainly by a reduction in surface winds over dust
1270 source regions rather than changes in land surface properties in modeling studies (Chin et al., 2014;
1271 Ridley et al., 2014).

1272 The Arabian Peninsula experiences increasing AOT, which may result from the observed
1273 decreasing precipitation for the similar time period (Almazroui et. al., 2012). The negative AOT trend
1274 over the Southern Indian Ocean is consistent with the trend analysis using MISR AOT data (Murphy,
1275 2013). However, this trend in our analysis results solely from trends in the source and sink function,
1276 because AOT is not assimilated in this region in our system. The decreasing trend in the southern Indian
1277 Ocean AOT in the model is mainly caused by a decreasing trend in the surface winds in the
1278 meteorological model, NOGAPS (not shown). Observational studies, however, have found that wind
1279 speed over the southern oceans has increased in the past two decades (Young et al., 2011; Hande et al.,
1280 2012). The question of why the surface wind in NOGAPS decreases and AOT decreases in the southern
1281 oceans during the 2003-2013 time period requires additional investigation but beyond the scope of this
1282 study.

1283 Figure 14 shows the monthly mean NAAPS reanalysis and AERONET L2 modal AOT at six AERONET
1284 sites chosen for their relatively long-term record under different aerosol regimes: Alta Floresta in the
1285 Amazon, dominated by biomass burning smoke during the burning season; Beijing in East Asia,
1286 dominated by anthropogenic fine mode aerosols year round with mixed dust and pollutions in the spring

1287 time; Capo Verde off the west coast of North Africa, dominated by Sahara/Sahel dust, GSFC in east
1288 CONUS, dominated by anthropogenic fine mode aerosols, Solar Village in the Arabian Peninsula,
1289 dominated by dust, and Venice in Italy, dominated by pollution-related fine mode aerosols and
1290 influenced by Saharan dust in spring time. Also shown are linear regression lines based on the total
1291 AOTs, indicative of AOT trends. Annotations in each time series show bias, RMSE and r^2 of the total AOT
1292 and the dominant modal AOT, calculated with reanalysis monthly averages (unpaired). Statistics from a
1293 paired comparison using reanalysis data sampled to match available AERONET data are shown in
1294 parentheses.

Formatted: Font: Not Italic

1295 Overall, the reanalysis follows the seasonal and interannual variability in AERONET data for the
1296 total AOT quite well, and to a lesser extent for the coarse and fine mode AOTs. The pairwise comparison
1297 shows better correlation with AERONET than that calculated with all data, and, generally smaller
1298 absolute bias and RMSE. The decreasing trends over Alta Floresta, GSFC and Venice, the increasing trend
1299 over Beijing (slight) and Solar Village, and the insignificant trend over Capo Verde are consistent with the
1300 regional trends shown in Fig. 13, and qualitatively agree with AERONET. Over GSFC, the reanalysis
1301 captures the evident decrease in total and fine mode AOT since 2008. The June-July-August average AOT
1302 drops about 0.14 (from 0.37 to 0.23) for the total AOT and 0.12 (from 0.29 to 0.17) for the fine mode
1303 AOT comparing the years before and after 2008. It drops about 0.09 (from 0.31 to 0.22) for the total
1304 AOT and 0.08 (from 0.27 to 0.19) for the fine mode AOT in the reanalysis, with a low bias in total AOT
1305 and a minimal bias in fine mode AOT for the season.

1306 **4 Summary and discussion**

1307 This paper describes a near 11-year global 550nm modal AOT reanalysis product developed at the
1308 Naval Research Laboratory, with a spatial resolution of 1x1 degree and a temporal resolution of 6 hours.
1309 The reanalysis uses the Navy Aerosol Analysis and Prediction System (NAAPS) with regionally-tuned

1310 source functions at its core and assimilates quality-controlled Terra and Aqua Collection 5 Moderate
1311 Resolution Imaging Spectroradiometer (MODIS) and Multi-angle Imaging SpectroRadiometer (MISR)
1312 AOT. Aerosol wet deposition in the tropics is constrained with satellite retrieved precipitation. Dry
1313 deposition parameters over ocean are also adjusted by minimizing AOT corrections in AOT assimilation.
1314 By validating the reanalysis fine and coarse mode AOTs and total AOT with Aerosol Robotic Network
1315 (AERONET) Level-2 product, we report the following findings:

1316 *4.1 Global representation:* Compared with 6-hr-average AERONET data, global mean RSME values for
1317 both fine and coarse mode AOTs are around 0.1, and the RMSE for the total AOT is ~ 0.14 . AOT
1318 RMSE decreases 50% when monthly averaging is applied. On a global average, coarse-mode AOT has
1319 a slight negative bias (-0.02) which is partially compensated by a slight positive bias of the fine mode
1320 AOT (0.01). In general, the fine mode AOT matches AERONET slightly better than the coarse mode
1321 AOT, reflected in the bias, RMSE and correlation. These numbers vary among different regions
1322 presumably because of regionally specific aerosol features.

1323 Since total AOT is being assimilated, the total AOT has a smaller uncertainty relative to the
1324 coarse and fine mode AOT. Currently, there is no way to validate speciated AOTs if two or more
1325 aerosol species are present in the same size mode. We would expect the relative uncertainty of the
1326 speciated AOTs to be larger than the modal AOTs. The data quality of satellite-retrieved AOT is
1327 generally better over water than over land because of the relatively simple surface optical
1328 properties of water (e.g., Levy et al., 2005, Remer et al., 2005). Under the same AOT data
1329 assimilation frequency (or same amount of data to be assimilated), the reanalysis performs
1330 relatively better over oceanic and coastal regions/sites than land regions/sites.

1331 *4.2 Regional representation:* The reanalysis captures the regional and seasonal AOT variations skillfully.
1332 The range of the regional reanalysis AOT values are generally smaller than those of AERONET (i.e.,
1333 high bias for small AOTs and low bias for high AOTs), which is commonly seen among aerosol

1334 models, especially with coarse spatial and temporal resolution (e.g., Kinne et al., 2006; Sessions et.
1335 al., 2015). Challenging regions for the reanalysis are East Asia, Indian subcontinent and Sahel, where
1336 there are often mixed fine and coarse mode aerosols. The reanalysis generally performs better in
1337 the long-range transport regions than the source regions. For example, the reanalysis AOT of the
1338 Caribbean islands sites, which are the receptor sites of African dust, matches AERONET observations
1339 better than the land sites within the African continent. A field campaign analysis of remotely
1340 transported smoke aerosols from Borneo and Sumatra islands found good agreement between the
1341 reanalysis AOT and the smoke concentrations therein and in-situ measurements taken in the open
1342 ocean west of the Philippines (Reid, et al., 2014).

1343 *4.3 Trends:* The trends calculated from the reanalysis are similar to other studies using standalone
1344 satellite products (Zhang and Reid, 2010; Hsu et al., 2012) in both aerosol transport regions and
1345 source regions. Over regionally representative sites, the reanalysis trend in modal AOT also agrees
1346 qualitatively well with the trend in AERONET data. This provides a reassurance of the quality of the
1347 reanalysis product. It is also worth noting that without trending source functions for sulfate and
1348 organic aerosols precursors, the data assimilation system has successfully reproduced regional AOT
1349 trends that are related to emission changes in the past decade. For example, a positive trend over
1350 India is attributed to emission growth. Signals of other low-frequency climate variability are also
1351 discernable in the reanalysis AOT. For example, using an earlier version of the NAAPS AOT analysis,
1352 the modulation effect of the Madden-Julian Oscillation on smoke AOT over the Maritime Continent
1353 is found (Reid, et al., 2012).

1354 *4.4 Role of AOT data assimilation:* Overall, the data assimilation system is very effective in correcting
1355 the modeled AOT and bringing it as close as possible to the satellite observations, and spreading the
1356 information to the neighboring grid cells through a correlation length scale. In the time steps
1357 following assimilation, the information is further propagated downstream. The data assimilation

1358 system plays an indispensable role in picking up AOT trends in the regions affected by emission
1359 changes that are not represented in the model. However, the data assimilation system, associated
1360 with the assimilatable data, also has limitations. **Satellite AOT retrievals characterize the optical**
1361 **properties of a column, and it does not carry any information about aerosol vertical profiles or**
1362 **speciation. So the total AOT is constrained through AOT data assimilation. The relative vertical**
1363 **profile in 3-D extinction and speciation of the aerosols are uniformly varied to match the posterior**
1364 **AOT.** The geographical coverage of the MODIS+MISR data to be assimilated can cover only up to
1365 about a quarter of the Earth in one data assimilation cycle (Fig. 1). AOT of one area can be updated
1366 by the data assimilation system only once per day on average (at most twice per day) and only
1367 during the local daytime. This affects the aerosol diurnal cycle in the reanalysis, as all the nighttime
1368 AOT are purely driven by the natural model while daytime AOT can be controlled by the data
1369 assimilation system. Repetitively adding or shedding aerosol mass and thus AOT in one area through
1370 data assimilation can make the AOT evolution unphysical. Because AERONET measurements occur
1371 during the local daytime, the validation results here may not represent the reanalysis skill for other
1372 times of day.

1373 *4.5 Data consistency in time:* Even though the data assimilation system has the capability of capturing
1374 the trend observed in stand-alone satellite or AERONET AOT analyses, the inconsistency in the
1375 meteorological analysis of Navy Operational Global Atmospheric Prediction System (NOGAPS) in the
1376 past decade poses a big challenge in the development of a long term global AOT reanalysis product.
1377 NOGAPS experienced several upgrades in the reanalysis period, including improved land surface
1378 parameterization, which impacts dust production trends.

1379 A meteorological reanalysis is intended to provide a more consistent atmospheric state for
1380 aerosol simulations. But meteorological reanalyses have a data consistency issue as well, because
1381 observations being assimilated change significantly with time (e.g., Dee et al., 2011). For example,

1382 with the ever-increasing satellite observations of the past two decades, more and more satellite
1383 data are being assimilated for one or more meteorological variables. With the demise or periodic
1384 malfunction of some satellite instruments, some data became unavailable. This impacts the final
1385 meteorological reanalysis, and consequently the AOT reanalysis. The NOAA Climate Prediction
1386 Center MORPHing (CMORPH) precipitation data, which is used to replace NOGAPS precipitation in
1387 the Tropics, is only available after December 2002. Its usage can impact regional AOT significantly in
1388 a natural model run (Xian et al., 2009). For areas not covered by the CMORPH product, any model
1389 precipitation performance change in time can be a potential issue for AOT trend analysis.

1390 *4.6 Recommendations for application*

- 1391 a) It is ideal for quick and consistent identification of large aerosol events globally or regionally. It
1392 can serve as a reference and provide the general background aerosol information without
1393 temporal or spatial discontinuity for field campaign analysis.
- 1394 b) The reanalysis AOT can be used to provide global and regional AOT climatologies for climate and
1395 applied science applications.
- 1396 c) The reanalysis AOT can be used in different scale analysis, from daily to inter-annual. The diurnal
1397 AOT analysis should be performed with caution considering the possible artifact feature
1398 introduced by the AOT assimilation cycle.

1399 Our future direction for the NAAPS aerosol reanalysis will be focused on 3-D extinction and mass
1400 concentration of single aerosol species, with special emphasis on the vertical dimension. The ability of
1401 NAAPS assimilating the Cloud-Aerosol Lidar with Orthogonal Polarization (CALIOP) lidar backscatter
1402 coefficient data (Campbell et al., 2010; Zhang et al., 2011, 2014) will aid in this effort.

1403

1404 **Code and data availability:**

1405 The NAAPS model code is a property of the U.S. Naval Research Laboratory and is not available to the
1406 public. However, the NAAPS reanalysis data is available at [http://usgodae.org/cgi-](http://usgodae.org/cgi-bin/datalist.pl?dset=nrl_naaps_reanalysis&summary=Go)
1407 [bin/datalist.pl?dset=nrl_naaps_reanalysis&summary=Go](http://usgodae.org/cgi-bin/datalist.pl?dset=nrl_naaps_reanalysis&summary=Go) . The data on this server are updated as model
1408 improvements are made and reruns are completed.
1409

1410 **Acknowledgement:**

1411 The development of the NAAPS reanalysis was an outcome of the needs of multiple projects, and largely
1412 supported by the Office of Naval Research Code 322 and the NASA Interdisciplinary Science Program.
1413 Additional support was provided by the NRL Base Program and the Office of Naval Research 35. The
1414 development team is grateful to the effort of the operational NASA-MODIS and MISR aerosol teams for
1415 the development and implementation of their level two products. We are likewise grateful to the NASA
1416 land team for the development of their fire products. The NASA Aerosol Robotic Network (AERONET)
1417 data is key to verifying models such as the NAAPS reanalysis and the use of this federated network's
1418 data is gratefully acknowledged.

1419 **References:**

- Ahmadov R., McKeen S.A., Robinson A.L., Bahreini R., Middlebrook A., deGouw J., Meagher J., Hsie E.-Y., Edgerton E., Shaw S., Trainer M.: A volatility basis set model for summertime secondary organic aerosols over the eastern U.S. in 2006. *J. Geophys. Res.*, 117, D06301, doi:10.1029/2011JD016831, 2012.
- Almazroui, M., Nazrul Islam, M., Athar, H., Jones, P. D. and Rahman, M. A.: Recent climate change in the Arabian Peninsula: annual rainfall and temperature analysis of Saudi Arabia for 1978–2009. *Int. J. Climatol.*, 32, 953–966, 2012.
- Antoine, D., and Nobileau, D.: Recent increase of Saharan dust transport over the Mediterranean Sea, as revealed from ocean color satellite (SeaWiFS) observations, *J. Geophys. Res.*, 111, D12214, doi:10.1029/2005JD006795, 2006.
- [Bathe, K.J.](#) : Finite Element Procedures. Cambridge, MA: Klaus-Jürgen Bathe. [ISBN 097900490X](#), 2006.
- Beirle, S., Hörmann, C., Penning de Vries, M., Dörner, S., Kern, C., and Wagner, T.: Estimating the volcanic emission rate and atmospheric lifetime of SO₂ from space: a case study for Kīlauea volcano, Hawai'i, *Atmos. Chem. Phys.*, 14, 8309-8322, 2014.
- Benedetti, A., Morcrette, J.-J., Boucher, O., Dethof, A., Engelen, R. J., Fisher, M., Flentje, H., Huneeus, N., Jones, L., Kaiser, J. W., Kinne, S., Mangold, A., Razinger, M., Simmons, A. J., and Suttie, M.: Aerosol analysis and recast in the European centre for Medium-Range Weather Forecasts Integrated Forecast System: 2. Data assimilation, *J. Geophys. Res.*, 114, D13205, doi:10.1029/2008JD011115, 2009.
- Benkovitz, C. M., T. Scholtz, L. Pacyna, L. Tarrson, J. Dignon, E. Voldner, P. A. Spiro, and T. E. Graedel : Global gridded inventories of anthropogenic emissions of sulphur and nitrogen. *J. Geophys. Res.*, 101, 29239-29253, 1996.
- Bond, T. C., D. G. Streets, K. F. Yarber, S. M. Nelson, J.-H. Woo, and Z. Klimont, A technology-based global inventory of black and organic carbon emissions from combustion, *J. Geophys. Res.*, 109, D14203, doi:10.1029/2003JD003697, 2004.
- Bond, T. C., et al.: Bounding the role of black carbon in the climate system: A scientific assessment, *J. Geophys. Res. Atmos.*, 118, 5380–5552, 2013.

- Buchard, V., da Silva, A. M., Colarco, P. R., Darmenov, A., Randles, C. A., Govindaraju, R., Torres, O., Campbell, J., and Spurr, R.: Using the OMI aerosol index and absorption aerosol optical depth to evaluate the NASA MERRA Aerosol Reanalysis, *Atmos. Chem. Phys.*, 15, 5743-5760, 2015.
- Campbell, J. R., J. S. Reid, D. L. Westphal, J. Zhang, E. J. Hyer, and E. J. Welton: CALIOP aerosol subset processing for global aerosol transport model data assimilation, *J of Sel. Topics in Appl. Earth Obs. and Rem. Sens.*, 3, 203-214, 2010.
- Campbell, J. R., Reid, J. S., Westphal, D. L., Zhang, J., Tackett, L., Chew B. N., Welton, E. J., Shimizu, A., Sugimoto, N., Aoki, K., Winker, D. M., Characterizing the vertical profile of aerosol particle extinction and linear depolarization over Southeast Asia and the Maritime Continent: The 2007–2009 view from CALIOP, *Atmos. Res.*, 122, 520-543, 2013.
- Chew, B. N., J. R. Campbell, J. S. Reid, D. M. Giles, E. J. Welton, S. V. Salinas and S. C. Liew: Tropical cirrus cloud contamination in sun photometer data, *Atmos. Environ.*, 45, 6724-6731, 2011.
- Chin, M., Diehl T, Tan Q, Prospero J, Kahn R, Remer L, Yu H, Sayer A, Bian H, Geogdzhayev I, Holben B, Howell S, Huebert B, Hsu N, Kim D, Kucsera T, Levy R, Mishchenko M, Pan X, Quinn P, Schuster G, Streets D, Strode S, Torres O, Zhao X.: Multi-decadal aerosol variations from 1980 to 2009: a perspective from observations and a global model. *Atmos. Chem. Phys.* 14, 3657-3690, 2014.
- Christensen, J. H. :The Danish eulerian hemispheric model—A three dimensional air pollution model used for the Arctic, *Atmos. Environ.*, 31, 4169-4191, 1997.
- Colarco, P., A. da Silva, M. Chin, and T. Diehl: Online simulations of global aerosol distributions in the NASA GEOS-4 model and comparisons to satellite and ground-based aerosol optical depth, *J. Geophys. Res.*, 115, D14207, doi:10.1029/2009JD012820, 2010.
- Collins, W. D., P. J. Rasch, B. E. Eaton, B. V. Khattatov, J.-F. Lamarque, and C. S. Zender: Simulating aerosols using a chemical transport model with assimilation of satellite aerosol retrievals: Methodology for INDOEX, *J. Geophys. Res.*, 106, 7313–7336, 2001.
- Dai, A.: Precipitation characteristics in eighteen coupled climate models, *J. Climate*, 19, 4605-4630, 2006.
- Daley, R. and Barker, E.: NAVDAS: Formulation and diagnostics, *Mon. Weather Rev.*, 129, 869-883, 2001.
- Dee, D. P., Uppala, S. M., Simmons, A. J., Berrisford, P., Poli, P., Kobayashi, S., Andrae, U., Balmaseda, M. A., Balsamo, G., Bauer, P., Bechtold, P., Beljaars, A. C. M., van de Berg, L., Bidlot, J., Bormann, N., Delsol, C., Dragani, R., Fuentes, M., Geer, A. J., Haimberger, L., Healy, S. B., Hersbach, H., Hólm, E. V., Isaksen, I., Kållberg, P., Köhler, M., Matricardi, M., McNally, A. P., Monge-Sanz, B. M., Morcrette, J.-J., Park, B.-K., Peubey, C., de Rosnay, P., Tavolato, C., Thépaut, J.-N. and Vitart, F. : The ERA-Interim reanalysis: configuration and performance of the data assimilation system. *Q.J.R. Meteorol. Soc.*, 137, 553–597, 2011.
- Diehl, T., Heil, A., Chin, M., Pan, X., Streets, D., Schultz, M., and Kinne, S.: Anthropogenic, biomass burning, and volcanic emissions of black carbon, organic carbon, and SO₂ from 1980 to 2010 for hindcast model experiments, *Atmos. Chem. Phys. Disc.* 12 : 24895-24954, 2012.
- Donahue, N. M., A. L. Robinson, C. O. Stanier, and S. N. Pandis: Coupled partitioning, dilution, and chemical aging of semivolatile organics. *Environ. Sci. Technol.* 40, 2635 – 2643, 2006.
- Dubovik, O., Holben, B., Eck, T. F., Smirnov, A., Kaufman, Y. J., King, M. D., Tanré, D. and Slutsker, I.: Variability of Absorption and Optical Properties of Key Aerosol Types Observed in Worldwide Locations. *J. Atmos. Sci.*, 59, 590–608, 2002.
- Evan, A. T., A. K. Heidinger, and P. Knippertz: Analysis of winter dust activity off the coast of West Africa using a new 24-year over-water advanced very high resolution radiometer satellite dust climatology, *J. Geophys. Res.*, 111, D12210, doi:10.1029/2005JD006336, 2006.
- Fromm, M. D., and R. Servranckx: Transport of forest fire smoke above the tropopause by supercell

- convection, *Geophys. Res. Lett.*, 30(10), 1542, doi:10.1029/2002GL016820, 2003.
- Giglio, L., J. T. Randerson, and G. R. van der Werf: Analysis of daily, monthly, and annual burned area using the fourth-generation global fire emissions database (GFED4), *J. Geophys. Res. Biogeosci.*, 118, doi:10.1002/jgrg.20042, 2013.
- Ginoux, Paul, M Chin, I Tegen, J M Prospero, B Holben, O Dubovik, and Shian-Jiann Lin: Sources and distributions of dust aerosols simulated with the GOCART model. *J. Geophys. Res.*, 106(D17), 20255-20273, 2001.
- Gordon, H. R. : Atmospheric correction of ocean color imagery in the Earth Observing System era, *J. Geophys. Res.*, 102(D14), 17081–17106, 1997.
- Granier, Claire et al., Evolution of anthropogenic and biomass burning emissions of air pollutants at global and regional scales during the 1980–2010 period, *Climate Change* 109 (1-2): 163-190, 2011.
- Hande, L. B., S. T. Siems, and M. J. Manton: Observed Trends in Wind Speed over the Southern Ocean, *Geophys. Res. Lett.*, 39, L11802, doi:10.1029/2012GL051734, 2012.
- Hanel, G.: The properties of atmospheric aerosol particles as functions of relative humidity at thermodynamic equilibrium with surrounding moist air, *Geophys. Res. Lett.*, 19, 73-188., 1976.
- Heald, C. L., D. J. Jacob, P. I. Palmer, M. J. Evans, G. W. Sachse, H. B. Singh, and D. R. Blake, Biomass burning emission inventory with daily resolution: Application to aircraft observations of Asian outflow, *J. Geophys. Res.*, 108(D21), 8811, doi:10.1029/2002JD003082, 2003.
- Hegg, D. A., D. S. Covert, K. Crahan, and H. H. Jonsson, The dependence of aerosol light-scattering on RH over the Pacific Ocean, *Geophys. Res. Lett.*, 29(8), doi:10.1029/2001GL014495, 2002.
- Hertel, O., Christensen, J., Runge, E., Asman, W. A. H., Berkowicz, R., Hovmand, M. and Hov, O.: Development and testing of a new variable scale air pollution model-ACDEP. *Atmos. Env.*, 29, 1267-1290, 1995.
- Hess, M., P. Koepke, P., and Schult, I.: Optical Properties of Aerosols and Clouds: The Software Package OPAC. *Bull. Amer. Meteor. Soc.*, 79, 831–844, 1998.
- Hoffmann, M. R. and Calvert, J. G.: Chemical Transformation Modules for Eulerian Acid Deposition Models: Volume II, the Aqueous-phase Chemistry, U.S. Environmental Protection Agency, Research Triangle Park, NC. 1985.
- Hogan, T. F. and L. Brody: Sensitivity Studies of the Navy's Global Forecast Model Parameterizations and Evaluation of Improvements to NOGAPS. *Mon. Wea. Rev.*, 121, 2373-2395, 1993.
- Hogan, T. F., Liu, M., Ridout, J. S., Peng, M. S., Whitcomb, T. R., Ruston, B. C., Reynolds, C. A., Eckermann S. D., Moskaitis, J. R., Baker, N. L., McCormack, J. P., Viner, K. C., McLay, J. G., Flatau, M. K., Xu, L., Chen, C., and Chang, S. W.,: The Navy Global Environmental Model. *Oceanography, Special Issue on Navy Operational Models*, 27, No. 3. 2014.
- Hogan, T.F. and T.E. Rosmond: The description of the Navy Operational Global Atmospheric Prediction System's spectral forecast model. *Mon. Wea. Rev.*, 119, 1786-1815, 1991.
- Holben, B. N., Eck, T. F., Slutsker, I., Tanre, D., Buis, J. P., Setzer, A., Vermote, E., Reagan, J. A., Kaufman, Y. J., Nakajima, T., Lavenu, F., Jankowiak, I., and Smirnov, A.: AERONET - A federated instrument network and data archive for aerosol characterization, *Remote Sens. Environ.*, 66, 1-16, 1998.
- Holben, B. N., Tanré, D., Smirnov, A., Eck, T. F., Slutsker, I., Abuhassan, N., Newcomb, W. W., Schafer, J. S., Chatenet, B., Lavenu, F., Kaufman, Y. J., Castle, J. V., Setzer, A., Markham, B., Clark, D., Frouin, R., Halthore, R., Karneli, A., O'Neill, N. T., Pietras, C., Pinker, R. T., Voss, K., and Zibordi, G.: An emerging ground-based aerosol climatology: Aerosol optical depth from AERONET, *J. Geophys. Res.-Atmos.*, 106, 12067-12097, 2001.
- Houweling, S., W. Hartmann, I. Aben, H. Schrijver, J. Skidmore, G.-J. Roelofs, and F.-M. Breon: Evidence of systematic errors in SCIAMACHY-observed CO₂ due to aerosols, *Atmos. Chem. Phys.*, 5, 3003–3013, 2005.
- Hsu, N. C., Gautam R, Sayer A, Bettenhausen C, Li C, Jeong M, Tsay S, Holben B. Global and regional

- trends of aerosol optical depth over land and ocean using SeaWiFS measurements from 1997 to 2010. *Atmos. Chem. Phys.* 12, 8037-8053, 2012.
- Hsu, N. C., Tsay, S.-C., King, M. D., and Herman, J. R.: Aerosol properties over bright-reflecting source regions, *IEEE T. Geosci. Remote Sens.*, 42, 557–569, 2004.
- Huang, J., N. C. Hsu, S.-C. Tsay, M.-J. Jeong, B. N. Holben, T. A. Berkoff, and E. J. Welton: Susceptibility of aerosol optical thickness retrievals to thin cirrus contamination during the BASE-ASIA campaign, *J. Geophys. Res.*, 116, D08214, doi:10.1029/2010JD014910, 2011.
- Hyer, E. J., Reid, J. S., Prins, E. M., Hoffman, J. P., Schmidt, C. C., Miettinen, J. I., Giglio L., Patterns of fire activity over Indonesia and Malaysia from polar and geostationary satellite observations, *Atmos. Res.*, 122, 504-519, 2013
- Hyer, E. J., Reid, J. S., and Zhang, J.: An over-land aerosol optical depth data set for data assimilation by filtering, correction, and aggregation of MODIS Collection 5 optical depth retrievals, *Atmos. Meas. Tech.*, 4, 379–408, 2011.
- Inness, A., Baier, F., Benedetti, A., Bouarar, I., Chabrillat, S., Clark, H., Clerbaux, C., Coheur, P., Engelen, R. J., Errera, Q., Flemming, J., George, M., Granier, C., Hadji-Lazaro, J., Huijnen, V., Hurtmans, D., Jones, L., Kaiser, J. W., Kapsomenakis, J., Lefever, K., Leitão, J., Razinger, M., Richter, A., Schultz, M. G., Simmons, A. J., Suttie, M., Stein, O., Thépaut, J.-N., Thouret, V., Vrekoussis, M., Zerefos, C., and the MACC team: The MACC reanalysis: an 8 yr data set of atmospheric composition, *Atmos. Chem. Phys.*, 13, 4073-4109, 2013.
- IPCC: Climate Change 2007: The Physical Science Basis. Contribution of Working Group I to the Fourth Assessment Report of the Intergovernmental Panel on Climate Change [Solomon, S., D. Qin, M. Manning, Z. Chen, M. Marquis, K.B. Averyt, M.Tignor and H.L. Miller (eds.)]. Cambridge University Press, Cambridge, United Kingdom and New York, NY, USA, 2007.
- IPCC: Climate Change 2013: The Physical Science Basis. Contribution of Working Group I to the Fifth Assessment Report of the Intergovernmental Panel on Climate Change [Stocker, T.F., D. Qin, G.-K. Plattner, M. Tignor, S.K. Allen, J. Boschung, A. Nauels, Y. Xia, V. Bex and P.M. Midgley (eds.)]. Cambridge University Press, Cambridge, United Kingdom and New York, NY, USA, 2013.
- Iversen, T.: Numerical modeling of the long range atmospheric transport of sulphur dioxide and particulate sulphate to the arctic, *Atmos. Environ.*, 23, 2571–2595, 1989.
- Janowiak, J.E., Kousky, V.E., Joyce, R.J.: Diurnal cycle of precipitation determined from the CMORPH high spatial and temporal resolution global precipitation analyses. *J. Geophys. Res.* 110, D23105, 2005.
- Jeong, J. I., Park, R., Woo, J.-H., Han Y.-J. and Yi, S.-M.: Source contributions to carbonaceous aerosol concentrations in Korea. *Atmos. Environ.*, 45, 1116-1125, 2011.
- Jimenez, J. L. et al.: Evolution of organic aerosols in the atmosphere. *Science*, 326, 1525-1529, 2009.
- Joyce, R.J., Janowiak, J.E., Arkin, P.A., Xie, P.: CMORPH: a method that produces global precipitation estimates from passivemicrowave and infrared data at high spatial and temporal resolution. *J. Hydromet.* 5, 487–503, 2004.
- Kahn, R. A., B. J. Gaitley, M. J. Garay, D. J. Diner, T. F. Eck, A. Smirnov, and B. N. Holben: Multiangle Imaging Spectroradiometer global aerosol product assessment by comparison with the Aerosol Robotic Network, *J. Geophys. Res.*, 115, D23209, doi:10.1029/2010JD014601, 2010.
- Kahn, R. A., Nelson, D. L., Garay, M., Levy, R. C., Bull, M. A., Diner, D. J., Martonchik, J. V., Paradise, S. R., and Hansen, E. G., and Remer, L. A.: MISR Aerosol product attributes, and statistical comparisons with MODIS. *IEEE Trans. Geosci. Remt. Sens*, 47, 4095–4114, 2009.
- Kahn, R. A., Y. Chen, D. L. Nelson, F.-Y. Leung, Q. Li, D. J. Diner, and J. A. Logan: Wildfire smoke injection heights: Two perspectives from space, *Geophys. Res. Lett.*, 35, L04809, doi:10.1029/2007GL032165. 2008.
- Kaku, K. C., J. S. Reid, N. T. O'Neill, P. K. Quinn, D. J. Coffman, and T. F. Eck: Verification and application of the extended spectral deconvolution algorithm (SDA+) methodology to estimate aerosol fine and

- coarse mode extinction coefficients in the marine boundary layer, *Atmos. Meas. Tech.*, 7, 3399-3412, 2014.
- Kalnay, E., M. Kanamitsu, R. Kistler, W. Collins, D. Deaven, L. Gandin, M. Iredell, S. Saha, G. White, J. Woollen, Y. Zhu, A. Leetmaa, R. Reynolds, M. Chelliah, W. Ebisuzaki, W. Higgins, J. Janowiak, K. C. Mo, C. Ropelewski, J. Wang, R. Jenne, D. Joseph: The NCEP/NCAR 40-year reanalysis project, *Bull. Amer. Meteor. Soc.*, 77, 437-470, 1996.
- Kappos, A. D., Brickmann, P., Elkmann, T., et al.: Health effects of particles in the ambient air, *Int. J. of Hygiene and Environ. Health*, 207, 399-407, 2004.
- Kinne, S., et al.: An AeroCom initial assessment -- optical properties in aerosol component modules of global models. *Atmos. Chem. Phys.* 6, 1815-1834, 2006.
- Kinne, S., et al., Monthly averages of aerosol properties: A global comparison among models, satellite data, and AERONET ground data, *J. Geophys. Res.*, 108(D20), 4634, doi:10.1029/2001JD001253, 2003.
- Laden, F., Neas, L. M., Dockery, D. W., and Schwartz, J.: Association of fine particulate matter from different sources with daily mortality in six US cities, *Environ. Health Perspectives*, 108, 941-947, 2000.
- Lana, A., et al.: An updated climatology of surface dimethylsulfide concentrations and emission fluxes in the global ocean, *Global Biogeochem. Cycles*, 25, GB1004, doi:10.1029/2010GB003850. 2011.
- Levy, R. C., Remer, L. A., Kleidman, R. G., Mattoo, S., Ichoku, C., Kahn, R., and Eck, T. F.: Global evaluation of the Collection 5 MODIS dark-target aerosol products over land, *Atmos. Chem. Phys.*, 10, 10399-10420, 2010.
- Levy, R. C., Remer, L. A., Mattoo, S., Vermote, EF, Kaufman, Y. J.: Second-generation operational algorithm: Retrieval of aerosol properties over land from inversion of Moderate Resolution Imaging Spectroradiometer spectral reflectance. *J. Geophys. Res.-Atmos.* 112, D13211, doi:10.1029/2006JD007811, 2007.
- Levy, R. C., et al.: Evaluation of the MODIS aerosol retrievals over ocean and land during CLAMS, *J. Atmos. Sci.*, 62(4), 974-992, 2005.
- Li-Jones X, H. B. Maring, J. M. Prospero: Effect of relative humidity on light scattering by mineral dust aerosol as measured in the marine boundary layer over the tropical Atlantic Ocean, *J. Geophys. Res.* 103, 31113-31121, 1998.
- Martonchik, J. V., R. A. Kahn, and D. J. Diner, "Retrieval of aerosol properties over land using MISR observations," in *Satellite Aerosol Remote Sensing Over Land*, A. Kokhanovsky, Ed. Berlin, Germany: Springer-Verlag, 2009.
- May, D. A., Stowe, L. L., Hawkins, J. D., McClain, E. P.; A correction for Saharan dust effects on satellite sea-surface temperature-measurements, *J. Geophys. Res.*, 97, 3611-3619, 1992.
- Miettinen, J., E. Hyer, A. S. Chia, L. K. Kwoh, and S. C. Liew: Detection of vegetation fires and burnt areas by remote sensing in insular Southeast Asian conditions: current status of knowledge and future challenges, *Int. J. Remote Sens.*, 34(12), 4344-4366, 2013.
- Miller, R.L., R.V. Cakmur, J.P. Perlwitz, I.V. Geogdzhayev, P. Ginoux, K.E. Kohfeld, D. Koch, C. Prigent, R. Ruedy, G.A. Schmidt, and I. Tegen: Mineral dust aerosols in the NASA Goddard Institute for Space Sciences ModelE atmospheric general circulation model. *J. Geophys. Res.*, 111, D06208, doi:10.1029/2005JD005796, 2006.
- Ming, Y, Russell L. M.: Predicted hygroscopic growth of sea salt aerosol. *J. Geophys. Res.-Atmos.*, 106, 28259-28274, 2001.
- Mishchenko, M. I., Geogdzhayev, I. V., Cairns, B., Rossow, W. B. and Lacis, A. A.: Aerosol retrievals over the ocean using channel 1 and 2 AVHRR data: A sensitivity analysis and preliminary results, *Appl. Opt.*, 38, 7325-7341, doi:10.1364/AO.38.007325, 1999.
- Monahan, E. C., D. E. Spiel, and K. L. Davidson: A model of marine aerosol generation via whitecaps and

- wave disruption, in *Oceanic Whitecaps and Their Role in Air-Sea Exchange Processes*, edited by E.C. Monahan and G. MacNiocaill, 167–174, Springer, New York, 1986.
- Morcrette, J.-J., Boucher, O., Jones, L., Salmond, D., Bechtold, P., Beljaars, A., Benedetti, A., Bonet, A., Kaiser, J. W., Razinger, M., Schulz, M., Serrar, S., Simmons, A. J., Sofiev, M., Suttie, M., Tompkins, A. M., and Untch, A.: Aerosol analysis and forecast in the European Centre for Medium-Range Weather Forecasts Integrated Forecast System: Forward modeling, *J. Geophys. Res.*, 114, D06206, doi:10.1029/2008JD011235, 2009.
- Murphy, D. M.: Little net clear-sky radiative forcing from recent regional redistribution of aerosols, *Nature Geoscience*, 6, 258-262, 2013.
- Obukhov, A.M : Turbulence in an atmosphere with a non-uniform temperature (English Translation). *Boundary-Layer Meteorology* 2: 7–29, 1971.
- Olivier J., J. Peters, C. Granier, G. Petron, J.F. Muller and S. Wallens, Present and future surface emissions of atmospheric compounds , POET report #2, EU project EVK2-1999-00011, 2003.
- O'Neill, N.T., T.F.Eck, B.N.Holben, A.Smirnov, O.Dubovik, and A.Royer: Bimodal size distribution influences on the variation of Angstrom derivatives in spectral and optical depth space, *J. Geophys. Res.*, 106, 9787-9806, 2001.
- O'Neill, N. T., Eck, T. F., Smirnov, A., Holben, B. N., and Thulasiraman S.: Spectral discrimination of coarse and fine mode optical depth. *J. Geophys. Res.*, 108, D05212, doi:10.1029/2002JD002975, 2003.
- Pankow, J. F., An absorption model of gas/particle partitioning of organic compounds in the atmosphere, *Atmos. Environ.*, 28, 189-193, 1994.
- Pérez, C., Haustein, K., Janjic, Z., Jorba, O., Huneus, N., Baldasano, J. M., Black, T., Basart, S., Nickovic, S., Miller, R. L., Perlwitz, J. P., Schulz, M., and Thomson, M.: Atmospheric dust modeling from meso to global scales with the online NMMB/BSC-Dust model – Part 1: Model description, annual simulations and evaluation, *Atmos. Chem. Phys.*, 11, 13001–13027, doi:10.5194/acp-11-13001-2011, 2011.
- Reid, J. S., R. Koppmann, T. Eck, and D. Eleuterio: A review of biomass burning emissions part II: Intensive physical properties of biomass burning particles, *Atmos. Chem. Phys.*, 5, 99–825, 2005a.
- Reid, J. S., T. Eck, S. Christopher, O. Dubovik, R. Koppmann, D. Eleuterio, B. Holben, E. Reid, and J. Zhang: A review of biomass burning emissions part III: Intensive optical properties of biomass burning particles, *Atmos. Chem. Phys.*, 5, 827–849, 2005b.
- Reid, J. S., Hyer, E. J., Prins, E. M., Westphal, D. L., Zhang, J., Wang, J., Christopher, S. A., Curtis, C. A., Schmidt, C. C., Eleuterio, D. P., Richardson, K. A., and Hoffman, J. P.: Global Monitoring and Forecasting of Biomass-Burning Smoke: Description of and Lessons from the Fire Locating and Modeling of Burning Emissions (FLAMBE) Program, *IEEE J. Sel. Top. Appl.*, 2, 144–162, JSTARS-2009-00034, 2009.
- Reid, J. S., N. D. Lagrosas, H. H. Jonsson, E. A. Reid, W. R. Sessions, J. B. Simpas, S. N. Uy, T. J. Boyd, S. A. Atwood, D. R. Blake, J. R. Campbell, S. S. Cliff, B. N. Holben, R. E. Holz, E. J. Hyer, P. Lynch, S. Meinardi, D. J. Posselt, K. A. Richardson, S. V. Salinas, A. Smirnov, Q. Wang, L. E. Yu, and J. Zhang, Observations of the temporal variability in aerosol properties and their relationships to meteorology in the summer monsoonal South China Sea/East Sea: the role of monsoonal flows, the Madden–Julian Oscillation, tropical cyclones, squall lines and cold pools. *Atmos. Chem. Phys. Discuss.*, 14, 20521-20584, 2014.
- Reid, J. S., et al.: Observing and Understanding the Southeast Asian Aerosol System by Remote Sensing: An Initial Review and Analysis for the Seven Southeast Asian Studies (7SEAS) Program. *Atmos. Res.* 122, 403-468, 2013.
- Reid, J. S., Xian, P., Hyer, E. J., Flatau, M. K., Ramirez, E. M., Turk, F. J., Sampson, C. R., Zhang, C., Fukada, E. M., and Maloney, E. D., Multi-scale meteorological conceptual analysis of observed active

Formatted: Indent: Hanging: 0.19", Don't adjust space between Latin and Asian text, Don't adjust space between Asian text and numbers

Formatted: Font: (Default) +Body (Calibri), (Asian) Chinese (PRC)

- fire hotspot activity and smoke optical depth in the Maritime Continent, *Atmos. Chem. Phys.*, 12, 1–31, 2012.
- Remer, L. A., Kleidman, R. G., Levy, R. C., Kaufman, Y. J., Tanré, D., Mattoo, S., Martins, J. V., Ichoku, C., Koren, I., Yu, H. and Holben, B. N.: Global aerosol climatology from the MODIS satellite sensors, *J. Geophys. Res.-Atmos.*, 113, D14S07, doi:10.1029/2007JD009661, 2008.
- Remer, L. A., Y. J. Kaurman, D. Tanre, S. Mattoo, D. A. Chu, J. V. Martins, R.-R. Li, C. Ichoku, R. C. Levy, R. G. Kleidman, T. F. Eck, E. Vermote, and B. N. Holben: The MODIS aerosol algorithm, products, and validation, *J. Atmos. Sci.*, 62, 947–973, 2005.
- Reynolds, R. W., Folland, C. K., and Parker, D. E.: Biases in satellite-derived sea-surface-temperature data, *Nature*, 341, 728-731, 1989.
- Ridley, D. A., C. L. Heald, and J. M. Prospero: What Controls the Recent Changes in African Mineral Dust Aerosol Across the Atlantic? *Atmos. Chem. Phys.* 14, 5735–5747, 2014.
- Ritchie, H.: Semi-Lagrangian Advection on a Gaussian Grid, *Mon. Wea. Rev.*, 115, 608-619, 1987.
- Robock, A.: Satellite data contamination, *Nature*, 341, 695-695, 1989.
- Saltzman, E.S., D.B. King, K. Holmen, C. Leck : Experimental determination of the diffusion coefficient of dimethylsulfide in water. *J. Geophys. Res.*, 98, 16481–16486, 1993.
- Sapiano, M. R. P. and P. A. Arkin: An intercomparison and validation of high resolution satellite precipitation estimates with three-hourly gauge data. *J. Hydromet.*, 10, 149-166, 2009.
- Sekiyama, T. T., T. Y. Tanaka, A. Shimizu, and T. Miyoshi: Data assimilation of CALIPSO aerosol observations, *Atmos. Chem. Phys.*, 10, 39–49, 2010.
- Sen, P. K.: "Estimates of the regression coefficient based on Kendall's tau", *J. Amer. Stat. Association*, 63, 1379–1389, 1968.
- Sessions, W. R., Reid, J. S., Benedetti, A., Colarco, P. R., da Silva, A., Lu, S., Sekiyama, T., Tanaka, T. Y., Baldasano, J. M., Basart, S., Brooks, M. E., Eck, T. F., Iredell, M., Hansen, J. A., Jorba, O. C., Juang, H.-M. H., Lynch, P., Morcrette, J.-J., Moorthi, S., Mulcahy, J., Pradhan, Y., Razinger, M., Sampson, C. B., Wang, J., and Westphal, D. L.: Development towards a global operational aerosol consensus: basic climatological characteristics of the International Cooperative for Aerosol Prediction Multi-Model Ensemble (ICAP-MME), *Atmos. Chem. Phys.*, 15, 335-362, 2015.
- Shi, Y., J. Zhang, J. S. Reid, B. Liu, and R. Deshmukh: Multi-sensor analysis on data-assimilation-quality MISR aerosol products, Abstract A53C-0358 presented at 2011 Fall Meeting, AGU, San Francisco, Calif., 5-9 Dec, 2011c.
- Shi, Y., Zhang, J., Reid, J. S., Holben, B., Hyer, E. J., and Curtis, C.: An analysis of the collection 5 MODIS over-ocean aerosol optical depth product for its implication in aerosol assimilation, *Atmos. Chem. Phys.*, 11, 557–565, 2011a.
- Shi, Y., Zhang, J., Reid, J. S., Hyer, E. J., Eck, T. F., Holben, B. N., and Kahn, R. A.: A critical examination of spatial biases between MODIS and MISR aerosol products – application for potential AERONET deployment, *Atmos. Meas. Tech.*, 4, 2823–2836, 2011b.
- Shi, Y., Zhang, J., Reid, J. S., Liu, B., and Hyer, E. J.: Critical evaluation of cloud contamination in the MISR aerosol products using MODIS cloud mask products, *Atmos. Meas. Tech.*, 7, 1791-1801, 2014.
- Shi, Y., Zhang, J., Reid, J. S., Hyer, E. J., and Hsu, N. C.: Critical evaluation of the MODIS Deep Blue aerosol optical depth product for data assimilation over North Africa, *Atmos. Meas. Tech.*, 6, 949-969, 2013.
- Slinn, A. A., and W. G. Slinn: Predictions for particle deposition on natural waters, *Atmos. Environ.*, 14, 1013– 1016, 1980.
- Smirnov, A., B. N. Holben, T. F. Eck, O. Dubovik, and I. Slutsker: Cloud screening and quality control algorithms for the AERONET data base, *Remote Sens. Environ.*, 73, 337– 349, 2000.
- Song C., Woodcock, C. E., Seto, K. C., Lenny, M. P., Macomber, S. A., Classification and change detection using Landsat TM data: When and how to correct atmospheric effects? *Remote Sens. of Environ.*,

- 75, 230-244, 2001.
- Staniforth, A. and Côté, J.: Semi-Lagrangian integration schemes for atmospheric models—a review. *Mon. Weather Rev.*, 119, 2206–2223, 1991.
- Sun, Y., S. Solomon, A. Dai and R. W. Portmann: How often does it rain? *J. Clim.*, 19, 916-934, 2007.
- Tanaka, T. Y., Orito, K., Sekiyama, T. T., Shibata, K., Chiba, M., and Tanaka, H.: MASINGAR, a global tropospheric aerosol chemical transport model coupled with MRI/JMA98 GCM: Model description, *Pap. Meteorol. Geophys.*, 53, 119–138, 2003.
- Theil, H.: "A rank-invariant method of linear and polynomial regression analysis. I, II, III", *Nederl. Akad. Wetensch., Proc.* 53: 386–392, 521–525, 1397–1412. 1950.
- Torres, O., Bhartia, P. K., Herman, J. R., Sinyuk, A., Ginoux, P. and Holben, B.: A long-term record of aerosol optical depth from TOMS observations and comparison to AERONET measurements, *J. Atmos. Sci.*, 59, 398–413, 2002.
- Tosca, M.G., Randerson, J.T., Zender, C.S., Nelson, D.L., Diner, D.J., Logan, J.A.: Dynamics of fire plumes and smoke clouds associated with peat and deforestation fires in Indonesia. *J. Geophys. Res.* 116, 2011.
- Toth, T.D., J. Zhang, J.R. Campbell, J.S. Reid, Y. Shi, R.S. Johnson, A. Smirnov, M.A. Vaughan, and D.M. Winker: Investigating enhanced Aqua MODIS aerosol optical depth retrievals over the mid-to-high latitude Southern Oceans through intercomparison with co-located CALIOP, MAN, and AERONET data sets, *J. Geophys. Res.-Atmos.*, 118, 4700-4714, 2013.
- Uppala, S.M., Kållberg, P.W., Simmons, A.J., Andrae, U., da Costa Bechtold, V., Fiorino, M., Gibson, J.K., Haseler, J., Hernandez, A., Kelly, G.A., Li, X., Onogi, K., Saarinen, S., Sokka, N., Allan, R.P., Andersson, E., Arpe, K., Balmaseda, M.A., Beljaars, A.C.M., van de Berg, L., Bidlot, J., Bormann, N., Caires, S., Chevallier, F., Dethof, A., Dragosavac, M., Fisher, M., Fuentes, M., Hagemann, S., Hólm, E., Hoskins, B.J., Isaksen, I., Janssen, P.A.E.M., Jenne, R., McNally, A.P., Mahfouf, J.-F., Morcrette, J.-J., Rayner, N.A., Saunders, R.W., Simon, P., Sterl, A., Trenberth, K.E., Untch, A., Vasiljevic, D., Viterbo, P., and Woollen, J.: The ERA-40 re-analysis. *Quart. J. R. Meteorol. Soc.*, 131, 2961-3012, 2005.
- van der Werf, G.R., et al.: Continental-scale partitioning of fire emissions during the 1997 to 2001 El Niño/La Niña period. *Science* 303, 73–76. 2004.
- Walcek, C. J., R. A. Brost, J. S. Chang and M. L. Wesely: SO₂, sulfate and HNO₃ deposition velocities computed using regional landuse and meteorological data. *Atmos. Environ.*, 20, 949-964, 1986.
- Walker, A. L., M. Liu, S. D. Miller, K. A. Richardson, and D. L. Westphal: Development of a dust source database for mesoscale forecasting in southwest Asia, *J. Geophys. Res.*, 114, D18207, doi:10.1029/2008JD011541, 2009.
- Wang, Chunzai, Shenfu Dong, Amato T. Evan, Gregory R. Foltz, Sang-Ki Lee: Multidecadal covariability of north atlantic sea surface temperature, african dust, sahel rainfall, and atlantic hurricanes. *J. Climate*, 25, 5404–5415. 2012.
- Wang, J., Ge, C., Yang, Z., Hyer, E. J., Reid, J. S., Chew, B. N., Mahmud, M., Zhang, Y., Zhang, M., Mesoscale modeling of smoke transport over the Southeast Asian Maritime Continent: Interplay of sea breeze, trade wind, typhoon, and topography, *Atmos. Res.*, 122, 486-503, 2013.
- Weatherhead, E. C., Reinsel, G. C., Tiao, G. C., Meng, X.-L., Choi, D., Cheang, W.-K., Keller, T., DeLuisi, J., Wuebbles, D. J., Kerr, J. B., Miller, A. J., Oltmans, S. J., and Frederick, J. E.: Factors affecting the detection of trends: Statistical considerations and applications to environmental data, *J. Geophys. Res.*, 103(D14), 17149–17161, 1998.
- Weaver, C., da Silva, A., Chin, M., Ginoux, P., Dubovik, O., Flittner, D., Zia, A., Remer, L., Holben, B., and Gregg, W.: Direct insertion of MODIS radiances in a global aerosol transport model, *J. Atmos. Sci.*, 64, 808–827, 2007.
- Westphal, D. L., Curtis, C. A., Liu, M., and Walker, A. L.: Operational aerosol and dust storm forecasting, in WMO/GEO Expert Meeting on an International Sand and Dust Storm Warning System, IOP

- Conference Series Earth and Environmental Science, 7, doi: 10.1088/1755-1307/7/1/012007, 2009.
- Westphal, D. L., O. B. Toon, and T. N. Carlson: A case study of mobilization and transport of Saharan dust. *J. Atmos. Sci.*, 45, 2145-2175, 1988.
- Wiedinmyer, C., S.K. Akagi, R.J. Yokelson, L.K. Emmons, J.A. Al-Saadi, J.J. Orlando, and A.J. Soja: The Fire INventory from NCAR (FINN): A high resolution global model to estimate the emissions from open burning. *Geoscientific Model Development*, 4, 625-641, 2011.
- Wilcox E. M. and V. Ramanathan: The impact of observed precipitation upon the transport of aerosols from South Asia, *Tellus-B*, 56, 435-450, 2004.
- Wilkinson, S. M., Dunn, S., Ma, S.: The vulnerability of the European air traffic network to spatial hazards, *Natural hazards*, 60, 1027-1036, 2012
- Witek, M. L., P. J. Flatau, P. K. Quinn, and D. L. Westphal: Global sea-salt modeling: Results and validation against multicampaign shipboard measurements, *J. Geophys. Res.*, 112, 2007.
- Xian, P., J. S. Reid, J. F. Turk, E. J. Hyer and D. L. Westphal: Impact of models versus satellite measured tropical precipitation on regional smoke optical thickness in an aerosol transport model, *Geophys. Res. Lett.*, 36, L16805, doi:10.1029/2009GL038823, 2009.
- Xian, P., J. S. Reid, S. A. Atwood, R. S. Johnson, E. J. Hyer, D. L. Westphal, W. Sessions: Smoke aerosol transport patterns over the Maritime Continent. *Atmos. Res.*, 122, 469-485, 2013.
- Young, I. R., S. Zieger, and A. V. Babanin: Global trends in wind speed and wave height, *Science*, 332, 451-455, 2011.
- Zhang, J. and Reid, J. S.: A decadal regional and global trend analysis of the aerosol optical depth using a data-assimilation grade over-water MODIS and Level 2 MISR aerosol products, *Atmos. Chem. Phys.*, 10, 10949-10963, 2010.
- Zhang, J. and Reid, J. S.: An analysis of clear sky and contextual biases using an operational over ocean MODIS aerosol product, *Geophys. Res. Lett.*, 36, L15824, doi:10.1029/2009GL038723, 2009.
- Zhang, J. and Reid, J. S.: MODIS Aerosol Product Analysis for Data Assimilation: Assessment of Level 2 Aerosol Optical Thickness Retrievals, *J. Geophys. Res.-Atmos.*, 111, 22207, doi:10.1029/2005JD006898, 2006.
- Zhang, J., J. R. Campbell, E. J. Hyer, J. S. Reid, D. L. Westphal, and R. S. Johnson: Evaluating the impact of multisensory data assimilation on a global aerosol particle transport model, *J. Geophys. Res. Atmos.*, 119, 4674-4689, 2014.
- Zhang, J., J. R. Campbell, J. S. Reid, D. L. Westphal, N. L. Baker, W. F. Campbell, and E. J. Hyer: Evaluating the impact of assimilating CALIOP-derived aerosol extinction profiles on a global mass transport model, *Geophys. Res. Lett.*, 38, L14801, doi:10.1029/2011GL047737, 2011.
- Zhang, J., Reid, J. S., Westphal, D. L., Baker, N. L., and Hyer, E. J.: A system for operational aerosol optical depth data assimilation over global oceans, *J. Geophys. Res.*, 113, D10208, doi:10.1029/2007JD009065, 2008.
- Zhang, Q., et al: Ubiquity and dominance of oxygenated species in organic aerosols in anthropogenically-influenced Northern Hemisphere midlatitudes, *Geophys. Res. Lett.*, 34, L13801, doi:10.1029/2007GL029979. 2007.

1420

1421

1422 Table 1. Optical properties for dry aerosol particles at 550nm in NAAPS.

Species	$a_{eff}(\mu\text{m})$	$\alpha_{ext}(\text{m}^2 \text{g}^{-1})$	$\alpha_{scat}(\text{m}^2 \text{g}^{-1})$	$\alpha_{abs}(\text{m}^2 \text{g}^{-1})$	ω_0	g
ABF	0.14	3.48	3.13	0.35	0.90	0.60
Dust	2.50	0.59	0.52	0.07	0.88	0.73
Smoke	0.17	4.48	3.99	0.50	0.89	0.58
Sea Salt	1.50	1.42	1.41	0.01	0.99	0.68

1423 where α_{ext} , α_{scat} , and α_{abs} are the bulk mass extinction, scattering, and absorption efficiencies, ω_0 the
 1424 single scattering albedo and g the asymmetry factor. a_{eff} is the bulk effective radius. "ABF" stands for
 1425 anthropogenic and biogenic fine particles.

1426

1427 Table 2. List of AERONET sites for further validation and *statistics of the reanalysis total AOT at 550nm*
1428 *compared with AERONET at these sites for December 2011-November 2012 breaking into two seasons*
1429 *DJFMAM (winter) and JJASON (summer). The selected sites and time periods match Sessions et al.*
1430 *(2015), where the International Cooperative for Aerosol Prediction (ICAP) Multi Model Ensemble (ICAP-*
1431 *MME) AOT is described and evaluated. The mean of total AOT of AERONET L2 data, the paired*
1432 *reanalysis data bias, root mean square error (RMSE), square of the Pearson correlation coefficient (r^2)*
1433 *and the total number of AERONET 6-hrly data (N) are shown. Values in bold, bold with underline and*
1434 *italic mean that the reanalysis is equally good, better and worse than the ICAP MME mean respectively*
1435 *(Such comparison is not available in terms of r^2 or for the fine mode AOT).*

1436 *Note: Correlation is not calculated for sites with dynamical range of the AOT data less than 0.1;*
1437 *correlation is marked with "N/A*" for these sites. "N/A" means data is not available.*

1438 *Seasonal AOT means for sites with only a few AERONET data (N) may not be representative.*

Formatted: Font: Not Italic

Formatted: Font: Not Italic

Site	Location	Main Aerosol type	Mean AERONET total 550nm AOT winter summer		Bias		RMSE		χ^2		N	
					winter summer	winter summer	winter summer	winter summer	winter summer	winter summer		
Alta Floresta	Brazil, 9S, 56W	Smoke	0.12	0.29	0.00	-0.03	0.05	0.11	0.49	0.82	35	203
Baengnyeong	Yellow Sea, 37N, 124E	ABF, Dust	0.39	0.34	0.04	0.00	0.16	0.18	0.77	0.75	213	215
Banizoumbou	Sahel, 13N, 2E	Dust	0.67	0.42	-0.11	-0.08	0.35	0.21	0.53	0.51	493	396
Beijing	China, 39N, 116E	ABF, Dust	0.60	0.62	-0.14	-0.17	0.50	0.45	0.54	0.76	322	110
Capo Verde	Sub-tro. Atlantic, 16N, 22W	Dust	0.36	0.39	0.02	0.00	0.12	0.12	0.88	0.77	283	312
Cart Site	Great Plains, 36N, 97W	Clean	0.10	0.14	0.00	-0.01	0.05	0.05	0.65	0.63	335	419
Chapais	Quebec, 49N, 74W	Clean	N/A	0.12	N/A	0.00	N/A	0.05	N/A	0.72	0	112
Chiang Mai	Thailand, 18N, 98E	Smoke	0.63	0.23	-0.14	-0.05	0.27	0.11	0.82	0.44	297	161
Crozet Island	Southern Ocean, 46S, 51E	Sea Salt	0.04	0.05	0.03	0.03	0.05	0.05	N/A*	N/A*	18	41
Gandhi College	Rural India, 25N, 84E	Dust, ABF	0.60	0.70	-0.08	-0.08	0.15	0.30	0.71	0.35	315	311
GSFC	EAST CONUS, 38N, 76W	ABF	0.11	0.18	0.00	-0.01	0.05	0.07	0.63	0.71	272	297
Ilorin	Sahel, 8N, 4E	Smoke, Dust	0.99	0.30	-0.09	0.02	0.31	0.13	0.75	0.55	411	182
Kanpur	Urban India, 26N, 80E	ABF, Dust	0.61	0.70	-0.08	-0.02	0.19	0.27	0.61	0.21	385	281
Minsk	Western Asia, 53N, 27E	ABF, Smoke	0.14	0.15	0.00	-0.01	0.06	0.07	0.52	0.51	156	180
Moldova	Eastern Europe, 47N, 28E	ABF	0.19	0.17	0.00	0.00	0.07	0.07	0.42	0.59	197	347
Monterey	WEST CONUS, 36N, 121W	Clean	0.08	0.07	0.02	-0.01	0.04	0.03	0.53	0.31	80	77
Palma de Mallorca	Mediterranean, 39N, 2E	Dust, ABF	0.08	0.20	0.00	-0.02	0.02	0.06	0.85	0.85	24	401
Ragged Point	Caribbean, 13N, 59W	African Dust	0.15	0.21	0.00	0.01	0.05	0.06	0.81	0.87	285	227
Rio Branco	Brazil, 9S, 67W	Smoke	0.08	0.22	0.00	-0.02	0.04	0.08	N/A*	0.86	144	328
Singapore	Maritime Cont., 1N, 103E	ABF, Smoke	0.31	0.47	-0.12	-0.16	0.20	0.24	0.15	0.55	71	192
Solar Village	Southwest Asia, 24N, 46E	Dust	0.63	0.38	0.02	0.07	0.27	0.13	0.25	0.68	77	318

Formatted: Font: Not Italic

1439

1440

1441

1442 Table 3. Same as Table 2, except for fine-mode AOT at 550nm.

Site	Mean AERONET fine AOT		Bias		RMSE		r^2		N	
	winter	summer	winter	summer	winter	summer	winter	summer	winter	summer
Alta Floresta	0.07	0.21	0.02	0.02	0.04	0.11	0.49	0.77	35	203
Baengnyeong	0.26	0.25	0.04	0.01	0.14	0.16	0.75	0.74	213	215
Banizoumbou	0.15	0.07	-0.03	0.07	0.14	0.11	0.17	0.16	493	396
Beijing	0.37	0.47	-0.05	-0.10	0.32	0.34	0.57	0.79	322	110
Capo Verde	0.08	0.06	0.01	0.03	0.07	0.05	0.33	0.30	283	312
Cart Site	0.06	0.09	0.01	0.02	0.03	0.04	0.69	0.70	335	419
Chapais	N/A	0.08	N/A	0.02	N/A	0.05	0.00	0.73	0	112
Chiang Mai	0.50	0.14	-0.04	0.02	0.22	0.08	0.82	0.48	297	161
Crozet Island	0.01	0.02	-0.01	-0.01	0.01	0.01	N/A*	N/A*	18	41
Gandhi College	0.31	0.43	0.02	0.05	0.11	0.23	0.71	0.41	315	311
GSFC	0.07	0.13	0.01	0.01	0.04	0.06	0.59	0.72	272	297
Ilorin	0.36	0.13	0.00	0.08	0.15	0.13	0.50	0.23	411	182
Kanpur	0.34	0.41	0.01	0.06	0.14	0.26	0.71	0.27	385	281
Minsk	0.09	0.10	0.01	0.01	0.04	0.05	0.53	0.47	156	180
Moldova	0.11	0.11	0.02	0.02	0.06	0.06	0.44	0.59	197	347
Monterey	0.03	0.04	0.02	0.00	0.02	0.02	N/A*	N/A*	80	77
Palma de Mallorca	0.05	0.09	0.00	0.00	0.02	0.03	0.91	0.61	24	401
Ragged Point	0.03	0.03	0.02	0.01	0.03	0.02	N/A*	N/A*	285	227
Rio Branco	0.04	0.16	0.01	0.03	0.02	0.08	N/A*	0.86	144	328
Singapore	0.21	0.34	-0.04	-0.07	0.14	0.18	0.13	0.58	71	192
Solar Village	0.11	0.13	0.07	0.06	0.09	0.07	0.09	0.36	77	318

Formatted: Font: Not Italic

1443

1444

1445

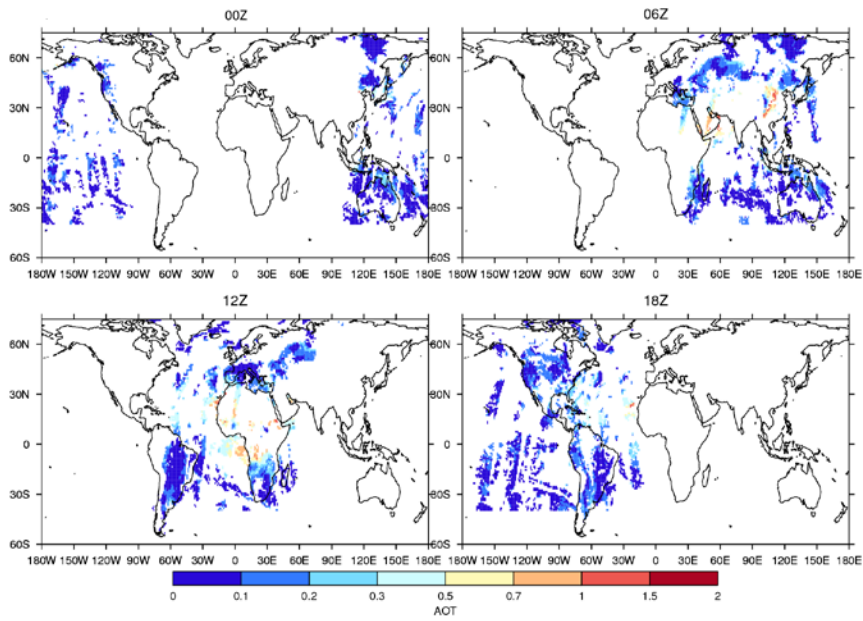
1446 Table 4, same as Table 2, except for coarse-mode AOT at 550nm and for sites in which the coarse mode
 1447 is dominated by dust.

1448

Site	Mean AERONET coarse AOT		Bias		RMSE		r^2		N	
	winter	summer	winter	summer	winter	summer	winter	summer	winter	summer
Baengnyeong	0.13	0.09	0.00	-0.01	0.07	0.05	0.47	0.63	213	215
Banizoumbou	0.52	0.35	-0.08	-0.15	0.29	0.23	0.50	0.55	493	396
Beijing	0.24	0.15	-0.09	-0.07	0.31	0.16	0.12	0.37	322	110
Capo Verde	0.28	0.33	0.01	-0.04	0.09	0.12	0.89	0.74	283	312
Gandhi College	0.29	0.27	-0.10	-0.13	0.14	0.23	0.50	0.57	315	311
Ilorin	0.63	0.17	-0.09	-0.06	0.30	0.11	0.65	0.49	411	182
Kanpur	0.27	0.29	-0.09	-0.09	0.14	0.15	0.65	0.69	385	281
Palma de Mallorca	0.03	0.11	0.00	-0.02	0.01	0.05	0.53	0.83	24	401
Ragged Point	0.12	0.18	-0.02	-0.01	0.06	0.06	0.72	0.85	285	227
Solar Village	0.52	0.25	-0.05	0.01	0.24	0.10	0.24	0.71	77	318

Formatted: Font: Not Italic

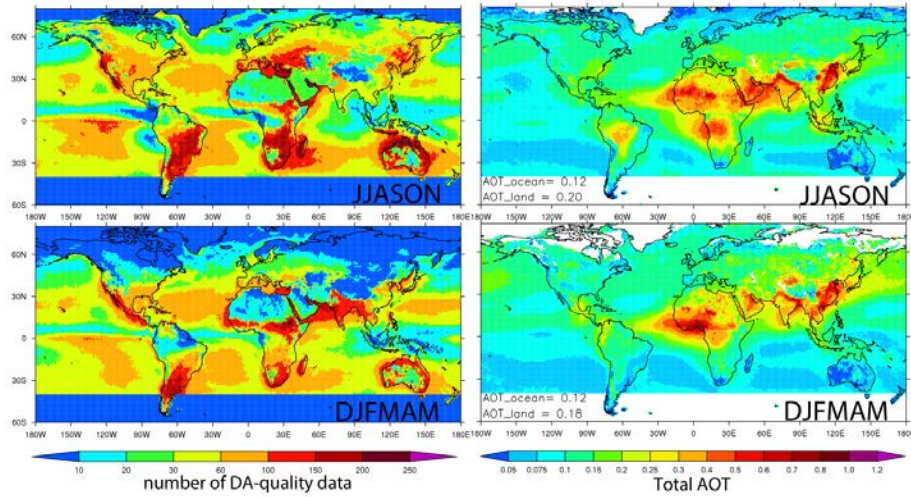
1449



1450

1451 Figure 1. An example of the general pattern of data coverage from MODIS (Aqua + Terra) and MISR for
1452 each AOT assimilation cycle at the valid time of the analysis, ie., 0, 6, 12 and 18 UTC, in NAVDAS-AOT.
1453 The MODIS and MISR AOT data displayed here is after strict QA/QC processes for Aug 11, 2011. The
1454 MODIS and MISR data assimilated in each NAVDAS-AOT cycle were acquired in a 6-hour range centered
1455 on the nominal valid time of the analysis.

1456



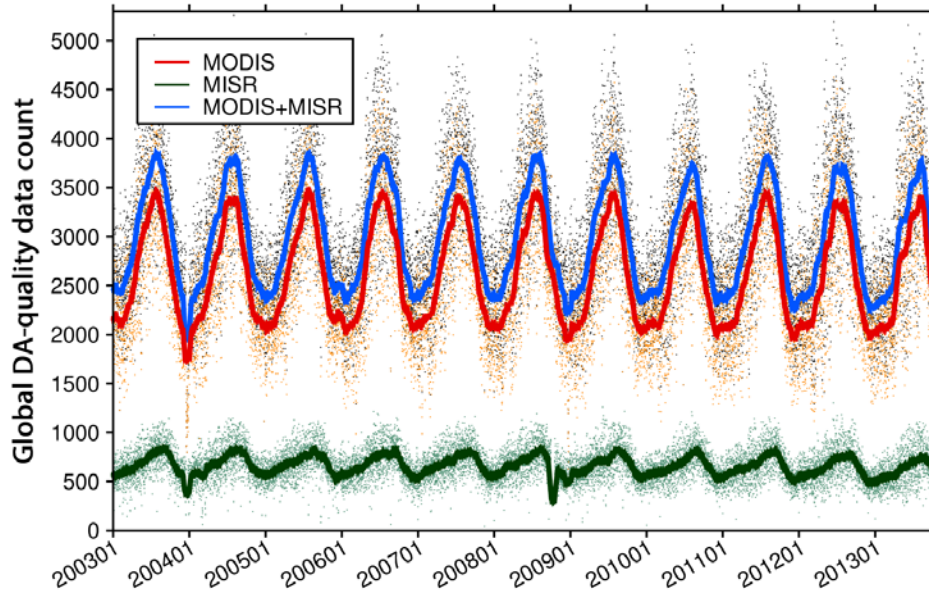
1457

1458 Figure 2. Properties of the 6-hrly 1x1 degree MODIS+MISR data assimilation quality AOT data for
1459 JJASON (June–November, upper) and DJFMAM (Previous year December–May, lower) averaged over
1460 2003–2013 (June 2003–May 2013): Left) total number of the DA-quality data, Right) seasonal mean of
1461 the total AOT at 550nm. Blank area indicates no available data. Annotations at the bottom left in the
1462 AOT figures show the area mean AOTs over ocean and over land averaged for 40°S–60°N.

1463

1464

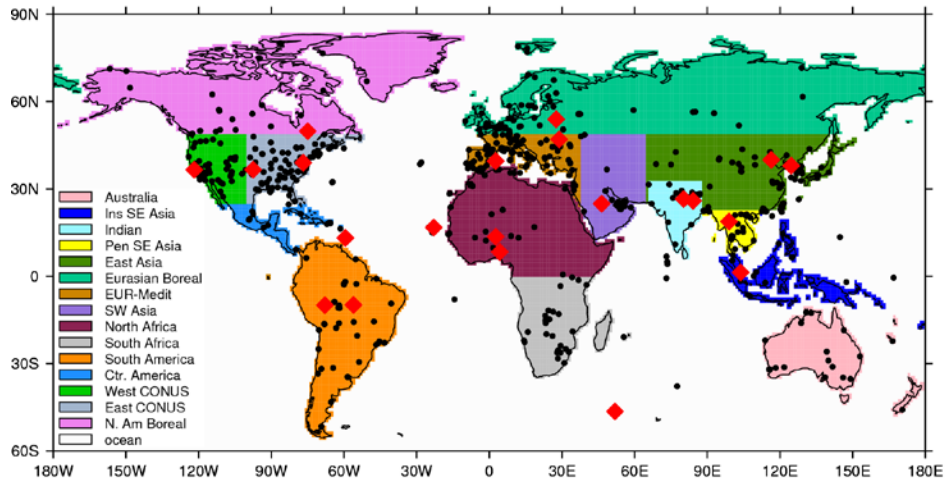
1465



1466

1467 Figure 3. The time series of 6-hrly data count of the global 1x1 grid MODIS (Terra+Aqua) (red), MISR
1468 (green), and fused MODIS-MISR data assimilation quality AOT (blue). Dots show 6-hrly data counts, and
1469 the solid lines represent the 30-day running average. The seasonal variation of the data volume is mainly
1470 related to the fact that more AOT data are discarded for the southern hemisphere high latitudes than
1471 the northern hemisphere high latitudes considering cloud contamination (see text for details).

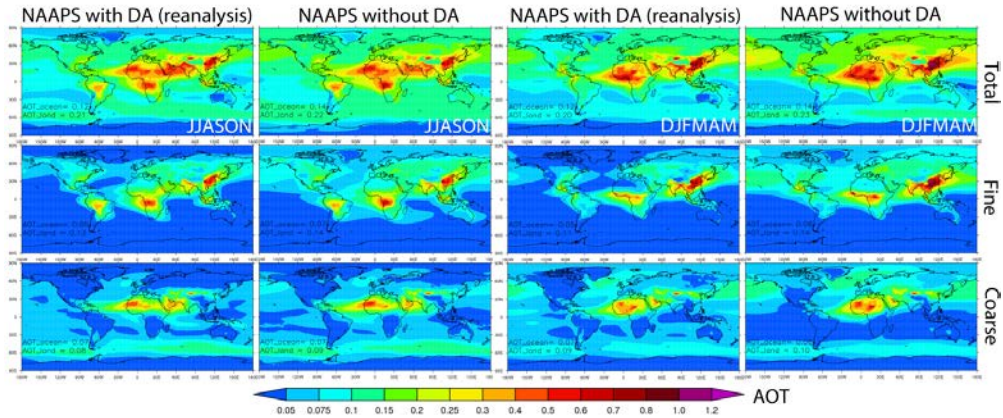
1472



1473

1474 *Figure 4. Selection of regions for this study. Antarctica is excluded. All AERONET sites that have valid L2*
 1475 *data for the study period (2003-2013) are in black dots. The selected sites for detailed validation (Section*
 1476 *3.2.3) are highlighted with red diamonds.*

1477



1478

1479 Figure 5. 2003-2013 averaged biseseasonal (June-November, ie., JJASON, and
 1480 December-May, ie., DJFMAM) total (upper), fine (middle) and coarse (bottom)
 1481 AOTs at 550nm from NAAPS with and without
 1482 AOT data assimilation. Annotations at the bottom left in the figures show the area mean AOTs over
 ocean and over land averaged for 40°S-60°N.

1483

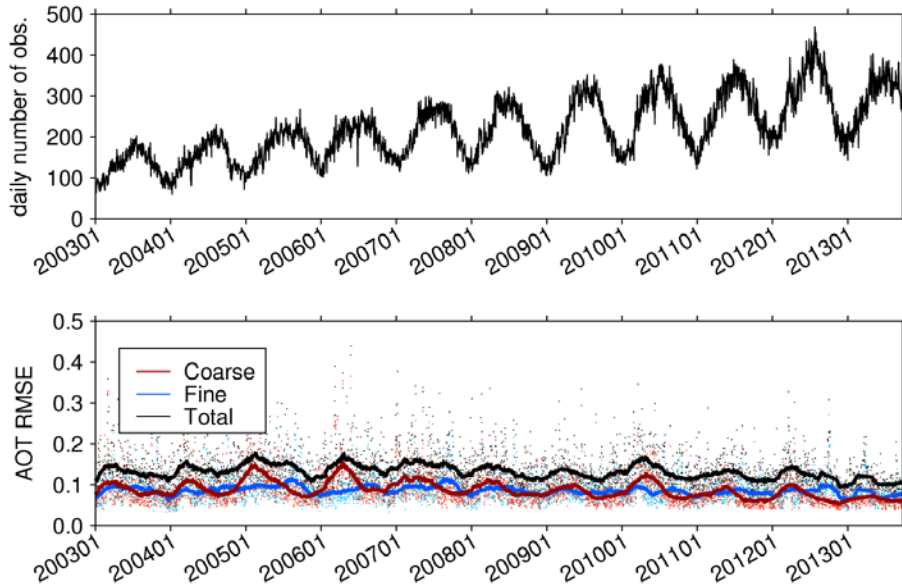


Figure 6. a) Time series of the daily total number of global regular AERONET L2 observations (excluding observations at DRAGON sites) binned into 6-hrly intervals (to match the model output resolution) for the AOT reanalysis period. b) Time series of the RMSE of the reanalysis total AOT (black), fine-mode AOT (blue) and coarse-mode AOT (red), all at 550nm, validated with AERONET. The daily average 6-hr RMSEs are in small dots and the corresponding 90-day running averages are in solid lines.

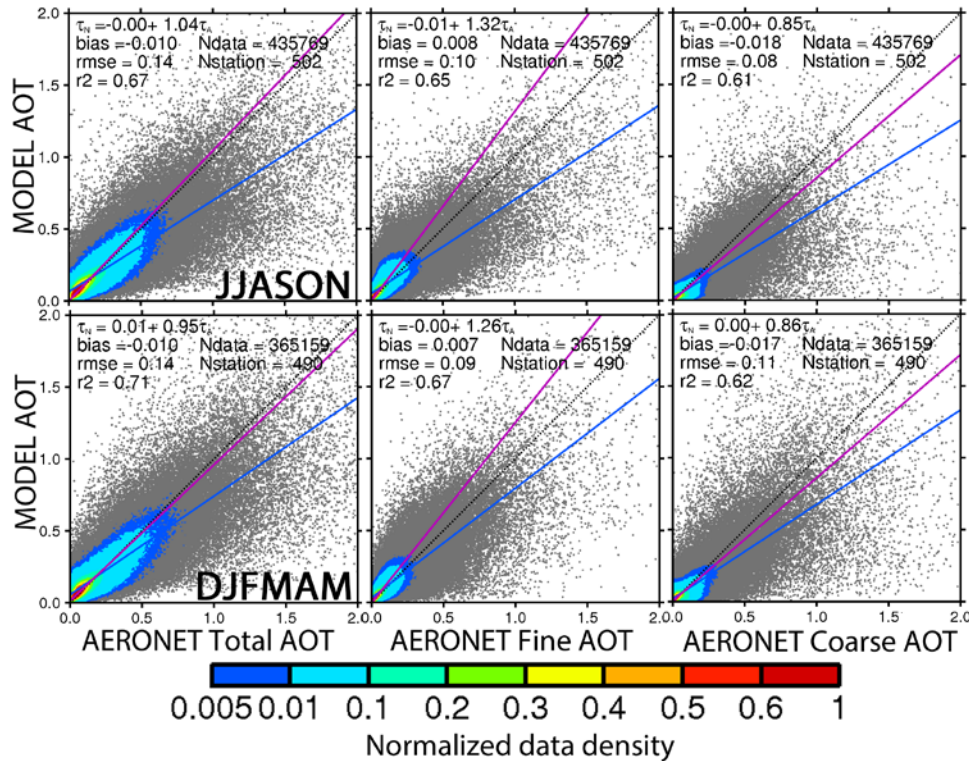


Figure 7. Pair-wise comparison of the global 6-hrly reanalysis AOT and AERONET AOT with respect to total (left), fine (middle) and coarse (right) modes at 550nm for JJASON (upper) and DJFMAM (bottom) for the entire reanalysis time (2003-2013). The normalized data density is shown in color. The solid magenta line represents a Theil-Sen linear regression and the corresponding equation is shown, where τ_N is the NAAPS reanalysis AOT and τ_A is the AERONET AOT. The solid blue line is a least-squares linear regression and the corresponding equation is not shown. Also shown are the bias, root mean square error (rmse), square of the pearson's correlation coefficient (r^2), total number of stations (Nstation) and total number of 6-hrly AERONET data (Ndata).

Formatted: Superscript

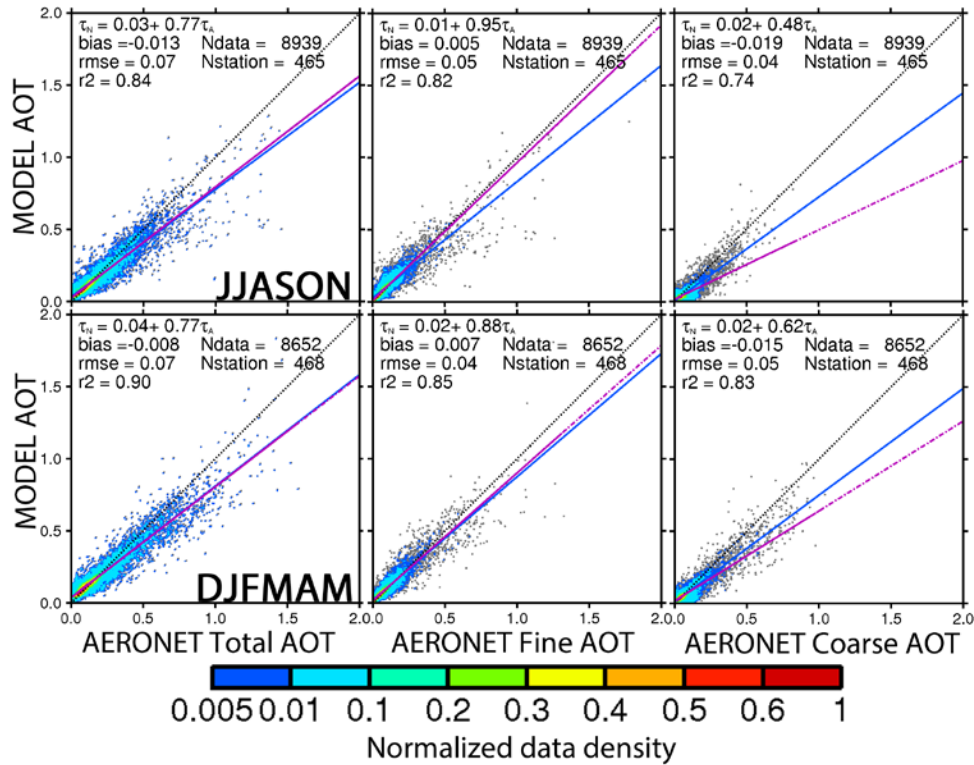


Figure 8. Same as Fig. 7, except for the monthly average of pair-wised 6-hrly mode AOTs at 550nm. Monthly average is obtained only when the total number of 6-hrly AERONET data exceeds 10 to ensure temporal representativeness. The monthly average reanalysis AOT here is calculated based on the available 6-hrly data that can be paired with AERONET data.

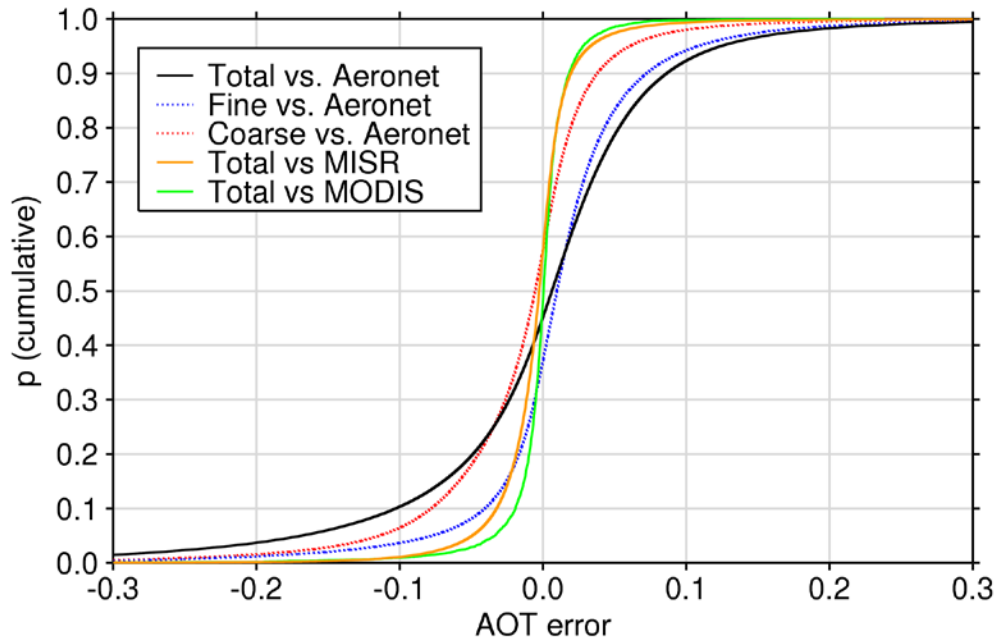
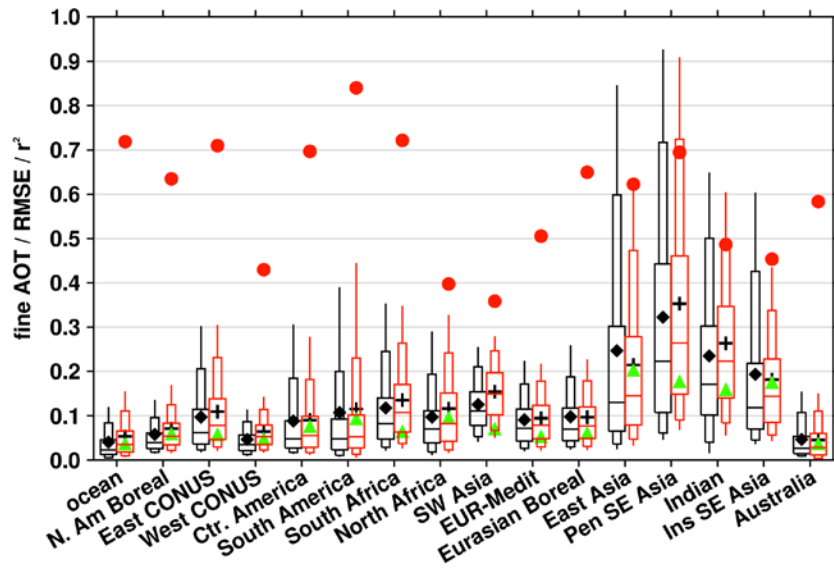


Figure 9. Cumulative distribution function for the reanalysis 6-hrly AOT errors compared to AERONET L2, MODIS and MISR data assimilation quality data with respect to the available total, fine and coarse modes at 550nm for the entire reanalysis time period (2003-2013).



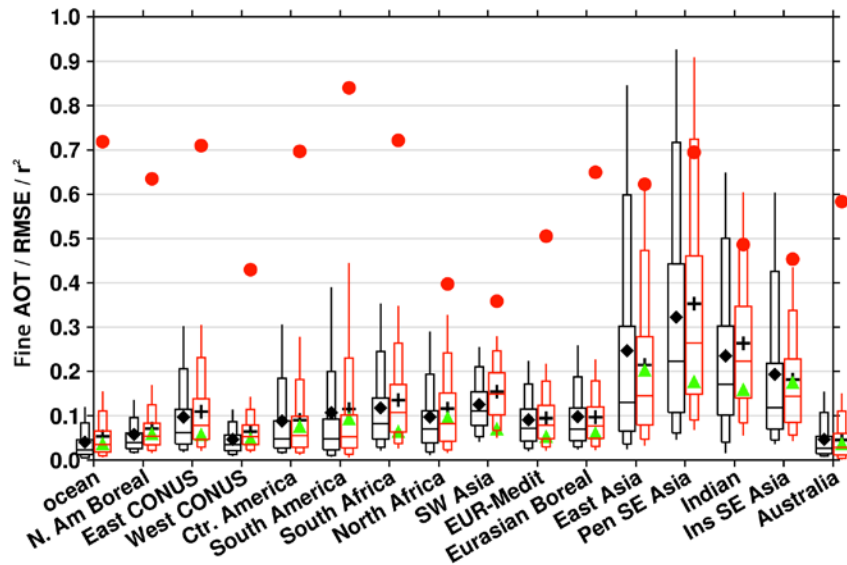
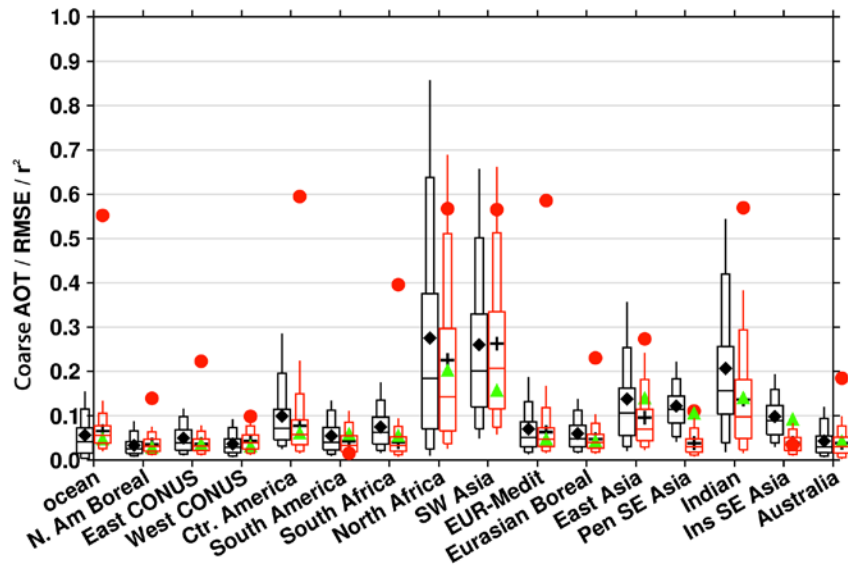


Figure 10. Comparison of regional fine mode AOT at 550nm of the reanalysis (red) at 95%, 90%, 75%, 50%, 25%, 10% and 5% percentiles to the pair-wised AERONET L2 data (black) for the regions defined in Figure 4 for the 10 year time period (June 2003-May 2013). Also shown are the regional mean of the reanalysis and AERONET fine mode AOTs in “+” and diamond respectively. Green triangles represent the root mean square error (RMSE) of the reanalysis. Red dots represent the square of the Pearson correlation coefficient (r^2) between the reanalysis and the AERONET observations.

Formatted: Font: Not Italic



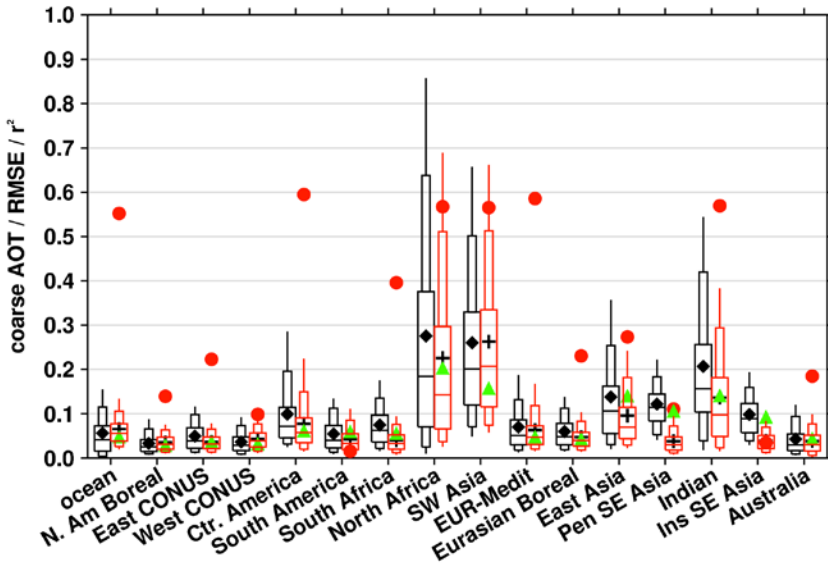
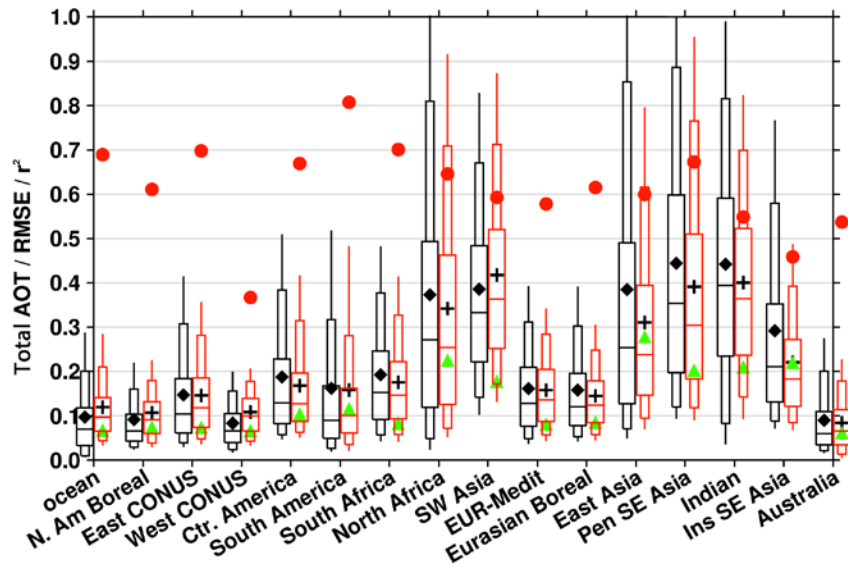


Figure 11. Same as Fig. 10, except for coarse mode AOT at 550nm.



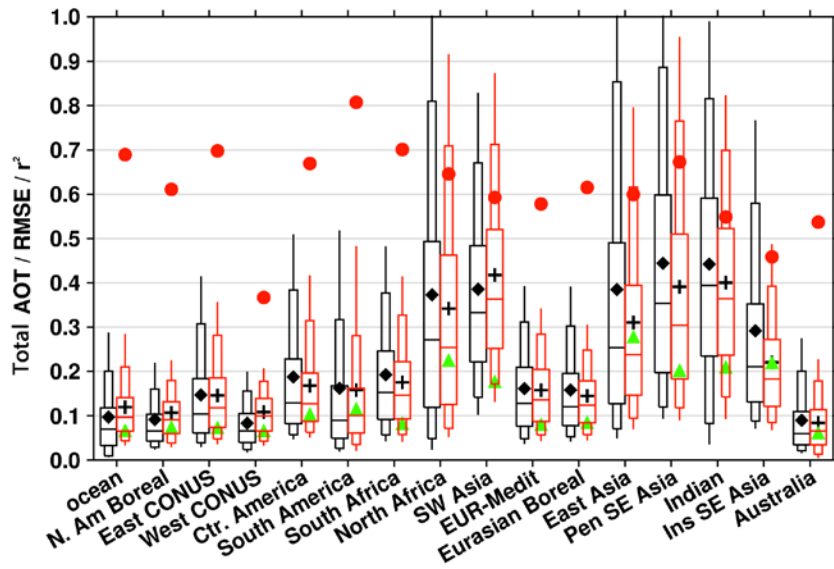


Figure 12. Same as Fig. 10, except for total AOT at 550nm. Also, AOT value greater than 1.0 is cropped in this figure.

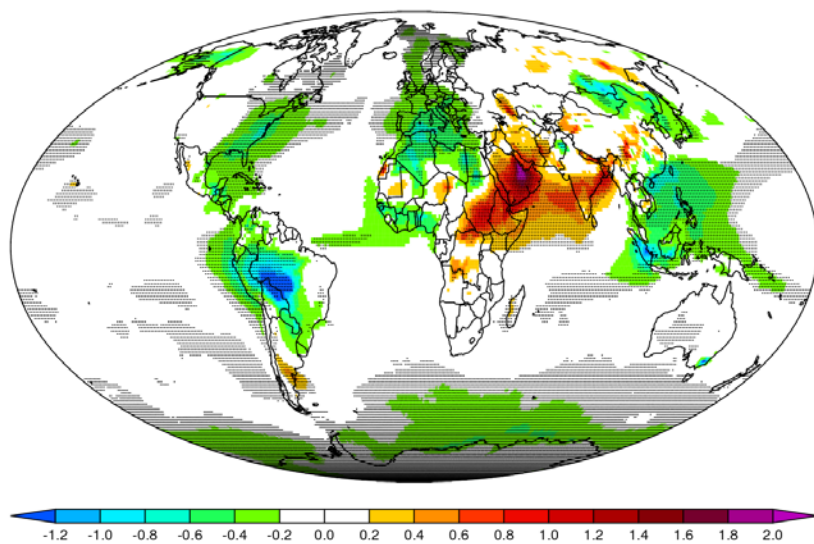


Figure 13. Trends of the deseasonalized reanalysis total AOT at 550nm over 2003-2013 (unit: 100xAOT/year). The dotted areas have passed 95% statistical significance level (see text and Zhang and Reid (2010) for details).

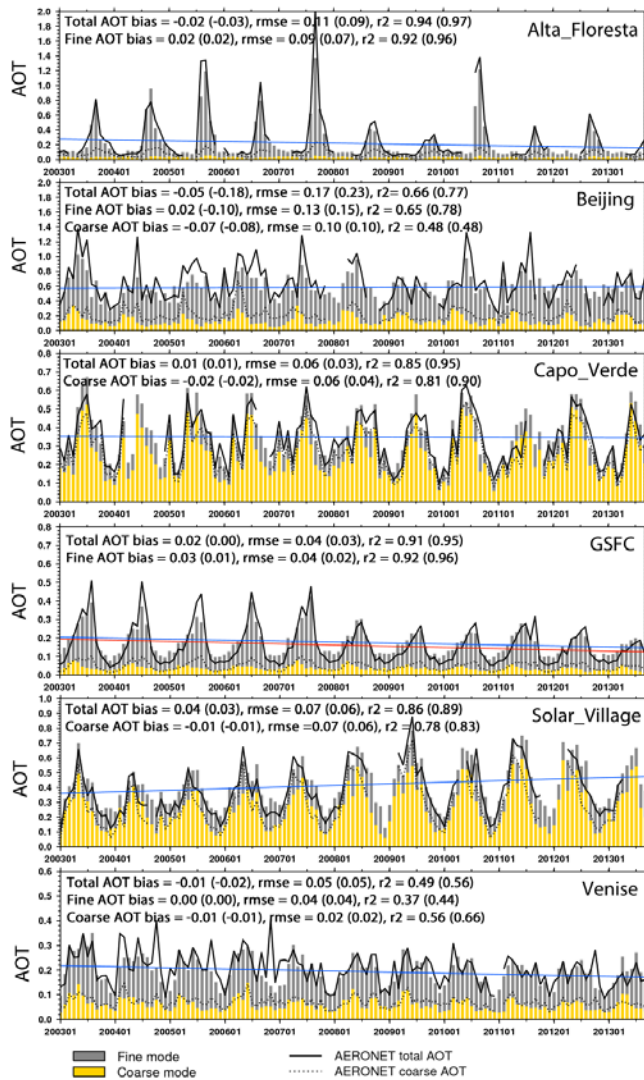


Figure 14. Monthly mean 550nm reanalysis and AERONET L2 mode AOTs at 6 AERONET sites, Alta Floresta in the Amazon, Beijing in East Asia, Capo Verde off the west coast of North Africa, GSFC in East CONUS, Solar Village in Arabian Peninsula, and Venice in Italy. The solid blue line is a linear regression of the reanalysis total AOT. The red solid line is a linear regression of the AERONET total AOT, only available when there is continuous data through the time. Monthly mean AERONET AOT is obtained only when the total number of 6-hrly AERONET data exceeds 10 to ensure temporal representativeness. Annotations for each time series show bias, RMSE and r^2 of monthly averages for unpaired comparisons; paired comparisons, using reanalysis values sampled to match available AERONET data, are shown in parentheses.

Formatted: Font: Not Italic

APPENDIX: Impact of tuning of sources and sinks vs. AOT data assimilation upon model performance

To show the relative importance of the tuning process on sources and sinks versus the AOT data assimilation to reanalysis performance, four model runs with difference configurations were conducted. AOT results from these four runs were inter-compared and validated with AERONET L2 data. The four model configurations are NAAPS without tuning (that is to say the original native version of NAAPS from which the reanalysis was originally based), NAAPS with tuning, NAAPS without tuning but with AOT data assimilation, and the final reanalysis version, which is with both tuning and AOT assimilation. The four model runs all cover Dec 2010-Nov 2011 one year time period. Interannual tuning was not conducted to preserve a measure of consistency within the model itself. The AOT data assimilation process, the input data and its pre-DA treatment are kept the same for the DA runs. The “tuning” processes on the sources and sinks include the addition of organic aerosols, updated SO₂ and DMS emissions, use of CMORPH precipitation to replace model precipitation within 30°S-30°N, usage of the FLAMBE MODIS 2-day-maximum regionally tuned smoke emissions and applying regional tuned factors on dust erodible fraction. For example, through the tuning exercises dust emission for 2011 is reduced from 1510 Tg to 953 Tg, and biomass turning smoke emission is reduced from 180 Tg to 85 Tg globally.

The appendix table shows the 550nm total, fine and coarse mode AOT bias, RMSE, r^2 and Theil-Sen linear regression slope against AERONET from the four model runs. With the tuning of sources and sinks, RMSE decreases about half, bias and r^2 also significantly improved for coarse, fine and total AOTs for the natural model run. The linear regression slope is also much closer to 1 for the fine and the total AOTs, and about unchanged for the coarse AOT compared to the NAAPS run without sources and sinks tuning. The absolute bias, RMSE and r^2 are comparable with those of the DA run without the tuning; i.e., through the tuning process on the baseline (“NAAPS_untuned”), similar validation result can be obtained as through the AOT assimilation on the baseline. This indicates that the tuning process on sources and sinks is as equally important as the AOT data assimilation process.

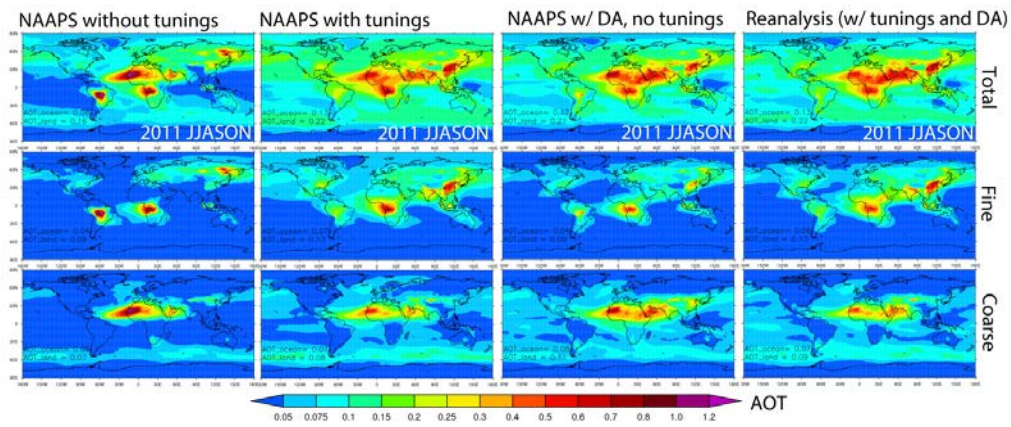
AOT data assimilation based on the tuned NAAPS further improves the validation statistics. For example, the RMSE is reduced about 20% for the coarse, fine and total AOTs comparing the reanalysis to the “NAAPS_tuned”. When comparing the DA runs (“reanalysis” vs. “DA_untuned”), there are also discernable improvements on bias, RMSE and r^2 resulted from the tuning process. The linear regression slope is improved for the fine AOT and about the same for the total AOT. The regression slope is worsened for the coarse AOT (0.64 for the reanalysis), because the model, like other aerosol models, faces challenges successfully resolving dust events over Sahel, East Asia and Indian subcontinent regions (e.g., Sessions et. al. 2015). While the untuned model has slight high biased coarse AOT, which makes the regression slope more tilted. The linear regression slope of the reanalysis based on all the 11-year data is 0.85 (Fig.7) though, better than the 2011 level.

The appendix Fig. 1 and Fig. 2 show the global coarse, fine and total AOT distributions from the four model runs for the two seasons of 2011, ie., JJASON and DJFMAM respectively. For both seasons, it is obvious that the natural NAAPS run without tunings has the most different AOT distributions and global averages among the four runs. The three other runs look more similar to each other, which is consistent with the validation statistics shown in appendix Table 1. For JJASON the natural NAAPS run without tunings has the lowest global mean AOTs among the four runs, yet the highest AOTs near dust and smoke source regions in South America and South Africa. This indicates possible excessive emissions in these regions and excessive removals over water, which are tuned through applying smaller emission factors for smoke and dust and lower dry deposition velocity for dust over water in the tuning process. For both seasons, the tuned NAAPS run without DA has slight high bias in the fine AOT (see also appendix Table 1) and the bias is slightly larger in DJFMAM than in JJASON, most probably resulted from excessive addition of organic aerosols during boreal winter.

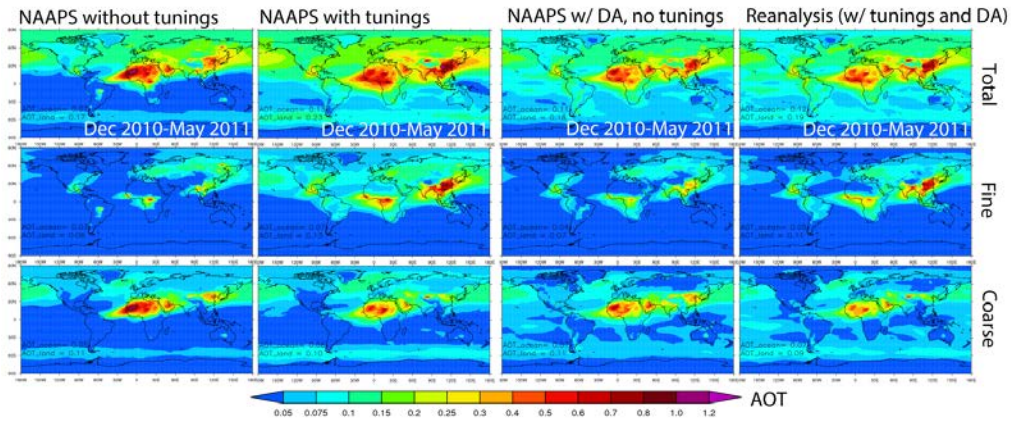
Compared to the reanalysis, the DA run without source and sink tuning, exhibits similar global total AOT distribution. However, some differences between the two are noticeable for the fine and coarse AOTs. For example, over the Indian subcontinent the AOT partitioning between the fine and coarse AOTs differs significantly. The contribution of the fine-mode aerosols to the total AOT dominates the contribution of the coarse-mode aerosols in the reanalysis. Whereas the total AOT is predominantly attributed to the coarse-mode aerosols in the DA run without tunings. Over the southern flank of the Himalayas, where fine-mode aerosols from industrial and biofuel emissions often prevails over coarse-mode (refer to Kanpur site in Tables 2-4), the fine mode fraction is increased from ~ 0.3 in the DA run without tunings to ~ 0.7 in the reanalysis. This illustrates the importance of the tuning processes in yielding a better AOT partitioning between the fine and coarse modes.

Appendix Table: Statistics of the coarse, fine and total AOTs at 550nm from four model runs compared with AERONET L2 data. The four model runs are from four different model configurations, including NAAPS without sources and sinks tuning, NAAPS with tuning, NAAPS without tuning but with AOT data assimilation, and the reanalysis version, which is with both the tuning and the AOT assimilation. The comparison is based on one year time period (Dec. 2010 to Nov. 2011). The global AERONET mean is 0.085, 0.102 and 0.187 for coarse, fine and total AOT respectively, obtained with averaging 97654 valid 6-hrly L2 data from 285 stations.

	AOT Bias	RMSE	r^2	Regression slope
	Coarse fine total	Coarse fine total	Coarse fine total	Coarse fine total
NAAPS_untuned	0.008 -0.030 -0.022	0.17 0.19 0.26	0.33 0.05 0.15	0.59 0.69 0.81
NAAPS_tuned	-0.005 0.021 0.016	0.10 0.10 0.16	0.45 0.47 0.48	0.58 0.98 0.89
DA_untuned	0.014 -0.025 -0.011	0.09 0.11 0.14	0.58 0.41 0.56	0.90 0.75 0.80
Reanalysis	-0.013 0.006 -0.007	0.08 0.08 0.13	0.59 0.63 0.65	0.64 1.00 0.77



Appendix Figure 1. 6-month-average (Jun-Nov 2011) total (upper), fine (middle) and coarse (bottom) AOTs at 550nm from four NAAPS runs with different configuration: NAAPS without tuning, NAAPS with tuning processes on sources and sinks, NAAPS without tuning but with AOT data assimilation, and the reanalysis version, which is with both tuning and AOT assimilation. Annotations at the bottom left in the figures show the area mean AOTs over ocean and over land averaged for 40°S-60°N.



Appendix Figure 2. Same as the Appendix Figure 1, except for Dec. 2010-May 2011 6-month-average.